Importance of numerical ocean modelling and in situ ocean bottom pressure observations for satellite gravimetry from GRACE and GRACE-FO

Dissertation

zur Erlangung des Grades eines Doktors der Naturwissenschaften.
Vorgelegt von

Lea Poropat

am Fachbereich Geowissenschaften der Freien Universität Berlin,
angefertigt am Deutschen GeoForschungsZentrum, Potsdam.

Berlin, 2019

Autor:	Lea Poropat
Erstgutachter:	Prof. Dr. Maik Thomas
Zweitgutachter:	Prof. Dr. Frank Flechtner (Technische Universität Berlin)
Datum der Einreichung:	13.12.2019
Datum der Disputation:	16.07.2020

Eidesstattliche Erklärung

Hiermit versichere ich, dass ich die vorliegende Dissertation selbstständig angefertigt habe und keine anderen als die angegebenen Quellen und Hilfsmittel benutzt habe, sowie Zitate kenntlich gemacht habe. Ein Promotionsverfahren zu einem früheren Zeitpunkt an einer anderen Hochschule oder bei einem anderen Fachbereich wurde nicht beantragt.

Ort, Datum

Lea Poropat

Contents

Abstract

The GRACE and GRACE-FO satellites observe the redistribution of mass in terrestrial water storage, ice sheets, oceans, atmosphere, and solid Earth. Because GRACE data is typically accumulated into monthly-mean gravity fields, an a priori background model, namely the Atmosphere and Ocean Dealiasing Level 1B (AOD1B) product, is applied to remove non-tidal variability that would otherwise alias into the monthly solutions. The main disadvantage of AOD1B RL06 compared to its previous release is that it does not simulate the dynamics beneath the Antarctic ice shelves, which can have a strong influence on global ocean circulation. The primary motivation for this work is the development of the new release of AOD1B, but the performed model experiments can also provide useful insight into the influence processes in the Southern Ocean have on global ocean dynamics.

To be able to test various model experiments, as well as to compare GRACE gravity field solutions, validation against in situ measured ocean bottom pressure (OBP) is used. The validation is somewhat better suited for submonthly variability of the ocean models than for long-term signals measured by GRACE because the in situ time series are affected by the errors in trend and drift removal on longer temporal scales. The difference between the pointwise in situ and the area-averaging GRACE measuring technique also influences the comparison. It is shown that post-processing choices can severely impact the results of the validation of GRACE fields, so if different solutions are compared, their post-processing needs to be identical. Validation against in situ OBP is used to compare the EGSIEM combined GRACE solution with its five contributing datasets. It is shown that the combined solution is very close to the leading CSR RL05 and ITSG-Grace2016 solutions, outperforming the others. To investigate whether GRACE is able to detect submonthly signals, the ITSG-Grace2016 daily Kalman solution, from which the submonthly atmospheric and oceanic variability has been removed with AOD1B RL05, is validated against in situ OBP. The results show that GRACE successfully captures some submonthly variability that is not predicted by the incorporated dealiasing model.

As a first step towards AOD1B RL07, the dynamics beneath the Antarctic ice shelves are implemented into the model used as the oceanic part of AOD1B, the Max Planck Institute Ocean Model (MPIOM). The bathymetry is modified to include the areas under the ice shelves and two new model experiments are performed: in one those regions are treated as open ocean, while in the other the atmospheric forcing is modified to simulate the ice shelves. The changes caused by such modifications are not limited only to the Southern Ocean, but also affect the Northern Atlantic, confirming the role the Weddell Sea has on the meridional overturning circulation. While surface changes exceed the typical variability only in a few regions, the differences at the bottom of the ocean are larger. The changes caused by ice shelf forcing are of the same order of magnitude in the vicinity of the ice shelves, but much smaller globally. A comparison with the GLORYS2v4 ocean reanalysis shows that the new model experiments are closer to the reanalysis, especially in the regions where the original MPIOM experiment performs the worst. The analysis of OBP variability points out some possible issues that need to be fixed before publishing the new AOD1B release. Validation against in situ OBP, however, shows that the modifications are without a doubt in the right direction: the new model experiment has increased relative explained variances in the $1 - 3$ days band by approximately 5 % throughout Pacific, and by more than 10 % in the Antarctic Circumpolar Current region.

Kurzfassung

Die GRACE- und GRACE-FO-Satelliten beobachten die Umverteilung von Masse in terrestrischen Wasserspeichern, Eisdecken, Ozeanen, Atmosphäre und fester Erde. Da GRACE-Daten in der Regel in monatlichen gemittelten Schwerefeldern gesammelt werden, wird ein a priori Hintergrundmodell *Atmosphere and Ocean Dealiasing Level 1B* (AOD1B) angewendet, um nicht-gezeitenbedingte Schwankungen zu beseitigen, die andernfalls zu einem Alias-Effekt in den monatlichen Lösungen führen würden. Der Hauptnachteil von AOD1B RL06 im Vergleich zu seiner Vorgängerversion besteht darin, dass die Dynamik unter den Antarktis-Eisschelfs, die einen starken Einfluss auf die globale Ozeanzirkulation haben kann, nicht simuliert wird. Die Hauptmotivation für diese Arbeit ist die Entwicklung des neuen Releases von AOD1B, die durchgeführten Modellexperimente können jedoch auch nützliche Einblicke in den Einfluss von Prozessen im Südpolarmeer auf die globale Ozeandynamik liefern.

Um verschiedene Modellexperimente testen und GRACE-Schwerefeldlösungen vergleichen zu können, wird eine Validierung gegen den in situ gemessenen Meeresbodendruck (OBP) durchgeführt. Die Validierung ist für die submonatliche Variabilität der Ozeanmodelle etwas besser geeignet als für die von GRACE gemessenen Langzeitsignale, da die In-situ-Zeitreihen auf längeren Zeitskalen von Trend- und Driftentfernungenfehlern beeinflusst werden. Der Unterschied zwischen der punktweisen in situ- und der flächenmittelnden GRACE-Messtechnik beeinflusst auch den Vergleich. Es wird gezeigt, dass die Auswahl der Postprozessierung die Validierungsergebnisse von GRACE-Feldern erheblich beeinflussen kann. Wenn also verschiedene Lösungen verglichen werden, muss die Postprozessierung identisch sein. Die Validierung gegen In-situ-OBP wird verwendet, um die in EGSIEM Projekt kombinierte GRACE-Lösung mit ihren fünf beitragenden Datensätzen zu vergleichen. Es wird gezeigt, dass die kombinierte Lösung den führenden CSR RL05- und ITSG-Grace2016-Lösungen sehr nahe kommt und die anderen übertrifft. Um zu untersuchen, ob GRACE in der Lage ist, submonatliche Signale zu erkennen, wird die tägliche ITSG-Grace2016-Kalman-Lösung, aus der die submonatliche atmosphärische und ozeanische Variabilität mit AOD1B RL05 entfernt

wurde, gegen in situ OBP validiert. Die Ergebnisse zeigen, dass GRACE gewisse submonatliche Variabilitäten erfolgreich erfasst, die vom integrierten Dealiasing-Modell nicht vorhergesagt werden.

Als erster Schritt in Richtung AOD1B RL07 wird die Dynamik unter den Antarktis-Eisschelfs in das *Max Planck Institute Ocean Model* (MPIOM) implementiert, das als ozeanischer Teil von AOD1B verwendet wird. Die Bathymetrie wird modifiziert, um die Bereiche unter den Eisschelfen einzubeziehen, und es werden zwei neue Modellexperimente durchgeführt: In einem Experiment werden diese als offener Ozean behandelt, während im anderen der atmosphärische Antrieb modifiziert wird, um die Eisschelfe zu simulieren. Die durch solche Modifikationen verursachten Veränderungen beschränken sich nicht nur auf das Südpolarmeer, sondern betreffen auch den Nordatlantik, was die Rolle des Weddellmeeres für die meridionale Umwälzzirkulation bestätigt. Während die Oberflächenveränderungen die typische Variabilität nur in wenigen Regionen überschreiten, sind die Unterschiede am Meeresboden größer. Die Veränderungen, die durch den Eisschelfantrieb verursacht werden, sind in der Nähe der Eisschelfs in der gleichen Größenordnung, global jedoch viel geringer. Ein Vergleich mit der Ozean-Reanalyse GLORYS2v4 zeigt, dass die neuen Modellexperimente näher an der Reanalyse liegen, insbesondere in den Regionen, in denen das ursprüngliche MPIOM-Experiment am schlechtesten abschneidet. Die Analyse der OBP-Variabilität zeigt einige mögliche Probleme auf, die vor der Veröffentlichung der neuen Version des AOD1B-Produkts behoben werden müssen. Die Validierung mit In-situ-OBP zeigt jedoch, dass die Modifikationen zweifellos in die richtige Richtung weisen: Das neue Modellexperiment hat die relativen erklärten Varianzen im Bereich von 1 – 3 Tagen im gesamten pazifischen Raum um ungefähr 5 % erhöht und um mehr als 10 % in der Region der Antarktische Zirkumpolarströmung.

1

Introduction

1.1 Historical background

For over a thousand years, people have been interested in the ocean because the knowledge of the winds and ocean currents was necessary to travel to new areas. Already the Vikings and the Polynesians made use of their experience with ocean currents in their exploration. First documented knowledge on the ocean currents was gathered during the expeditions of Christopher Columbus (1492–1494), Vasco da Gama (1497–1499), and Ferdinand Magellan (1519–1522) (*Dijkstra*, 2008). The early ocean exploration was usually motivated by the desire to find new areas to settle, extend trading routes, and facilitate the travels. Most of the measurements were incidental, made from the ships that normally had a purpose other than sea research. Only in 1925 the first dedicated physical oceanographic expedition was organised, the German Meteor expedition of the Atlantic Ocean (*Dijkstra*, 2008). Ever since then, more and more measurements of the ocean properties are made. Even with ever-increasing number of ocean research campaigns and observational networks, however, there are still areas of the ocean without in situ measurements because of their high price and difficult working conditions. Satellite observations partly solve that, by providing global coverage of surface quantities, but electromagnetic energy, the backbone of sensors and communications in the atmosphere, does not penetrate deep or propagate far in the ocean, making it very difficult to probe the ocean interior remotely (*Kantha and Clayson*, 2000).

Since collection of in situ data in the ocean is quite expensive, and since satellite-borne sensors provide information on mostly near-surface layers of the ocean, it is often thought that ocean models are central to understanding how oceans function (*Kantha and Clayson*, 2000). Same as the whole field of oceanography, ocean modelling is very young. The first comprehensive numerical global baroclinic ocean model was only formulated in the late sixties, by Kirk Bryan (*Bryan*, 1969). The development of high performance computing, however, has led to an exponential growth in the ocean model advancement, allowing us to understand and simulate the characteristics and the circulation of the ocean with increasing resolution and accuracy.

Today, we need both models and observations to study the ocean dynamics. In situ and satellite observations are assimilated into ocean models to produce reanalysis datasets, which combine the reality of the observations, while remaining in agreement with model physics. Observations are often used to check the quality of the models in regions where they are available, which increases the confidence into the model in regions without observations. Models of ocean and atmosphere are used as background models for processing of satellite data. The increasing number of in situ observations, an ever-growing number of satellites orbiting the Earth measuring sea surface height, temperature, and other quantities, and the rapid development of global and regional ocean models all provide us with a better understanding of the ocean than we would ever be able to obtain with only one method.

1.2 Motivation and context

The motivation for this work is dual. The main incentive is the development of the ocean model used for satellite gravimetry data processing and signal separation. Secondly, comparing the results from different model experiments allows the study of the impact of various processes on ocean dynamics, making it a great tool to understand the ocean.

Gravity Recovery and Climate Experiment (GRACE) is the first satellite mission dedicated to accurately map the spatial distribution and temporal variations of the Earth's gravity field. It was launched on the 17 March 2002, with an intended lifetime of 5 years. The satellites greatly surpassed it, ending their science operations in October 2017, after more than 15 years in orbit. The mission is continuing with GRACE Follow On (GRACE-FO), a new pair of satellites launched on the 22 May 2018. Both GRACE and GRACE-FO consist of two satellites tracking each other in a near-circular slowly declining orbit, at a starting altitude of ∼500 km, and 89.5° inclination, separated by approximately 220 km along-track (*Tapley et al.*, 2004). They are linked by a highly

accurate inter-satellite, K-band microwave ranging system. Each satellite is equipped with Global Positioning System (GPS) receivers, attitude sensors, and high precision accelerometers located at the satellite's center of mass. GRACE-FO in addition has a laser ranging interferometer, which increases the accuracy of the inter-satellite distance measurements. As the satellite pair circles the Earth, areas of greater mass concentration, and therefore slightly stronger gravity, affect the lead satellite first, pulling it away from the trailing satellite. As they continue, the trailing satellite is pulled toward the lead satellite as it also passes over the gravity anomaly. The changes in the distance are detected by the microwave ranging system and, in case of GRACE-FO, satellite interferometer. With the accelerometer measuring the non-gravitational accelerations, the accelerations caused by gravity can be isolated, while GPS is used to determine the position of the satellites. By tracking the distance between the two satellites, GRACE observes the variations in Earth's gravity field caused by changes in ice sheets (e.g. *Velicogna*, 2009; *Luthcke et al.*, 2013), terrestrial water storage (e.g. *Rodell et al.*, 2009; *Moore and Fisher*, 2012), ocean dynamics (e.g. *Chambers*, 2006; *Bergmann and Dobslaw*, 2012), and solid Earth (e.g. *Wahr and Velicogna*, 2003; *Davis et al.*, 2004).

While some datasets are provided with higher temporal resolution, GRACE observations are typically averaged to obtain monthly-mean gravity fields. As such, they are affected by the aliased submonthly signals that are dominant in the atmosphere and ocean. Those high frequency signals are usually removed by applying an a priori background model, namely the Atmosphere and Ocean Dealiasing Level 1B (AOD1B) product, which is used to predict and remove high-frequency non-tidal atmospheric and oceanic variability. Its atmospheric part comes from the European Centre for Medium-Range Weather Forecasts (ECMWF) reanalysis (*Dee et al.*, 2011) and for later years operational model, while the oceanic part is calculated by an ocean general circulation model, forced by aforementioned ECMWF products. The level of errors in GRACE data can be reduced by developing and improving the backround models. During the development of AOD1B RL06, a switch from Ocean Model for Circulation and Tides (OMCT; *Thomas*, 2002) to the Max Planck Institute Ocean Model (MPIOM; *Jungclaus et al.*, 2013) was made (*Dobslaw et al.*, 2017). Among the many improvements was also one disadvantage, namely, unlike OMCT, MPIOM does not simulate the dynamics beneath the Antarctic ice shelves.

Southern Ocean connects the three major oceans through the Antarctic Circumpolar Current (ACC). It is also a key region for the exchange of energy and gases between the atmosphere and the abyssal ocean as one of the regions where the oxygen rich surface waters sink to the ocean bottom. A multitude of processes important for the Southern Ocean circulation, and therefore also for the global ocean circulation and climate, are

affected by the presence of the Antarctic ice shelves. Despite that, many global ocean models, including MPIOM, do not take the ice shelves into account, often going as far as to not even include the areas beneath the ice shelves into their domain. It is therefore important to analyse the influence such differences in ocean bathymetry have on simulated ocean circulation. The new experiments demonstrate the sensibility of the model to bathymetry changes and give us important insights about the influence the Southern Ocean has to the global ocean circulation. Considering MPIOM is the basis for the dealiasing product for GRACE, the changes made to the bathymetry and forcing of MPIOM, will also eventually be implemented into the new release of AOD1B, thus improving the quality of GRACE observations and allowing us to discover new trends in terrestrial water storage, better detect the ice sheet melting, and observe the global sea level rise due to the changes of ocean mass.

1.3 Aims and structure of this thesis

This dissertation uses in situ and satellite observations along with numerical ocean modelling to study the circultion and the variability of the global ocean. It contributes to the research of oceanic signals from GRACE satellite gravimetry, as well as to the development of an ocean general circulation model for the purpose of processing and separating signals from GRACE. It also presents a study of model sensitivity to the changes in the Southern Ocean and their influence on ocean circulation. This dissertation contains work that was published as part of the following two first-author papers:

F1 **L. Poropat**, H. Dobslaw, L. Zhang, A. Macrander, O. Boebel, and M. Thomas (2018): **Time variations in ocean bottom pressure from a few hours to many years: in situ data, numerical models, and GRACE satellite gravimetry**, Journal of Geophysical Research: Oceans, 123, 5612–5623, doi: 10.1029/2018JC014108.

F2 **L. Poropat**, A. Kvas, T. Mayer-Gürr, and H. Dobslaw (2020): **Mitigating temporal aliasing effects of high-frequency geophysical fluid dynamics in satellite gravimetry**, Geophysical Journal International, 220(1), 257–266, doi: 10.1093/gji/ggz439.

Parts of the following co-authored publications are also included in the dissertation:

C1 H. Dobslaw, I. Bergmann-Wolf, R. Dill, **L. Poropat**, M. Thomas, C. Dahle, S. Esselborn, R. König, and F. Flechtner (2017): **A new high-resolution model of non-tidal atmosphere and ocean mass variability for de-aliasing of**

satellite gravity observations: AOD1B RL06, Geophysical Journal International, 211, 263–269, doi: 10.1093/gji/ggx302.

C2 Q. Chen, **L. Poropat**, L. Zhang, H. Dobslaw, M. Weigelt, and T. van Dam (2018): **Validation of the EGSIEM GRACE gravity fields using GNSS coordinate time series and in situ ocean bottom pressure records**, Remote Sensing, 10(12), 1976, doi: 10.3390/rs10121976.

Since only parts of some papers are relevant for the dissertation, and in other cases additional information not included in any of the papers is required, the content of the contributing papers is rewritten to fit within the main body of the thesis. Each chapter or section that is based on a scientific paper has a note at the beginning stating so and referencing the appropriate publication. The abstracts of all papers, as well as an overview of contributions of Lea Poropat to each of the publications is given in the appendix.

The thesis can be divided into four parts, each focusing on a separate subject and answering several research questions. The first topic is the intercomparison of ocean bottom pressure from in situ measurements, model simulations, and satellite gravimetry. The method of validation of simulated and GRACE-based ocean bottom pressure fields described in this part is used througout the dissertation. The second part focuses on the oceanic signals from GRACE, both in the sense of validation through well-known oceanographic records, as well as through discovery of new signals that are not predicted by ocean models. Third part is based on ocean modelling. It describes new model experiments and the impact they have on simulated temperature, salinity, sea ice thickness, and sea level. Finally, in the fourth part, the results from the model experiments are tested, to see if they can become a part of the new release of the dealiasing background model for GRACE, which will allow us to obtain even better information about global mass induced sea level variations.

Ocean bottom pressure signals

In the first study, Chapter 2, ocean bottom pressure (OBP) time series from in situ observations, satellite gravimetry, and a numerical ocean model are compared. The sources and processing of the in situ OBP time series are described, and the suitability of such a database for validation of ocean models and GRACE gravity fields is tested. This topic is based on publication F1, and it answers the following questions:

- Are OBP signals from in situ data, models, and GRACE comparable?
- Can in situ data be used to validate model experiments?

- Can in situ data be used to validate GRACE monthly-mean solutions?
- What affects the validation results?

GRACE

Chapter 3 focuses on oceanic signals captured by GRACE satellite gravimetry and their comparison with in situ data. It compares monthly GRACE gravity fields from different institutions and analyses the submonthly ocean bottom pressure signals observed by GRACE satellites, particularly those not predicted by the dealiasing model. It includes the work from publications C2 and F2, and the questions covered by this chapter are:

- Can we distinguish between different GRACE solutions with the help of OBP?
- Can GRACE capture submonthly signals not predicted by the dealiasing model?

MPIOM experiments

The topic from Chapter 4 represents the core of this dissertation. While the initial motivation for this research still comes from GRACE, it deviates from the field of satellite geodesy into numerical ocean modelling. It describes the changes made to MPIOM in order to include the ocean dynamics beneath the Antarctic ice shelves and the impact that has on the Southern Ocean, as well as on the global ocean circulation simulated by the model. The main questions answered in this study are the following:

- How much does extending the ocean model domain to the regions beneath the Antarctic ice shelves affect the ocean circulation?
- Is the impact of such changes local or does it have a global influence?
- Is it possible to include the influence of the ice shelves to the ocean model?
- What is the extent of changes caused by implementing the ice shelf influence?
- Are there any numerical issues associated with the bathymetry modifications?
- Do the new model experiments bring the simulation results closer to the "true" state of the ocean?

AOD1B development

In the last part, Chapter 5, the focus is returned to geodesy, in particular to the development of the AOD1B product for GRACE. It includes the description of in situ ocean

bottom pressure validation during the development of AOD1B RL06 (published as part of C1), and the potential use of MPIOM model experiments described in Chapter 4 for the development of the future AOD1B RL07. The answers to the following questions are a part of this topic:

- Can using in situ OBP time series help during the development of an ocean model?
- Are there any potential issues arising from the implementation of the dynamics beneath the Antarctic ice shelves?
- Do the new model experiments improve the ocean bottom pressure prediction?
- Can the new MPIOM experiment be included in the dealiasing model for GRACE?

Finally, the conclusions of the dissertation, including the answers to aforementioned questions, as well as the outlook on the possible future work are given in Chapter 6.

2

Ocean bottom pressure

This chapter is based on the publication F1:
L. Poropat, H. Dobslaw, L. Zhang, A. Macrander, O. Boebel, and M. Thomas (2018): **Time variations in ocean bottom pressure from a few hours to many years: in situ data, numerical models, and GRACE satellite gravimetry**, Journal of Geophysical Research: Oceans, 123, 5612–5623, doi: 10.1029/2018JC014108.

Throughout this dissertation, it is often necessary to check the quality of various ocean model experiments or GRACE gravity fields, which requires the use of independent datasets. Comparison with other models can be useful, but ultimately it can only illustrate the differences between the models and point out the areas in which one model stands out from the others. However, that does not necessarily mean that that model is wrong. Using observations for validation is more appropriate because they include an information about the "true" state of the ocean, but observations often have other issues, e.g. most of them are quite sparse compared to models. Even satellite measurements, despite usually covering very large areas, often have relatively low spatial resolution or are only provided as monthly values. In situ data usually has high temporal sampling, but for most variables only exist at a few hundred locations unevenly distributed over the globe. Another option is to use ocean reanalysis data, which combine the observations with the output of an ocean model. Which method and

dataset is used for validation depends on the characteristics of the analysed dataset, processes we wish to investigate, and the purpose of the validation.

Since the motivation of this work is within the field of satellite gravimetry, specifically in using oceanographic data and ocean models to improve GRACE and GRACE–FO gravity fields, the focus is usually on mass variations, which are over the ocean equivalent to ocean bottom pressure (OBP) variations. OBP is the pressure applied at the ocean floor by the combined weight of the column of sea water and the atmosphere above it. Therefore, the dataset that is frequently used for validation is a set of in situ measured OBP time series. Alternatively, it is possible to use satellite altimetry data or in situ measured sea level time series to validate GRACE, but they are not as suitable as OBP because, while GRACE measures only the mass contribution to the sea level, altimetry cannot distinguish between the mass induced and the steric component of the total sea level. An advantage of using in situ measurements is that doing the comparison only for a few hundred time series is much faster than comparing whole global fields, which is very convenient when many new model experiments with slight changes need to be checked during the development of an ocean model or when the impact of different steps in post-processing of GRACE data is investigated.

2.1 In situ data acquisition and processing

Temporal variations and spatial gradients in OBP reflect a wide range of regimes in the ocean, from ocean tides and other barotropic waves such as tsunamis, to low-frequency processes such as the barystatic sea level changes due to water influx from the continents. The majority of OBP variability is related to changes in wind-driven and thermohaline ocean circulation. It is measured in situ for diverse purposes, both in research campaigns and as part of long term operational networks.

The observations used for validation are a dataset of 167 time series from globally distributed OBP recorders from various institutions initially compiled by *Macrander et al.* (2010). The largest part of the dataset consists of the time series recorded within the Deep-ocean Assessment and Reporting of Tsunamis (DART) network (*Meinig et al.*, 2005), that monitors OBP throughout the Pacific to allow tsunami early warnings. The Kuroshio Extension System Study (KESS) array (*Park et al.*, 2012; *Bishop and Watts*, 2014) contributes many time series regularly distributed off the Japanese coast. They were recorded as a part of the study of the dynamics of an extension of the Kuroshio current in a region characterized by high eddy kinetic energy due to the confluence of warm salty tropical water with cold fresh subpolar water. Data from the Meridional Overturning Variability Experiment (MOVE) at 16°N (*Kanzow et al.*, 2006; *Send et al.*, 2011; *Köhler et al.*, 2014; *Frajka-Williams et al.*, 2019), which is originally

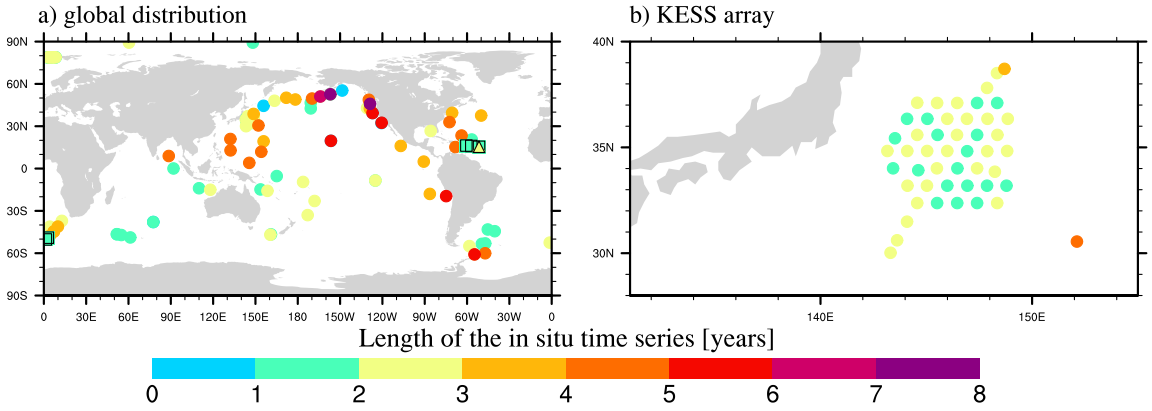

Figure 2.1: Time series length and temporal sampling for all OBP in situ stations utilized in this study in the world oceans (a) and in the Kuroshio region off the coast of Japan (b). Circles represent locations with in situ measurements with hourly or higher temporal sampling, triangles 12-hourly, and squares 24-hourly sampling.

conducted to study the Atlantic meridional overturning circulation (AMOC), are also part of the dataset. Several time series from the Fram Strait are taken within the Arctic–Subarctic Ocean Fluxes North (ASOF–N) project. They were originally used to study the exchange between the North Atlantic and the Arctic Ocean, that results in the most dramatic water mass conversion in the world's oceans (*Beszczynska-Möller et al.*, 2012). Several institutions collected data in the Southern Ocean: time series from the Alfred Wegener Institute (AWI) cover the region between Africa and Antarctica, the National Oceanography Centre from Liverpool (formerly called Proudman Oceanographic Laboratory) collected several time series off the coast of Argentina, and *Laboratoire d'Etudes en Géophysique et Océanographie Spatiales* (LEGOS) maintains tide gauges that also include OBP recorders in the Crozet–Kerguelen region, two of which are part of the *Macrander et al.* (2010) dataset. An important part of the OBP database are the two time series from the Arctic Ocean, obtained by the Polar Science Center of the University of Washington in Seattle, USA (*Peralta-Ferriz et al.*, 2014). The data from the two gauges are the first in situ bottom pressure measurements in the central Arctic Ocean and they were already successfully used for comparison with GRACE data over the Arctic Ocean (*Morison et al.*, 2007).

Observations of OBP are technically challenging because in situ sensors are required to detect variations of less than 1 hPa at depths of up to 10 km, which translates into a measurement sensitivity of 10^{-9} while being exposed to a highly corrosive environment. Such sensors only became available at affordable prices about three decades ago (*Watts and Kontoyiannis*, 1990), which allowed the deployment of a very irregularly

distributed network of OBP recorders. The DART time series, as well as the Crozet–Kerguelen and Arctic data, are taken with the bottom pressure recorders (BPRs), while most of the remaining data are taken with pressure inverted echo sounders (PIES). The pressure transducer in a BPR uses a very thin crystal beam, electronically induced to vibrate at its lowest resonant mode. It is attached to a Bourdon tube that is open on one end, so that changes in pressure cause the tube to curl or uncurl, which compresses or stretches the crystal, changing its vibrational frequency. These changes can be measured very precisely by the electronic system of the instrument (*Eble and Gonzales*, 1990). The PIES instruments, in addition to measuring OBP, are used to determine the depth of isothermal surfaces in the main thermocline, the geopotential height anomaly between two pressure levels, or other dynamic and descriptive quantities (*Meinen and Watts*, 1998).

The OBP time series have very different lengths, from a few months to several years, collectively covering the 1998 – 2010 years timespan (Fig. 2.1). Some of them have high temporal sampling, of 30 minutes or 1 hour, which allows clear separation of subdaily tidal constituents, while others have only 12-hourly or daily sampling. Many of them contain long term drifts because of the mechanical creep of materials subjected to high stress (*Watts and Kontoyiannis*, 1990), while some have very strong drifts at the beginning of the time series due to settling of the sensor on the ocean floor. It is not easy or sometimes even possible to determine whether the trends present in some time series are a proper oceanographic signal, or a measurement bias. Sensors, especially those at the longer lasting stations, sometimes have to be retrieved for data recovery, battery replacement, and general maintenance, and subsequently redeployed, causing gaps and discontinuities in the time series. They also contain tidal signals, which are often not simulated by ocean models and are normally removed from GRACE gravity fields. The pre-processing of the time series was also diverse: while some of them were already checked for outliers, and had some corrections applied, others were given as more or less raw. Therefore, to ensure uniformity of the time series used for validation, and to obtain a dataset suitable for comparison with simulated or GRACE-based OBP datasets, all time series are processed in the same way.

Time series are visually inspected for discontinuities and drifts that are present in many time series. The classic method of drift removal from oceanographic time series is a fit to a power-law, exponential or logarithmic function (*Watts and Kontoyiannis*, 1990). However, neither of these functions is suitable for all time series, so to allow a certain level of automation, short segments of data with significant non-linear drifts at the beginning or end of the time series are discarded, while the remaining drifts, as well as long-term trends, are removed with a quadratic fit (Fig. 2.2 a, b). Discontinuities are handled by calculating and removing the mean from each data segment separately

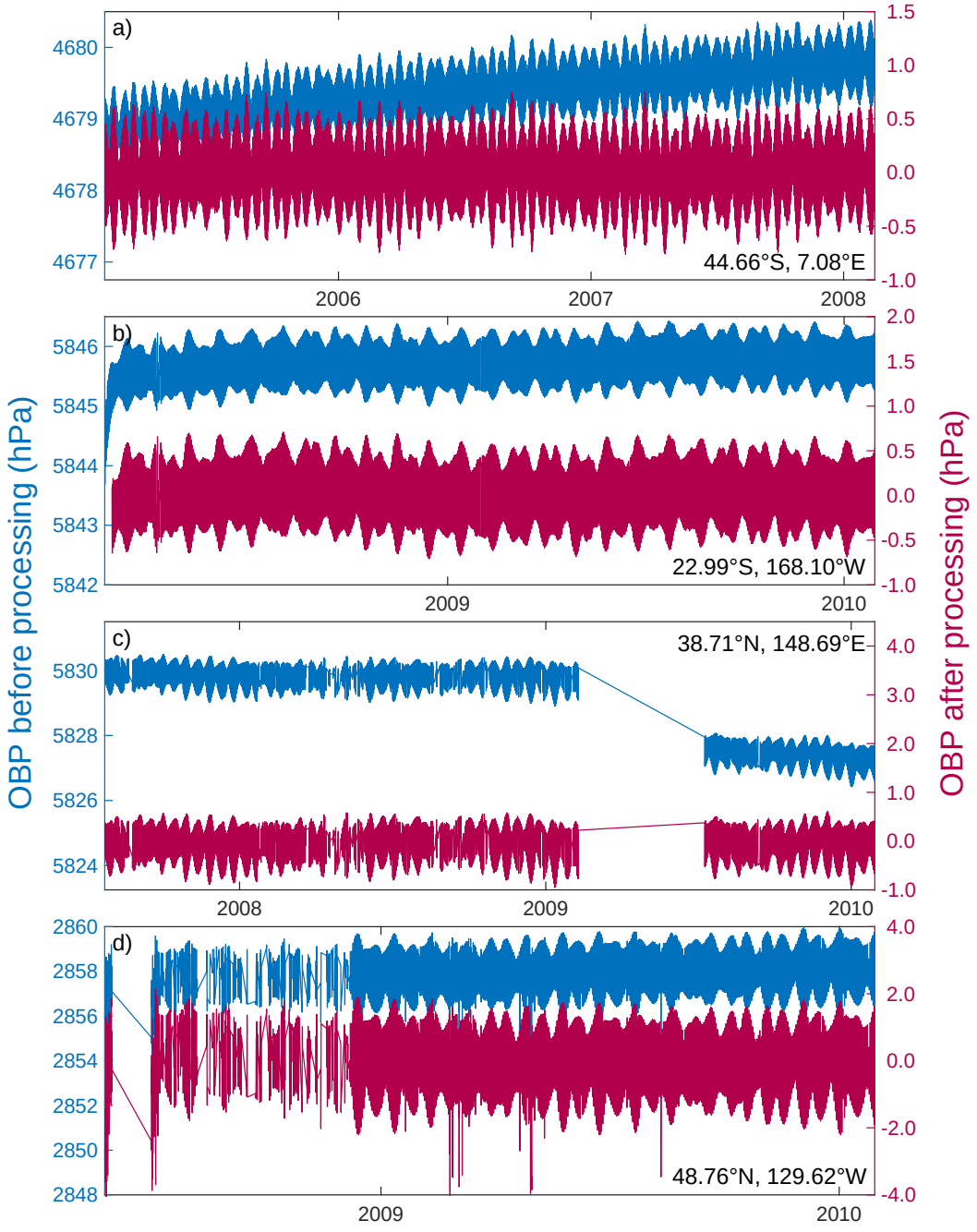

Figure 2.2: Examples of four in situ time series before and after removing temporal mean, trends, drifts, discontinuities, and outliers.

(Fig. 2.2 c), which is sometimes not fully successful, especially if the time series has too many gaps (Fig. 2.2 d).

To ensure uniformity of the database, temporal sampling is reduced to 1 h for sub-hourly sampled time series by calculating hourly means. Tidal signals are estimated and

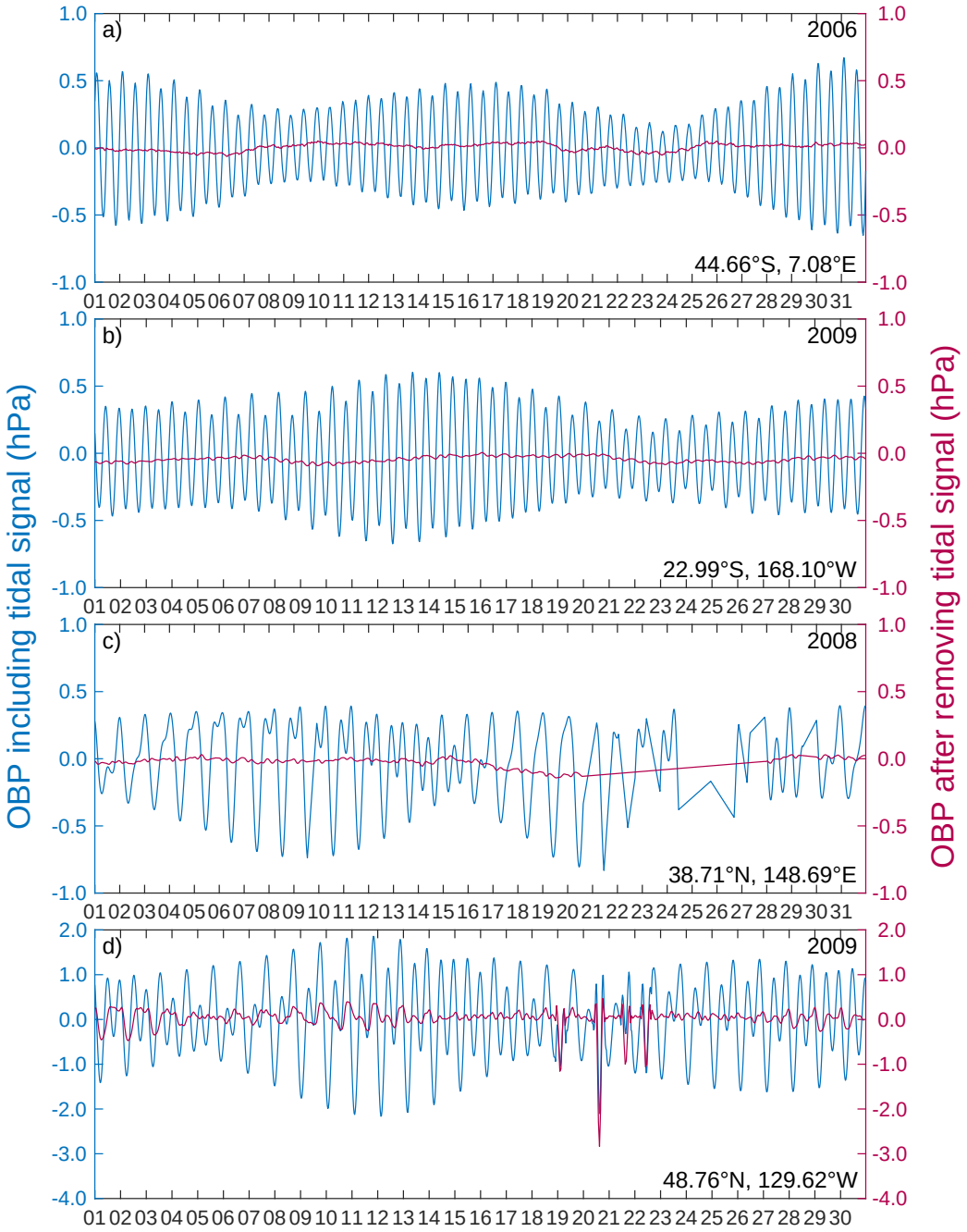

Figure 2.3: Examples of four in situ time series before and after removing tidal signal. Only one month of data is shown, January of the first year covered by observations.

removed with the T_TIDE package for classical harmonic analysis (*Pawlowicz et al.*, 2002). Since the package is intended for time series of approximately one year length, those significantly longer are split into appropriately long segments before performing the harmonic analysis. If possible, gaps present in the time series are used to determine

the exact location of the partition. The tidal constituents are automatically chosen based on the length and location of the time series and their number ranges from 18 for the shortest time series to 68 for the time series of approximately one year length. While the separation of tidal signal is generally successful (Fig. 2.3 a, b, c), if the time series has too many gaps or the discontinuities are not properly handled, there might be some residual signal left (Fig. 2.3 d). Finally, data from the same geographical position are stacked into a single time series, obtaining a database with in situ OBP time series suitable for quick comparison with ocean models or GRACE gravity fields.

2.2 Validation of an ocean model with in situ OBP

Due to relatively sparse observations of the oceans, models are an excellent tool to obtain the information about global ocean circulation. To ensure their quality, it is imperative to compare their output with as many different obsevations as possible, including the observations of OBP made in situ. As already pointed out, temporal variations of OBP are a manifestation of many physical processes in the ocean, some of them easily identifiable by the frequency of the produced fluctuations. Comparing simulated OBP with in situ measurements can pinpoint the locations and, by use of temporal filtering, also indicate the processes which could be improved in the model.

The Max Planck Institute Ocean Model (MPIOM; *Jungclaus et al.*, 2013) is an ocean general circulation model. OBP from an experiment that uses a tripolar grid with approximately 1° grid spacing and 40 layers in the vertical, from years 2003 – 2012, is compared with the in situ observations. Simulated OBP has 3-hourly temporal resolution, and is regridded to a regular 0.5° grid. To compare model output with in situ OBP time series, model data is extracted at each in situ station by means of bilinear interpolation from the four nearest grid points, and the appropriate time steps are taken from the in situ data to allow the comparison. Both simulated and in situ time series are separated into five frequency bands by 4th order Butterworth filters with cutoff periods of 1, 3, 10, and 30 days. Since moving-window filters distort data toward the ends of the time series, and since in situ records typically contain many gaps at whose ends the data would be distorted by a filter, the gaps are linearly interpolated before applying the filter. The interpolated segments are again removed after filtering. Gaps present in the in situ time series are considered in the simulated series as well to ensure that both time series have exactly the same number of data points. Additionally, the monthly averages are considered. For the considered timespan, 154 time series of varying length are available, from locations unevenly distributed over the ocean.

To ascertain how much of the observed signal at each in situ location is successfully

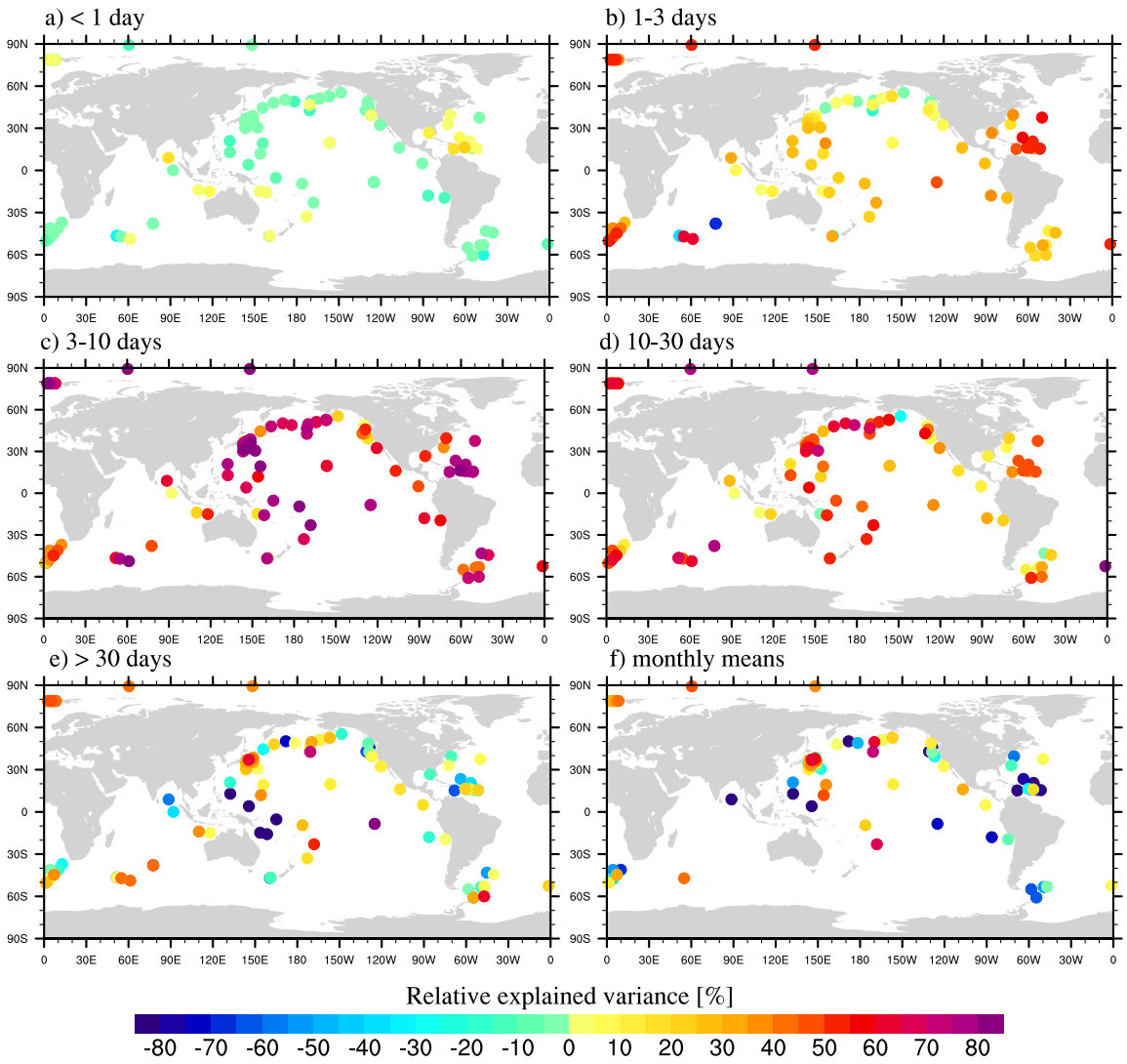

Figure 2.4: Percentage of variance in OBP observed at in situ stations that is explained by OBP simulated by the MPIOM model experiment for periods shorter than 24 hours (a), between 1 and 3 days (b), between 3 and 10 days (c), between 10 and 30 days (d), longer than 30 days (e) as separated by 4th order Butterworth filters. In addition, the relative explained variance for monthly-mean estimates is given (f).

represented in the model, relative explained variances are calculated (Fig. 2.4), i.e. the variance of the in situ data when modelled quantity is subtracted:

$$VE(m) = \frac{S^2(o) - S^2(o-m)}{S^2(o)}, \tag{2.1}$$

where $S^2(o)$ is the variance of the in situ observations, and $S^2(o-m)$ indicates the residual variance in the in situ observations after subtracting the model. For a perfect model, the relative explained variance would be 100 %, if the model does not simulate

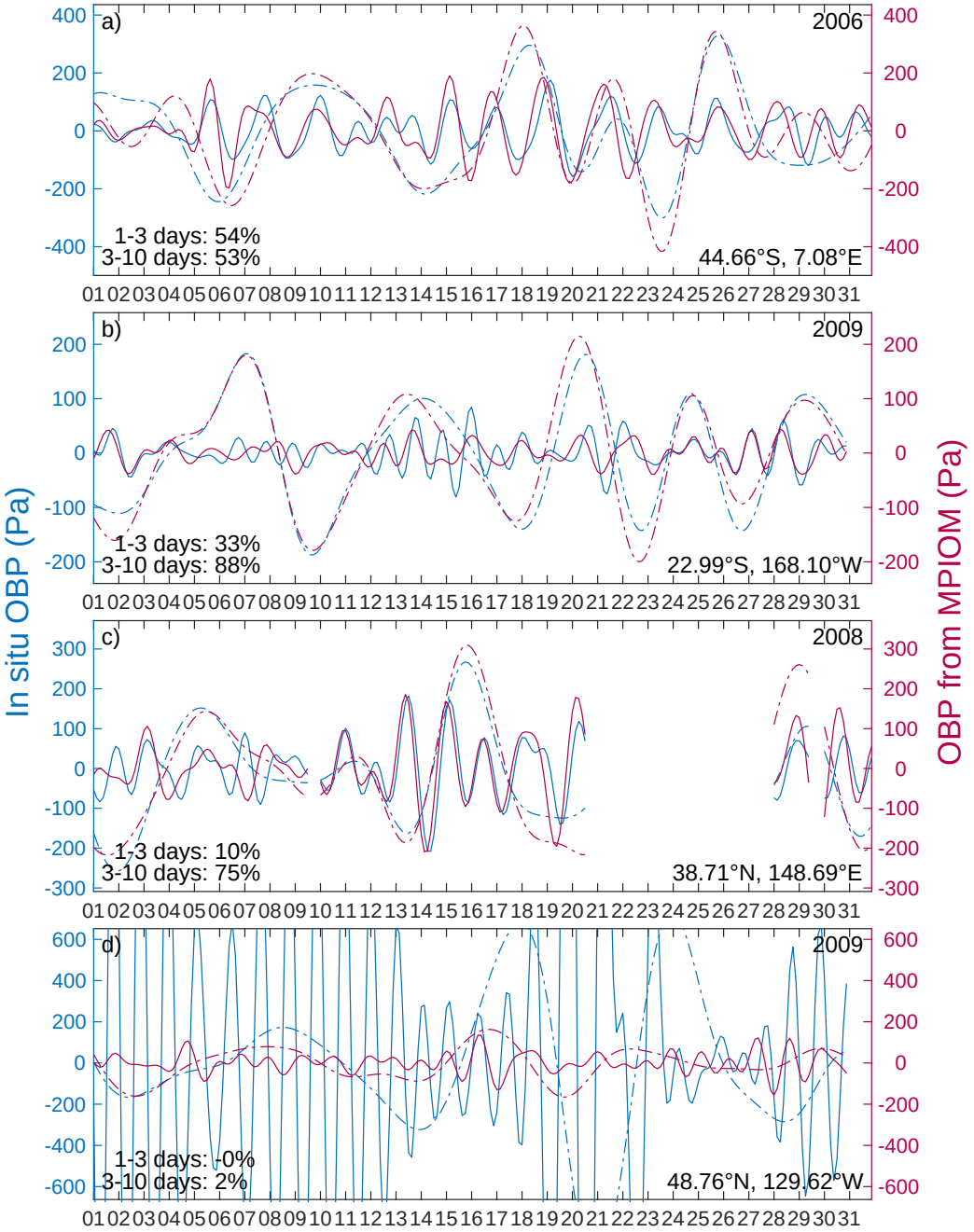

Figure 2.5: Comparison of OBP time series measured in situ and simulated by MPIOM at four in situ stations. Time series from only one month are shown (January of the first year completely covered by the time series), filtered by 1–3 days and 3–10 days band pass filters. The relative explained variance for each period band calculated from the whole series is noted for each in situ location.

the observed variability well, it is around zero or negative.

For the subdaily periods there is almost no agreement between the model and the observations because the observed variability is likely affected by residual tidal signals that are not properly removed and small timing errors in the onset of weather systems in the atmospheric data cause a delayed OBP response in the numerical ocean model. For the intermediate periods (1 – 30 days) most stations have a positive relative explained variance. The correspondence is especially good for the periods in the 3 – 10 days range, for which relative explained variances exceed 70 % in the majority of the stations. For periods longer than 30 days relative explained variances are much lower and often negative. This might be related to the subtraction of long-term signals and reduction of data gaps in the observations, as well as to the seasonal and interannual variations due to self-attraction and loading that are not considered in the model, and variations in the meridional overturning circulation that are not fully captured by MPIOM. Using monthly means degrades the results even further.

While explained variances provide a global overview of the similarity between the model and the in situ observations, it can also be useful to look at the time series

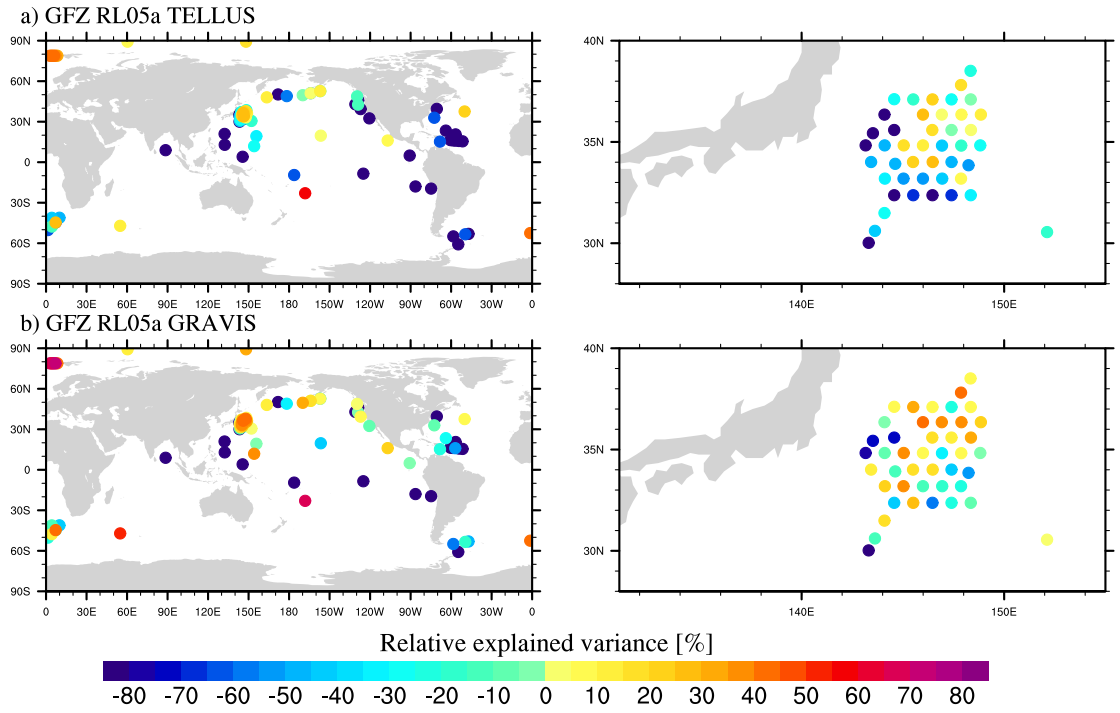

Figure 2.6: Percentage of variance in OBP observed at in situ stations that is explained by OBP from GRACE monthly grids after applying the pattern filter for GFZ RL05a from Tellus portal of NASA (a) and for GFZ RL05a GRAVIS grids (b).

comparison (Fig. 2.5). Time series comparison is especially necessary if the results at a specific in situ location seem suspicious, such as negative explained variance for a station surrounded by very high positive variances. That can be an indication of a faulty in situ time series (Fig. 2.5 d).

Comparison with in situ OBP has shown that this MPIOM experiment, which is also used as the oceanic part of the dealiasing model for GRACE, AOD1B RL06, performs very well in terms of simulating OBP on submonthly scale. Nevertheless, there is always room for improvement. While the low explained variances for the highest and the lowest periods can be explained by issues with the in situ time series, the results for the intermediate periods are most likely due to the physical processes captured by the model. During the development of AOD1B RL6, when the Ocean Model for Circulation and Tides (OMCT; *Thomas*, 2002) that was used in the previous release, was replaced by MPIOM, one major downgrade was that MPIOM does not simulate the dynamics beneath the Antarctic ice shelves. That is one possible reason for the relatively low explained variances for some period bands, and it is planned to be fixed by the next release.

2.3 Validation of monthly GRACE gravity fields with in situ OBP

GRACE satellites and their successor GRACE-FO have been monitoring the variations in the Earth's gravity field since their launch in 2002. Changes in the GRACE-measured gravity fields are related to changes in the mass distribution on Earth and can thus be converted into surface mass anomalies or consequently OBP variations. Therefore, in situ measured OBP can be used for their validation, to assess the impact of post-processing strategies applied to the GRACE data, and to compare the gravity field solutions from different institutions.

While for ocean models bilinear interpolation to the in situ measuring location works well, GRACE data are a spatial average over a region of 100,000 km^2 and larger. Therefore, a pattern filter approach is used instead, as suggested by *Böning et al.* (2008). The patterns of coherent OBP variability are determined for each OBP station by calculating autocorrelation maps from monthly MPIOM grids. GRACE data from areas with autocorrelation values larger than 0.7 and distances to the in situ station smaller than 20° are averaged to obtain time series that can be compared with the in situ data. After calculation of the monthly means from the in situ data, many of the in situ time series used for validation of MPIOM for the same 2003 – 2012 years timespan

are not long enough for validation of monthly GRACE gravity field solutions. As a result, relative explained variances are calculated for 103 in situ stations, almost half of which belong to the KESS array and are located off the coast of Japan.

The results are comparable with the results obtained for monthly averages calculated from MPIOM. Apart from the reasons already mentioned when discussing the results of the model validation, an additional reason for relatively poor corresponence of GRACE measurements with the in situ data is the area-averaging measuring technique used by the GRACE satellites opposed to the pointwise in situ measurements. It is possible that for some locations the in situ measured time series, while accurately displaying the variability in its location, is not representative for the larger surrounding area seen by GRACE.

Validation of the GFZ RL05a GRACE solution (*Dahle et al.*, 2016) post-processed in two different ways demonstrates that post-processing can have a non-negligible influence on the results (Fig. 2.6), highlighting the necessity to post-process all GRACE fields in the same way when comparing them through validation against in situ OBP. Some choices during the validation can also affect the results (Fig. 2.7). Using a pattern filter significantly improves the results compared to using only the bilinear interpolation. Due to the gaps in GRACE measurements, some GRACE monthly solutions cover an interval that differs from the exact calendar month. If the start and end of GRACE "months" are provided, it is possible to use them to calculate the appropriate means of the in situ data as well, but that improves the results only for a few stations that

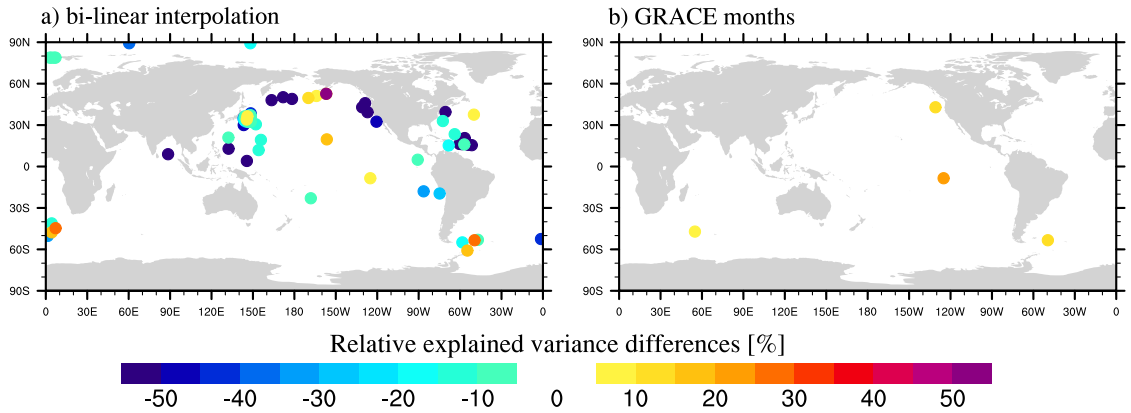

Figure 2.7: Change in percentage of variance in OBP observed at in situ stations that is explained by OBP derived from GRACE satellite gravimetry compared to Figure 2.6 b after bilinearly interpolating GRACE data to the in situ station's location instead of applying the pattern filter (a), and after considering actual GRACE months instead of the calendar months during the evaluation.

have data coverage during the very beginning or the late years of GRACE life, when gaps in the measurements are common, and it is therefore considered unnecessary.

OBP provedes a very precise measure of ocean mass redistribution due to a variety of different dynamical processes on very different temporal and spatial scales. Using already pre-processed OBP time series from approximately 150 locations worldwide is simple and fast. Since the results are best for intermediate periods (1 – 30 days), it is most suited for validation of ocean models and can be used to quantify the impact of changes during their development. Even though the results of OBP validation are not as good for the seasonal and interannual variations, in situ OBP can nevertheless be used to distinguish between different GRACE solutions, and therefore to assess the influence of new post-processing techniques, as well as to compare GRACE releases from different institutions. The main signals in GRACE come from terrestrial water storage and ice sheets, compared to which oceanic signals are minuscule. However, being able to monitor the global mass variations in the ocean is also important. In the time of rapid climate change and global warming, it is imperative to monitor the sea level rise due to ice sheet and glacier melting, and GRACE is the only satellite mission that allows us to distinguish between the mass induced and the steric component of the sea level. In situ measured OBP is the only independent dataset that can be compared with GRACE over the oceans, increasing the confidence in the GRACE data.

3

Oceanic signals in GRACE

Gravity Recovery and Climate Experiment (GRACE) satellites have been used for years to observe global mass induced changes in sea level (e.g. *Willis et al.*, 2008; *Cazenave et al.*, 2009), and in combination with altimetry to distinguish between the mass induced and the steric component of sea level rise (e.g. *Leuliette and Miller*, 2009; *Llovel et al.*, 2010). GRACE has been compared with satellite altimetry data to study the relationship between ocean bottom pressure and sea level (*Piecuch et al.*, 2013). There have also been several attempts in comparing GRACE data with in situ OBP time series. *Kanzow et al.* (2005) compared the GRACE gravity fields with the OBP data from the MOVE experiment in the tropical northwest Atlantic, *Morison et al.* (2007) used the data from two Arctic bottom pressure recorders, confirming from both datasets that the Arctic Ocean is reverting from the cyclonic state characterizing the 1990s to the anticyclonic state that was prevalent prior to the 1990s, and *Park et al.* (2008) used OBP data from the KESS array near Japan.

Gravity fields derived from GRACE observations can be compared with in situ measured OBP because they essentially measure the same quantity, fluctuations of mass. While there are some differences in the two measuring techniques that affect the comparison of two datasets, namely the difference between the pointwise in situ measurements and the area-averaging GRACE observations, in situ OBP records can be a great tool for validation of GRACE over the oceans. When comparing GRACE with in situ OBP, it always needs to be kept in mind that a standard GRACE post-processing step

is the application of the Atmosphere and Ocean Dealiasing Level 1B (AOD1B) product, which effectively removes the oceanic and atmospheric signals from the GRACE data. In order to obtain those signals again, the GAD product from AOD1B needs to be added back, which can also introduce errors from the model into the GRACE solution.

3.1 Comparison of monthly GRACE fields from different institutions

This section is based on the publication C2:
Q. Chen, **L. Poropat**, L. Zhang, H. Dobslaw, M. Weigelt, and T. van Dam (2018): **Validation of the EGSIEM GRACE gravity fields using GNSS coordinate time series and in situ ocean bottom pressure records**, Remote Sensing, 10(12), 1976, doi: 10.3390/rs10121976.

Since the start of the GRACE mission, a number of processing approaches to derive global gravity fields from the raw sensor data observed by the GRACE satellites have been developed and advanced. Within the European Gravity Service for Improved Emergency Management (EGSIEM) project (*Jaggi et al.*, 2019), a gravity solution combined from the solutions from different institutions was developed. To evaluate the quality of different gravity field solutions, two types of external datasets have been used: global navigation satellite system (GNSS) time series, and in situ OBP observations. The agreement of GRACE gravity fields with in situ OBP is expressed in terms of correlation (Fig. 3.1) and, because correlation is only sensitive to the differences in phase, but not in amplitude, in terms of reduction of standard deviation (Fig. 3.2) in the in situ time series after GRACE measured series has been subtracted from them:

$$SR(G) = \frac{S(o) - S(o - G)}{S(o)}, \tag{3.1}$$

where $S(o)$ is the standard deviation of the in situ observations, and $S(o - G)$ is the residual standard deviation in the in situ observations after subtracting GRACE observations. Standard deviation reduction is used instead of relative explained variance because they are calculated in a very similar way and provide virtually the same information, but using a standard deviation makes the validation against OBP more similar to the validation against GNSS data, which is presented in *Chen et al.* (2018).

Six monthly GRACE gravity solutions are compared in this study: EGSIEM combined long-term solution from *Jean et al.* (2018), CSR RL05 (*Bettadpur*, 2012), GFZ RL05a (*Dahle et al.*, 2012), JPL RL05.1 (*Watkins and Yuan*, 2012), AIUB RL02 (*Meyer et al.*,

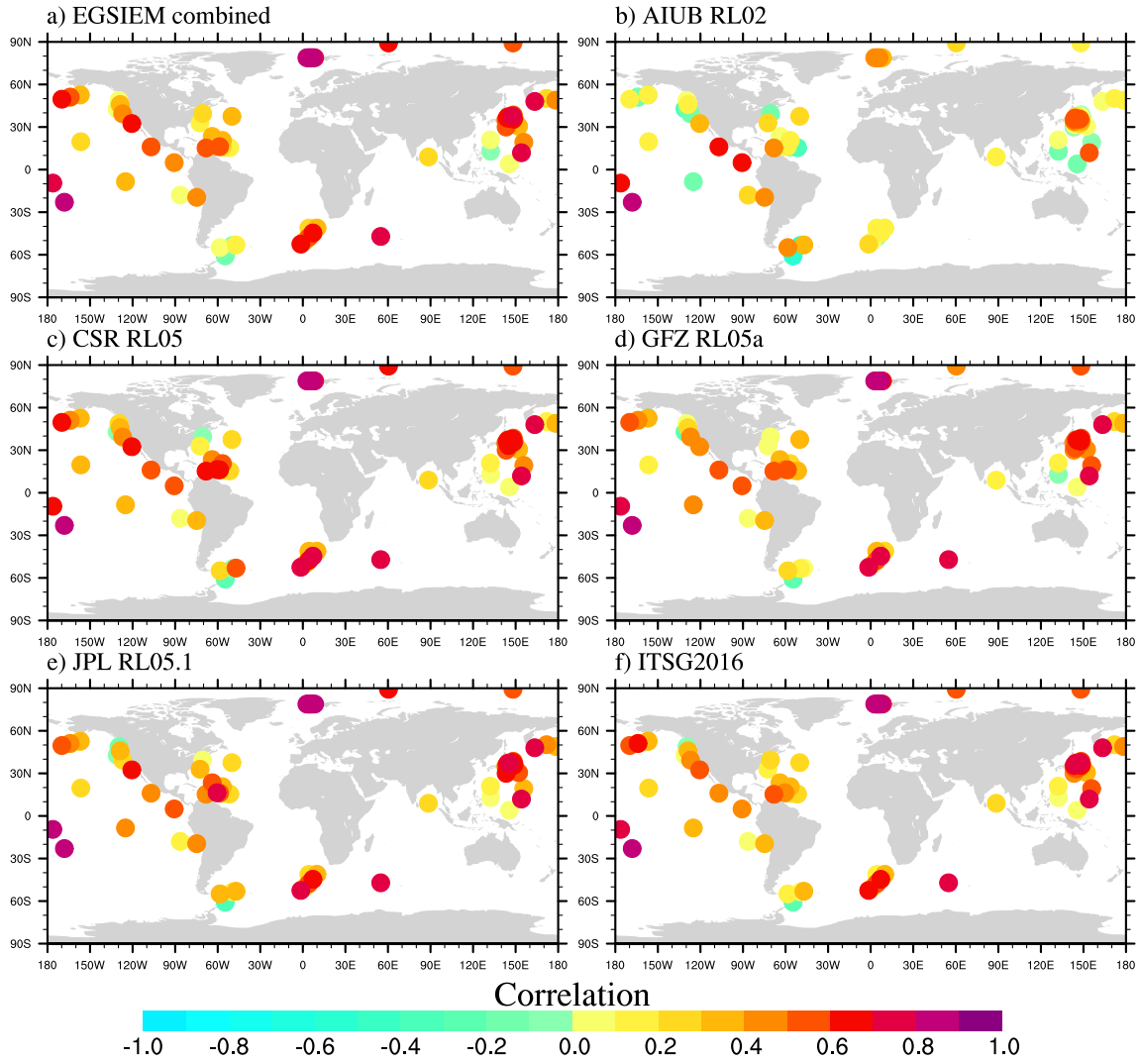

Figure 3.1: Correlations between in situ OBP and GRACE-derived pressure over 103 OBP in situ stations.

2016) from University of Bern, and ITSG2016 (*Mayer-Gürr et al.*, 2016) from TU Graz. Years 2003 – 2010 are used for validation against OBP due to the limitations of the in situ OBP database, even though the series used with GNSS data are longer (2003 – 2014).

Correlation between GRACE and in situ OBP is positive for almost all locations and solutions. The highest correlations are found in two geographical regions: Greenland Sea and Central Pacific Ocean. Both locations have relatively high variability of OBP and the regions of coherent variability calculated for in situ stations in those regions are very large, which is why the in situ time series can be considered representative for a larger area, resulting in a very high correlation between the area-averaging GRACE and pointwise measured in situ data. The highest calculated correlation is 0.90, obtained

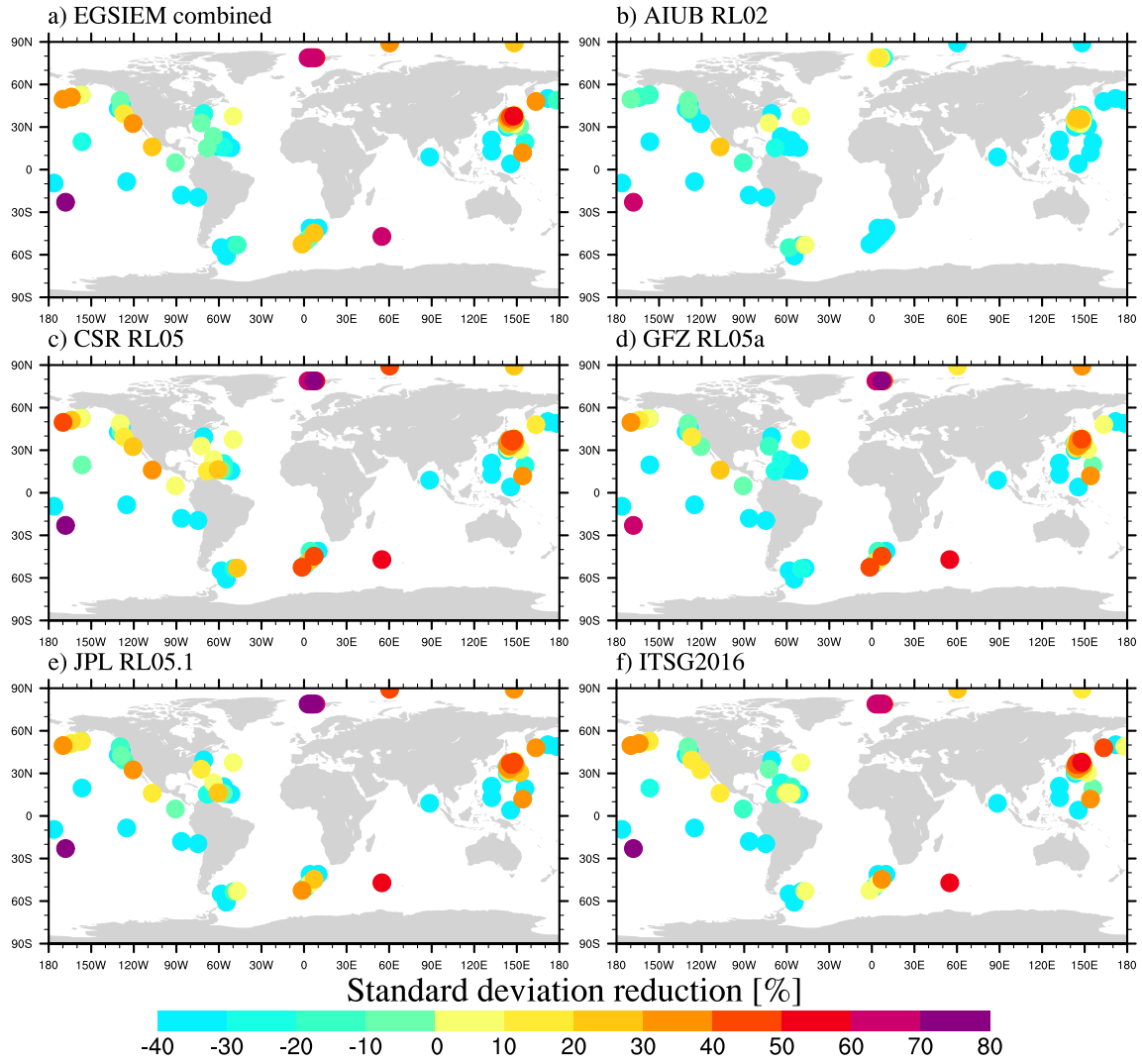

Figure 3.2: Standard deviation reductions over 103 OBP in situ stations with GRACE-derived pressure.

for the JPL RL05.1 GRACE solution. All GRACE solutions have so similar patterns in correlation that it is impossible to discriminate between them.

Unlike correlations, the standard deviation reductions are pretty low and often negative for all GRACE gravity field solutions. The results from the comparison with the GNSS data (Fig. 3 from *Chen et al.*, 2018) are much better because the monthly GRACE fields are dominated by seasonal and interannual signals in terrestrial water storage and ice mass. In comparison to those signals, the variability in OBP is much smaller, and consequently the signal to noise ratio is lower. Furthermore, the results are affected by errors in the dealiasing model and by the removal of trends from both datasets. It is nevertheless easier to discriminate between different solutions from standard deviation reductions than from correlations. While the geographical patterns are similar in all

GRACE solutions, there are some noticable differences, e.g. most solutions have negative standard deviation reductions in the North Atlantic, but CSR RL05 has a large number of positive values. Based on the differences in the standard deviation reduction maps, it is possible to conclude that CSR RL05, ITSG2016, and EGSIEM solutions outperform the other three GRACE time series in this study. The results from validation against GNSS time series confirm the conclusions obtained from comparison against in situ OBP.

3.2 Validation of daily GRACE fields from TU Graz

This section is based on the publication F2:
L. Poropat, A. Kvas, T. Mayer-Gürr, and H. Dobslaw (2020): **Mitigating temporal aliasing effects of high-frequency geophysical fluid dynamics in satellite gravimetry**, Geophysical Journal International, 220(1), 257–266, doi: 10.1093/gji/ggz439.

GRACE data is typically averaged to obtain monthly-mean gravity field solutions, but considering it only needs 90 minutes for one orbit, it also captures submonthly signals. Thus, there are some attempts to compute daily gravity fields from GRACE. One such set of daily solutions, the ITSG-Grace2016 daily Kalman smoother solutions (*Mayer-Gürr et al.*, 2016) from TU Graz, is analysed to determine how much realistic oceanic signal on submonthly frequencies they manage to capture.

In order to properly interpret the Kalman Smoother results in the spatial domain, the expected geophysical signals at submonthly periods induced by non-tidal mass transport processes that potentially contribute to temporal aliasing are analysed. Over the continents, they are calculated by the Land Surface Discharge Model (LSDM; *Dill*, 2008) in its latest configuration as applied for the prediction of Earth rotation excitations (*Dill et al.*, 2018). Over the oceans, MPIOM (*Jungclaus et al.*, 2013) in its configuration for AOD1B RL06 (*Dobslaw et al.*, 2017) is used. Water storage variability is converted into equivalent surface pressure (i.e., 1 cm of water equals 1 hPa) before combining with OBP. All model data is available with daily sampling over the period 2003 – 2012. Mass variations are separated into four frequency bands by means of a series of 4th order Butterworth filters, and standard deviations for every location on a global 1° grid are presented (Fig. 3.3). GRACE satellites also measure the signals from continental ice sheets, which is not represented in the numerical model data used here for comparison.

For periods shorter than 3 days there are almost no signals over the continents, whereas ocean areas have larger variability, in particular in coastal regions at higher latitudes.

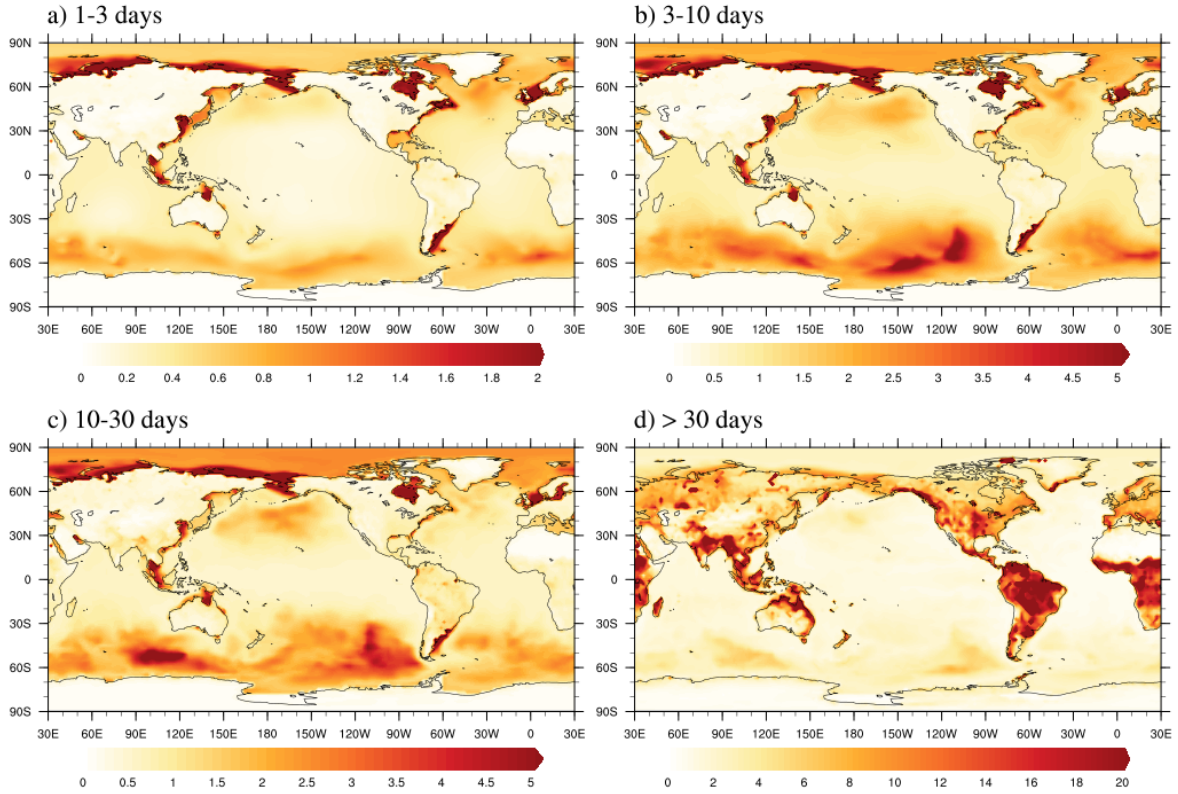

Figure 3.3: Standard deviation of daily mass anomalies expressed in surface pressure equivalent (hPa) due to water storage simulated by LSDM and OBP from MPIOM during 2003 – 2012 separated into periods shorter than 3 days (a); 3 – 10 days (b); 10 – 30 days (c); and longer than 30 days (d) obtained with a series of 4th order Butterworth filters.

All Nordic seas, Hudson Bay, East China Sea, Gulf of Thailand, Gulf of Carpentaria, and the Patagonian Shelf encounter mass variability exceeding 2 hPa. Furthermore, signals related to fast changes in the Antarctic Circumpolar Current (ACC) reach 1 hPa. For periods between 3 and 10 days the signals in similar coastal areas are still dominant, now exceeding 5 hPa, and the variability of the ACC is becoming even more important, with a very prominent maximum in variability just south of the East Pacific Rise. Water storage variations over the continents remain much smaller than the oceanic signals also for this frequency band.

For the periods between 10 and 30 days, variability remains strongest on the continental shelves and along the path of the ACC, but there are now also relevant signals on the continents. Terrestrial water storage variations reach 1 hPa in regions with humid tropical climate such as Brazil and Southeast Asia. Over the oceans, locations of strongest variability in the ACC shift somewhat in position in line with the eigenfrequencies of the most important resonant modes constituting the signal. For periods

longer than 30 days, the oceanic variability continues to have similar magnitude and spatial distribution as for the 10 – 30 days band, but the seasonal variations in terrestrial water storage now clearly dominate, with standard deviations reaching 10 hPa almost everywhere over the continents – a notable exception being the deserts – and often exceeding 20 hPa in the regions with high precipitation rates, especially if the climate is characterized by monsoons, and along the large river systems, such as the Amazon, Kongo, and Mekong.

It becomes obvious from Fig. 3.3 that the wind-driven OBP variability at high frequencies is so strong that reasonable ocean signals can only be deduced from monthly-mean gravity fields if those signals are accounted for at each overflight of the satellites. Non-tidal OBP variability is thus part of the standard dealiasing model AOD1B. Submonthly variations of terrestrial water storage are much smaller than the corresponding oceanic signals at identical frequencies, and also much smaller than the monthly-mean and seasonal variations, so that temporal aliasing errors would not dominate estimates over the continents.

The global gravity field estimates from GRACE, the ITSG-Grace2016 daily solutions (*Mayer-Gürr et al.*, 2016) as obtained with the Kalman smoother approach, are now discussed. Available over the period 2003 – 2012 up to d/o = 40, the data is synthesized onto an 1° equiangular grid and subsequently separated into four frequency bands by means of a series of 4th order Butterworth filters (Fig. 3.4). The oceanic and atmospheric variability reduced during the dealiasing process with AOD1B RL05 has not been restored here, meaning that only the so-called GSM products are used that reflect mass variablity either not considered a priori, or introduced erroneously by means of imperfect background models. While a significant portion of the signal is removed during dealiasing, if the dealiasing model is added back, it is not possible to distinguish if the signal in the GRACE solutions is really captured by GRACE or it comes from the model. Since GRACE is most commonly used to study seasonal and interannual signals, this study is meant to determine whether it also captures submonthly oceanic signals in addition to the signals successfully simulated by the dealiasing model.

For the shortest periods below 3 days, the day-to-day variability in ITSG-Grace2016 over the continents is very small and never exceeds 0.3 hPa. Variations in the open ocean are also small in tropical regions but somewhat higher at moderate latitudes. The largest variability is seen in several semi-enclosed ocean basins like North Sea, Yellow Sea, Gulf of Thailand, and Gulf of Carpentaria. All of these regions have very high variability also in MPIOM (see Fig. 3.3), and many of them are known today to be affected by errors in AOD1B RL05 (*Dobslaw et al.*, 2013) as discussed in *Dobslaw*

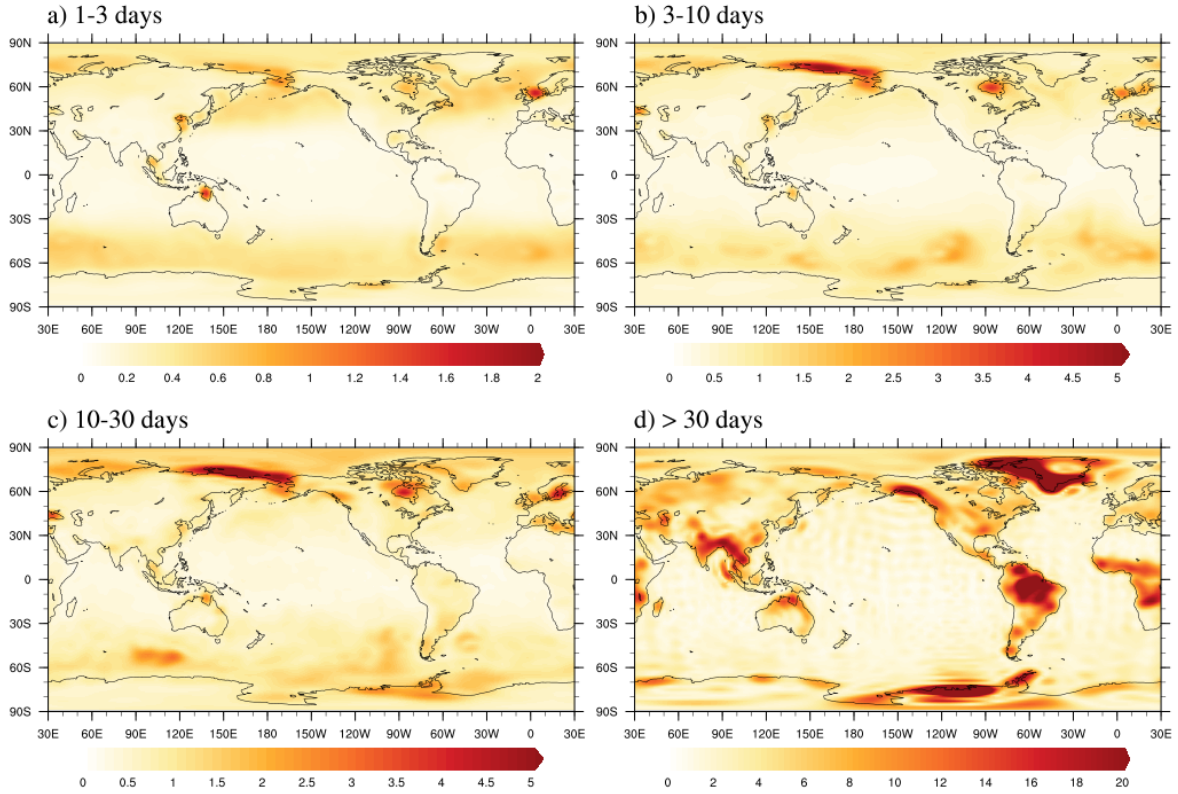

Figure 3.4: Standard deviation of mass anomalies expressed in surface pressure equivalent (hPa) derived from daily ITSG-Grace2016 Kalman solutions during 2003 – 2012 as separated into periods shorter than 3 days (a); 3 – 10 days (b); 10 – 30 days (c); and longer than 30 days (d) obtained with a series of 4th order Butterworth filters.

et al. (2016). Since ITSG-Grace2016 daily solutions use AOD1B RL05 for dealiasing, any errors in AOD1B RL05 are passed on to the ITSG-Grace2016 solutions. More recent GRACE solutions that use AOD1B RL06 and therefore MPIOM for dealiasing are consequently not affected by the same errors. For periods between 3 and 10 days, signals of more than 2 hPa are present everywhere in the Arctic Ocean and the Nordic seas and particularly strong variability is visible along the Siberian Shelf and in Hudson Bay. Other semi-enclosed basins like North, Mediterranean, and Black Sea, and some resonant basins in the Southern Ocean show enhanced variability as well. Increased variability in the regions of the ACC is also evident in this frequency band. Signals over the continents are still much smaller and hardly exceed 1 hPa.

Between 10 and 30 days, residual signals in the oceans are still dominating the ITSG-Grace2016 solutions. Most prominent areas are East Siberian, Baltic, and Black Sea. The signal variability over the continents approaches 2 hPa in West Antarctica and at the southern tip of Greenland. Both regions are characterized by marine climate

with strong snowfall events and the rapid passing of low pressure systems which might not be captured too well by the ECMWF numerical weather model utilized for the atmospheric part of AOD1B. Residual signals at periods of 30 days and longer are dominated by the seasonal and interannual variations in terrestrial water storage and ice mass change, while the oceanic signals are much weaker. Signals over the continents contained in ITSG-Grace2016 are generally in line with model predictions in terms of both regions and magnitudes. Note that LSDM does not simulate ice dynamics and thus does not reflect the variability in Antarctica and Greenland, as well as in glaciated high-mountain regions like Alaska and Patagonia to full extent. To conclude, while the regions with highest variability are the same in the simulated and in ITSG-Grace2016 fields on all period bands, the oceanic variability is significantly reduced in the GRACE fields due to the subtraction of the AOD1B product.

As an external validation measure, the in situ OBP time series are used. Since the AOD1B product has been removed during dealiasing, and has not been restored to the ITSG-Grace2016 fields, the daily means of the same AOD1B RL05 product have been removed from each in situ OBP time series. To compare daily bottom pressure estimates of ITSG-Grace2016 with in situ OBP, a reduction in standard deviation is calculated (Eq. 3.1). Positive values indicate that some variability measured by in situ ocean bottom sensors is also contained in ITSG-Grace2016 daily Kalman solutions. Since in situ measurements are pointwise, while GRACE measures averages over larger areas, perfect correspondence between them is not expected. Furthermore, since the submonthly atmospheric and oceanic variability removed during dealiasing has not been restored, good agreement between GRACE and in situ time series is expected only in regions where the AOD1B RL05 product is not performing well. In areas and for periods in which AOD1B RL05 performs very well, there is not much signal left in the GRACE and in situ data after AOD1B has been subtracted, resulting in time series with very low signal to noise ratio that are difficult to compare and usually have negative standard deviation reductions.

For periods below 3 days, only a few stations show positive results, mostly in the Arctic Ocean and in the Sargasso Sea. Over the poles, GRACE observations are available every 90 min, and AOD1B RL05 is well known to be affected by errors due to the generally limited number of meteorologic observations at polar latitudes. The reasons for positive results in the Sargasso Sea, however, are not as obvious because the dealiasing model performs quite well in that region (*Dobslaw et al.*, 2017; *Poropat et al.*, 2018). Similar results are also found at the Arctic polar stations in the period band between 3 and 10 days, with additional strong signals in two regions of the ACC. For the vast majority of stations away from the Arctic Ocean, however, ITSG-Grace2016 daily fields explain only a small portion or no signals seen by the in situ stations.

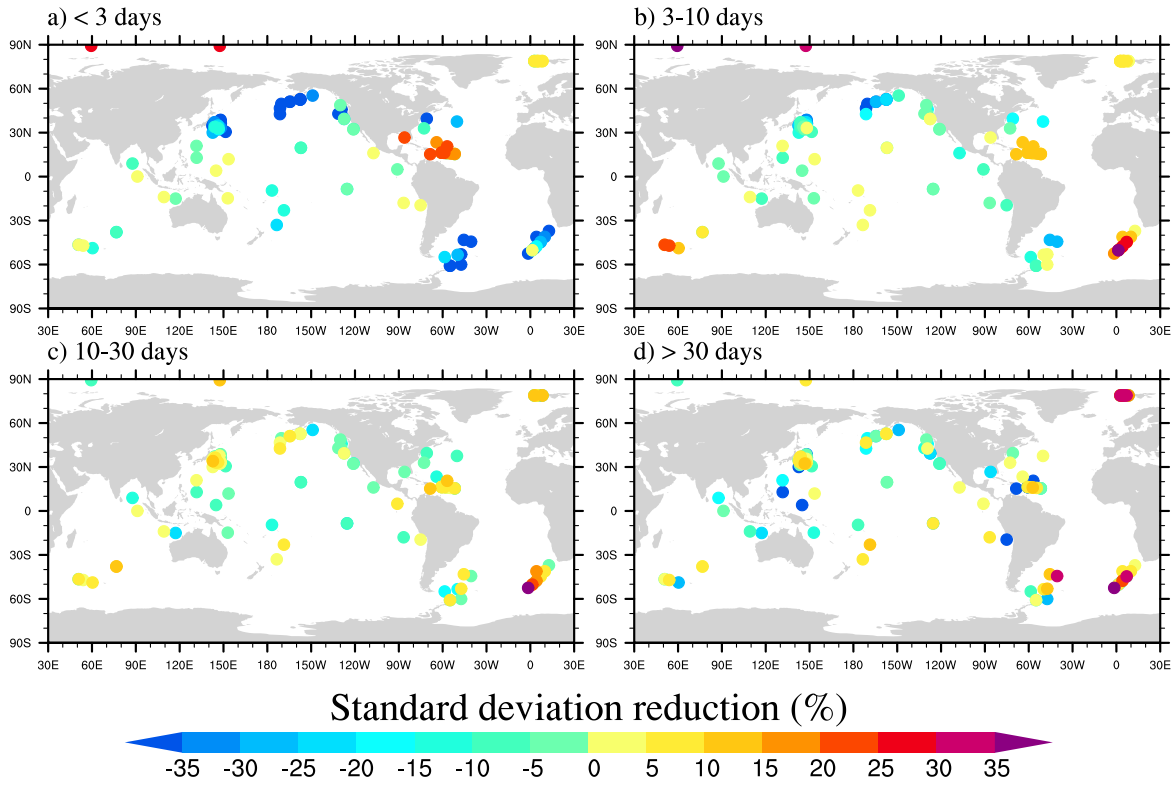

Figure 3.5: Standard deviation reduction of OBP when subtracting daily ITSG-Grace2016 estimates from the in situ observations separated into periods shorter than 3 days (a); 3 – 10 days (b); 10 – 30 days (c); and longer than 30 days (d) as obtained from a series of 4th order Butterworth filters.

However, most of the variability in the GSM fields is found in regions not covered by in situ stations used in this study. This applies in particular to most of the semi-enclosed seas, the Siberian Shelf, and many of the resonant regions in the Southern Ocean.

For periods between 10 and 30 days, 53 % of the in situ stations show reduced standard deviations when ITSG-Grace2016 is subtracted, the largest of them being in the ACC region, where for some stations around 40 % of variability is detected by GRACE, but obviously not captured by AOD1B RL05. This clearly indicates that some fraction of the OBP variability measured by the in situ gauges is captured by the daily ITSG-Grace2016 Kalman Smoother solutions, meaning that the sampling characteristics of GRACE allow to reliably observe signals at weekly periods and longer. For the longest periods, ITSG-Grace2016 Kalman solutions have a similar number of locations with positive reductions of standard deviation, but their spatial distribution is somewhat different. It can thus be concluded that the ITSG-Grace2016 solution indeed captures submonthly variability not predicted by the non-tidal dealiasing model AOD1B.

4

New experiments with MPIOM

The Southern Ocean is highly influential for global ocean circulation and climate. It is a key region for the exchange of energy and gases between the atmosphere and the abyssal ocean by converting surface waters to deep and bottom water that form the deepest branch of the meridional overturning circulation (*Hellmer et al.*, 2016). Cold, dense, and oxygenated Antarctic Bottom Water (AABW), the densest water mass in all oceans, is produced at the continental shelves around Antarctica during the winter, mostly in the shallow Weddell Sea. Its production is one of the drivers of the global thermohaline circulation and influences the properties of the world ocean. The Ice Shelf Water, a water mass with temperatures well below surface freezing temperature produced in contact with Antarctic ice shelves, is thought to be an important ingredient in the formation of the AABW (*Hellmer and Olbers*, 1989; *Foldvik et al.*, 2004). This cold, salty water produced at the continental shelves around Antarctica flows along the seafloor forming the bottom water that spreads into all ocean basins.

The Antarctic Circumpolar Current (ACC) flows eastwards around Antarctica. Despite its relatively slow speed, the ACC transports more water than any other current because it extends from the surface to the bottom and is up to 2000 km wide in some regions. As the only current that flows completely around the globe, it is primarily responsible for the water exchange of the deep and intermediate water between Atlantic, Pacific and Indian Ocean. Since it transports heat, salt and other quantities between the ocean basins, it has an important role in the climate system (*Dijkstra*, 2008).

Interaction of relatively warm water with ice sheets through the ice shelves is believed to be one of the major processes causing sea level rise and ice sheet mass loss (*Hellmer et al.*, 2016). While it was long thought that the ice loss through iceberg calving is the dominant process, *Rignot et al.* (2013) showed that basal melt of 1325±235 Gt/year exceeds the calving flux, making ice-shelf melting the largest ablation process in Antarctica. The freshwater flux due to basal melting also stabilizes the shelf water column both in front of the ice shelf, as well as further downstream after advection by the coastal current (*Hellmer*, 2004). On the other hand, the ACC maintains the Antarctic ice sheets by keeping warm water masses away from the Antarctic coast (*Rintoul et al.*, 2001).

Despite such an extensive influence of the interaction between seawater and Antarctic ice shelves on the ocean circulation, ocean dynamics beneath the ice shelves, and therefore any kind of interaction with them, are often not explicitly considered in global ocean circulation models. In some models the regions beneath ice shelves are treated as land and ocean is only defined at the edge of the ice shelf. Other models include the area covered by ice shelves, but treat them as open ocean, without taking into account that the ice shelf shields the water from the atmospheric influence. The Max-Plack-Institute Ocean Model (MPIOM; *Jungclaus et al.*, 2013) does not consider the dynamics beneath the ice shelves in its standard configuration used in the Atmosphere and Ocean Dealiasing Level 1B (AOD1B) RL06 product (*Dobslaw et al.*, 2017) for GRACE. Because of the effect ice shelves could have on the simulated ocean circulation, it is sensible to include that influence into the ocean model and to estimate its impact through comparison of ocean model experiments with and without ice shelves.

4.1 Experiment design

MPIOM is a baroclinic primitive equation general circulation model. A configuration with approximately 1° resolution on a tri-polar curvilinear grid and with 40 vertical levels, driven by atmospheric forcing from ERA-Interim (*Dee et al.*, 2011), is used.

Table 4.1: MPIOM model experiments

Experiment	Time step	Bathymetry	Forcing
T20B0F0	20 min	reference bathymetry	no ice shelf forcing
T20B1F0	20 min	modified bathymetry	no ice shelf forcing
T20B1F1	20 min	modified bathymetry	ice shelf forcing
T90B0F0	90 min	reference bathymetry	no ice shelf forcing

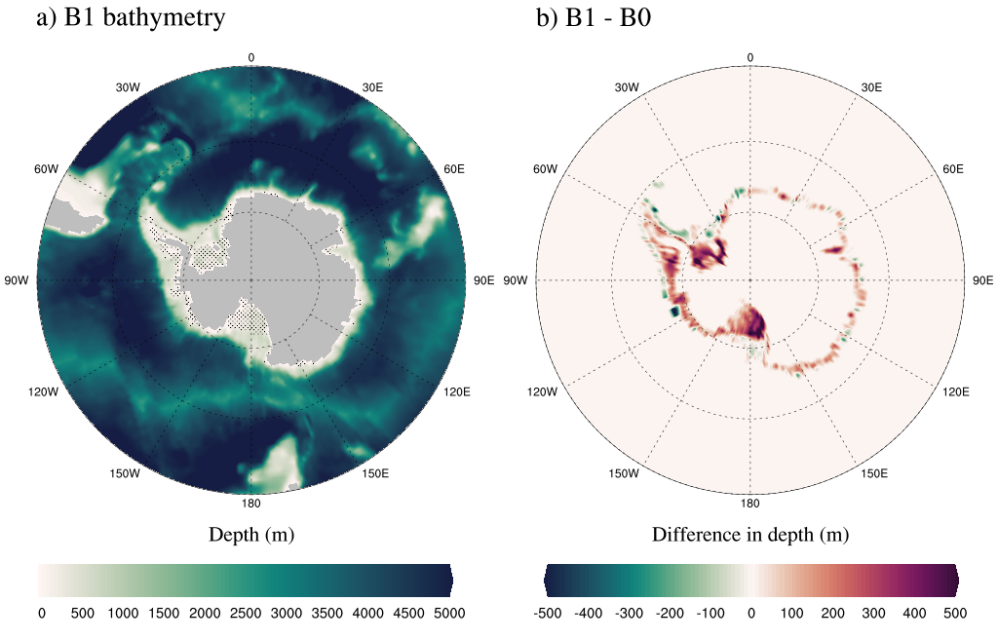

Figure 4.1: New MPIOM bathymetry (B1) in the Southern Ocean with stippled areas marking the ice shelves considered in the T20B1F1 model experiment (a), and the difference between the modified (B1) and the original (B0) bathymetry (b).

Three model experiments are performed to test the influence of the dynamics beneath the Antarctic ice shelves on ocean circulation (Table 4.1). In the first experiment (T20B0F0), oceanic areas beneath the ice shelves are treated as land.

As a first step in the implementation of Antarctic ice shelves, the bathymetry used in the model run is modified to include the areas of the ocean covered by them. The information about the bathymetry beneath the ice shelves is taken from the tidal model for the Southern Ocean CATS02.01. As described in *Padman et al.* (2002), the bathymetry used for the CATS model is based on the ETOPO-5 dataset (NOAA, 1998), but uses local depth grids for specific regions. Under the ice shelves the height of the water column (distance between ocean floor and ice shelf base) is used instead of depth. The dataset has a 1/4° resolution in the meridional and 1/12° in the zonal direction and is interpolated to the model grid using conservative remapping (*Jones*, 1998). The bathymetry in regions near the coast of Antarctica shallower than 1000 m are then replaced with the new dataset to obtain the B1 bathymetry. The new bathymetry dataset was thoroughly inspected and some grid points were manually edited to ensure that the new bathymetry is smooth and without discontinuities. An additional change of the bathymetry is applied to the Baltic Sea, where the bathymetry file is manually edited based on the information from GEBCO_2014 (BODC, 2014) to include the Bothnian Bay and the island Gotland, but since those changes have no influence outside

of the Baltic Sea, they are not discussed in this work. This model experiment is labeled as T20B1F0.

The atmosphere is the major driver of variability in the ocean. The ocean absorbes the heat from above, transports it and releases it through sensible and latent heat fluxes. The input of freshwater through precipitation, river inflow, and melting of ice modifies the salinity of seawater. Wind stress transfers the horizontal momentum from the atmosphere to the ocean and is thus driving ocean surface currents. However, when the dynamics beneath the ice shelves are considered, there is a layer of ice sometimes even 1 km thick between the ocean and the atmosphere that impedes direct atmosphere – ocean interaction. Therefore, the atmospheric forcing fields are modified to take into account the existence of ice shelves. Since some of the Antarctic ice shelves are rather small, the spatial resolution of MPIOM is not high enough to properly represent them. Hence, only the ice shelves shown in Fig. 4.1 are taken into account. The model experiment that includes modifications to the atmospheric forcing to simulate a simple version of ice shelf forcing is labeled as T20B1F1.

Winds are the main driving force for ocean surface currents. They are included in the ocean model through the use of wind stress atmospheric forcing. Since ice shelves represent an obstacle that blocks the transfer of momentum from the atmosphere to the ocean, an ice shelf mask is used to set the wind stress fields to zero in the areas covered by Antarctic ice shelves before using them to force the ocean model.

Ice shelves can lose mass because of basal melting induced by the comparatively warmer ocean. Melting ice produces fresh water at the ice shelf base that reduces the salinity of the ocean thus changing its density, which can have an effect on the thermohaline circulation. To include the input of fresh water because of the basal melting and at the same time to exclude the precipitation that does not reach the ocean because of the ice shelves, the precipitation atmospheric forcing is replaced by ice shelf melting rates in areas covered by ice shelves. The ice shelves are divided into 8 regions based on their geographic location and behavior and an average melt rate in equivalent water height is calculated for each region based on the melt rates from *Rignot et al.* (2013) (Table 4.2). Note that due to the low spatial resolution of the model (1°) and of the forcing file (0.75°), the smallest ice shelves are not directly included, but their melt rates are still part of the average in their region.

The exchange of sensible heat between the atmosphere and the ocean is usually considered through surface temperature forcing fields. When studying the ocean dynamics beneath the ice shelves, the ocean is not in direct contact with the atmosphere, so the ice temperature at the ice shelf base is used instead. There are few observations of the ice shelf base temperatures due to their inaccessibility, but for most ice shelf regions it

Table 4.2: Average melting rates for Antarctic ice shelves

Region	Melt rate (m/y)
Ross ice shelf and shelves in Ross Sea	0.17
East Antarctica between Ross Sea and Amery ice shelf	3.13
Amery and Publications ice shelves	0.59
East Antarctica between Amery and Filchner	0.43
Filchner-Ronne and Larsen ice shelves	0.35
Western side of Antarctic Peninsula	3.10
West Antarctica between peninsula and Ross Sea	5.63

is a safe assumption that the temperature of the ice shelf is the melting temperature of ice at the ice shelf base depth. While ice models provide those temperatures with a very high spatial resolution, due to the low resolution of both the global ocean model and the ERA-Interim atmospheric forcing, only a rough estimate is utilized here. A constant temperature forcing of -2 °C is applied for all the smaller ice shelves, while for the three largest ice shelves (Ross, Filchner, and Ronne) a lower temperature of -4 °C is used because an ice model (*Bernales et al.*, 2017) showed lower ice melting temperature for them, as well as very low and often even negative melting rates, which suggests that their temperature is probably even lower. The thermal forcing from the ice shelves will trigger re-freezing from the sea-ice module in the ocean model where necessary. Furthermore, since ice acts as insulation, the radiative forcing from the sun is also set to zero in the areas covered by ice shelves.

MPIOM in its configuration for AOD1B RL06 has a 90 minutes time step (T90B0F0). However, when using the modified bathymetry including the area under the Ross ice shelf, the domain approaches the polar singularity on Antarctica, which decreases the longitudinal distance between two grid points from approximately 23 km to 11 km in the Ross Sea. Since MPIOM uses a semi-implicit time stepping scheme for both the barotropic and the baroclinic subsystem, it is more stable than the explicit scheme and does not need to strictly fulfill the Courant-Friedrichs-Lewy (CFL) condition:

$$C = \frac{c\Delta t}{\Delta x} \leq 1\,, \tag{4.1}$$

where c is the characteristic wave speed of the system, Δt is the time step, and Δx is the spatial resolution in longitudinal direction. In latitudinal direction resolution does not change when approaching the pole. Nevertheless, it is still necessary that the Courant number C is not too large. An example of waves that are long enough to be simulated by MPIOM in that region and fast enough to potentially cause an instability so close to the polar singularity are topographic Kelvin waves, a type of gravity waves

that propagate along the coast with a non-dispersive speed:

$$c = \sqrt{gH}\,, \tag{4.2}$$

where g is the acceleration of gravity, and H is the water depth. Since the depth at the southernmost part of the Ross Sea is approximately 100 m, the speed of the Kelvin waves that could develop there is ~ 30 m/s. With $\Delta x = 11$ km and $\Delta t = 90$ minutes, the Courant number is $C \approx 15$. If the time step is kept at 90 min after implementing the bathymetry modifications near Antarctica, an instability arises at the coast of the Ross Sea and grows exponentially until the model simulation crashes. Therefore, the time step is reduced to 20 min, which brings the Courant number to 3.3 and keeps the model in stable conditions. That also increases the computing effort by approximately 30 %, which is an acceptable price to pay. Changing the time step, however, has an influence on the simulated ocean dynamics caused by the fast processes that can be represented by a 20 minute time step, but are not caught by the much longer 90 minutes time step. Since there are some changes caused by the time step difference, when studying the influence of bathymetry modifications and ice shelf forcing, all model experiments use the same 20 minutes time step.

The model is spun up for 500 years with climatological atmospheric forcing, both with original (B0) and with modified bathymetry (B1), after which all the model experiments are continued for 10 years with ERA-Interim forcing. To save computation time, the spin-up for T20B0F0 experiment is the same as for AOD1B RL06, so while the 10 years considered in the experiment have a 20 minute time step, the spin-up uses a 90 minute time step. Experiments T20B1F0 and T20B1F1 are continued from the spin-up with B1 bathymetry. Only the second half of the model run, i.e. years 2006 – 2010, are analysed to allow the model to adapt to the new forcing. The output is remapped to a regular 0.5° grid and the mean difference between the three model runs are calculated. If the changes depend on the season, austral summer (December, January, and February) and austral winter (June, July, and August) averages are considered separately.

4.2 Simulated mean circulation in the Southern Ocean

In order to assess the magnitude of changes caused by the bathymetry modifications and the implementation of ice shelf forcing into the ocean model, it is important to first examine the signals present in the Southern Ocean and their variability. In this section, temporal means and standard deviations of the potential temperature, salinity, and sea level are calculated from the MPIOM T20B1F0 experiment. Temperature and salinity control the sea water density, which is important for the formation of the bottom water,

while sea level can be used to study the ACC in the regions where its flow is mainly geostrophic. Since the surface (averaged uppermost 6 m layer) values can be highly dependent on the seasonal cycle, they are studied separately for the austral summer, and winter. Spatial distribution at 200 m depth (averaged 185.5 – 220 m layer), as well as a vertical cross section at 70°W, where the impact of changes to the model is expected to be large, are analysed.

Temperature variability can be inferred from the standard deviations, which display a large seasonal difference at the surface. During the summer (Fig. 4.2 a), surface temperature variability is largest along the coast, where the ocean is shallow enough to allow faster temperature changes than in the open ocean. In the Weddell and a portion

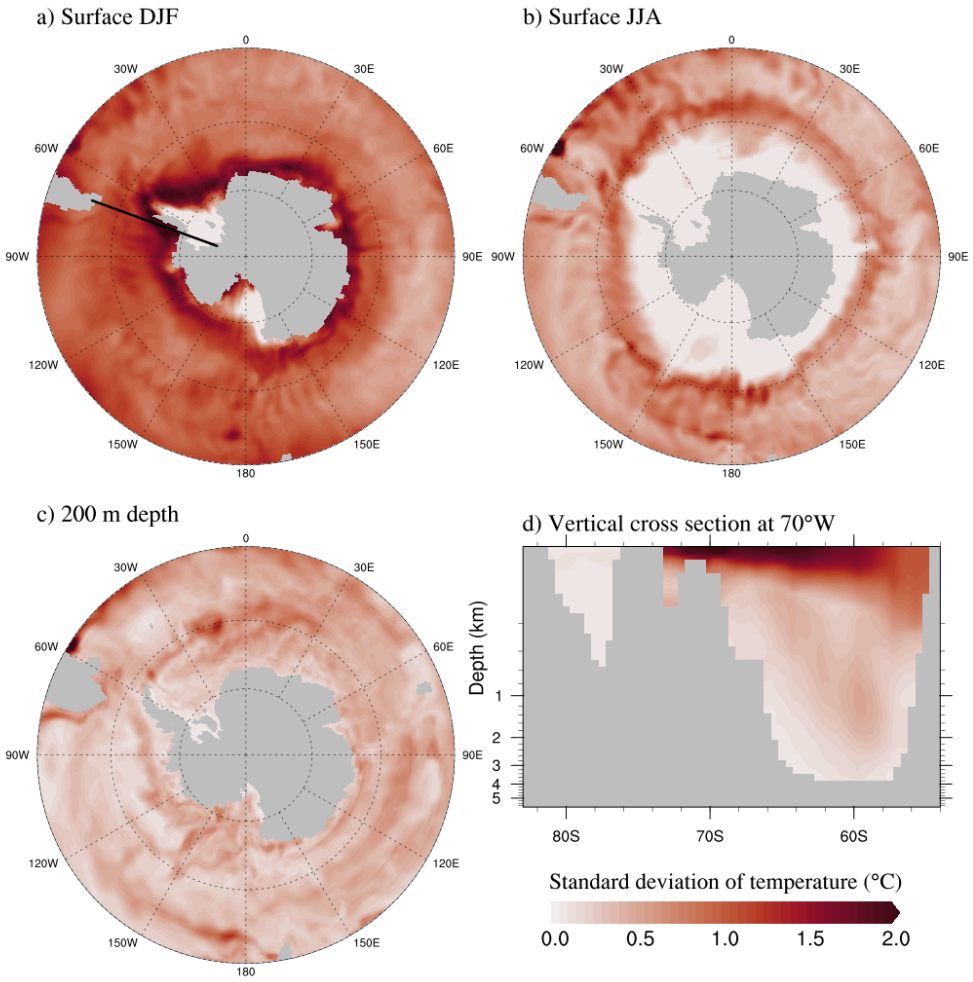

Figure 4.2: Standard deviation of temperature of the austral summer (a), and winter (b) at the surface; of the entire year at 200 m depth (c), and at a vertical cross section between Antarctica and South America at 70°W (d) simulated by the MPIOM T20B1F0 experiment. The black line in (a) marks the location of the vertical cross section.

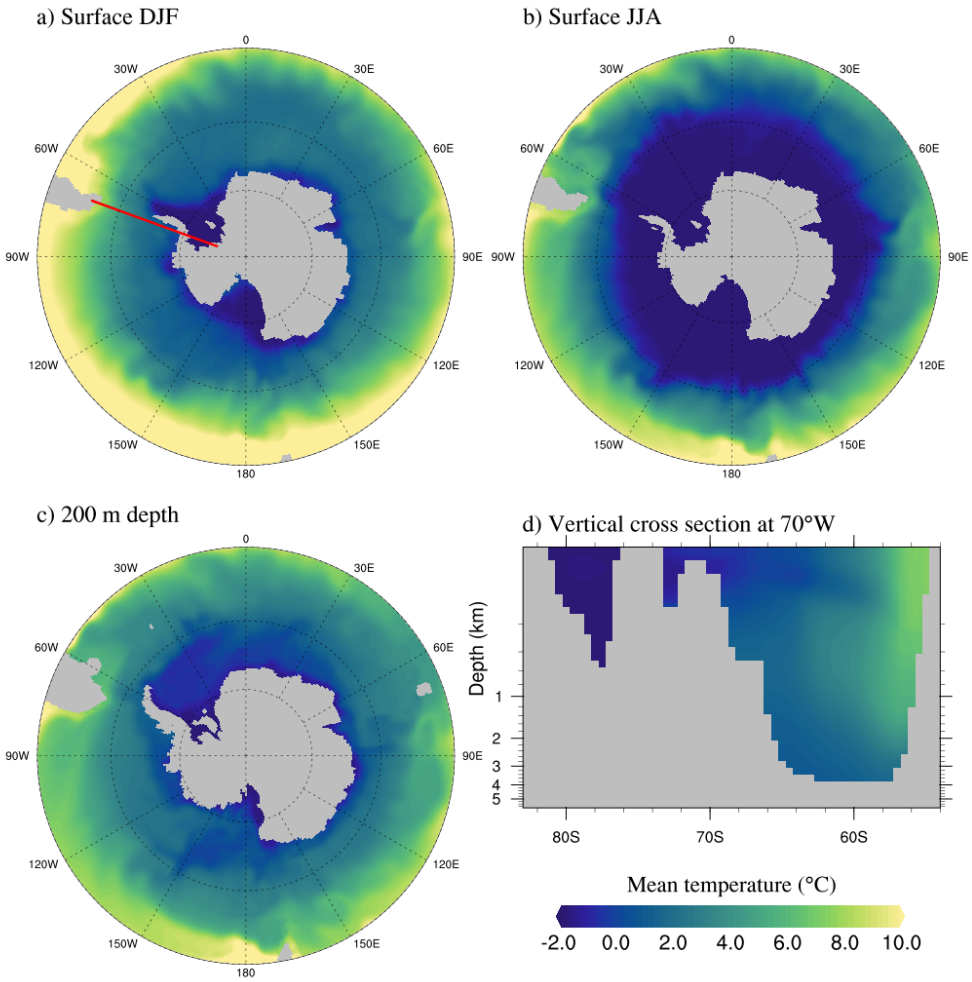

Figure 4.3: Mean temperature of the austral summer (a), and winter (b) at the surface; of the entire year at 200 m depth (c), and at a vertical cross section between Antarctica and South America at 70°W (d) simulated by the MPIOM T20B1F0 experiment. The red line in (a) marks the location of the vertical cross section.

of the Ross Sea, however, the temperature variability is practically zero because those areas are permanently covered by sea ice which insulates the sea from the atmosphere. During the winter (Fig. 4.2 b), almost all latitudes within the polar circle are covered by sea ice, resulting in very small standard deviations in the whole area. At 200 m depth (Fig. 4.2 c) variability is much smaller than at the surface, even though it includes the seasonal cycle. Some regions of slightly higher variability are located further away from the coast and are most likely related to the meanders in the ACC that form due to topographic steering. The vertical cross section (Fig. 4.2 d) confirms that the variability is much higher for the upper 200 m than in the deep ocean. An exception to that is the southernmost part of the cross section, the Weddell Sea, where the variability is virtually zero in the whole water column because it is permanently covered by sea ice

in this model experiment.

The mean sea surface temperature (Fig. 4.3 a, b) has a very strong latitudinal dependence, ranging from around -2 °C at the Antarctic coast to more than 10 °C when approaching 45°S. Seasonal dependence is also apparent: while during the austral summer only the Weddell and the Ross Sea as well as a short band next to the coast of Antarctica have near freezing surface temperatures, the whole area within the polar circle has temperatures below 0 °C during the austral winter. At 200 m depth (Fig. 4.3 c), the temperature also has a latitudinal dependence, but with a smaller range. In the vertical cross section at 70°W between Antarctica and South America (Fig. 4.3 d) a region of cold water on the Antarctic side and at the bottom is visible, revealing the cold AABW spreading along the continental slope into the Atlantic ocean. The permanently ice-covered Weddell Sea has an even lower temperature, well below -1 °C, in the whole water column.

The variability in salinity is vastly different between the seasons: while there is almost no variability anywhere in the Southern Ocean during the winter (Fig. 4.4 b) because the sea is covered with ice, summer variability (Fig. 4.4 a) around the Antarctic coast is rather large due to the melting of said ice that nudges the salinity towards its usual lower values. High variability is limited to the upper layer, at 200 m depth (Fig. 4.4 c) salinity practically does not vary with time. It is visible from the vertical cross section (Fig. 4.4 d), that the variability in salinity is limited to the upper 100 m of the ocean. It is the largest in the Weddell Sea, in this experiment covered by sea ice, where the seasonal melting and freezing of sea water generates large fluctuations of salinity at the surface, and it decreases with distance from the coast.

Mean sea surface salinity strongly depends on the season. While the minimum of salinity in the Southern Ocean is approximately 34 PSU in the ACC region in the western hemisphere throughout the entire year, it extends all the way to the Antarctic coast during the summer (Fig. 4.5 a). During the winter months (Fig. 4.5 b), however, salinity near the coast is much higher, exceeding 35.8 PSU at the coast of the Ross and Weddell Sea. This difference arises from the formation of the sea ice, which removes the fresh water from the surface ocean, substantially increasing its salinity. The low salinity of 34 PSU is restricted to the surface layer. Already at 200 m depth salinity is higher and much more uniformly distributed (Fig. 4.5 c). The vertical cross section (Fig. 4.5 d) demonstrates that there is a layer of low salinity at the surface, below which the salinity is increasing with depth, up to almost 35 PSU in the open ocean and much more in the semi-enclosed Weddell Sea. High salinity in the Weddell Sea is a result of brine rejection during the formation of the permanent sea ice cover. Because of its high density such salty water sinks to the bottom. Since it is observed that the

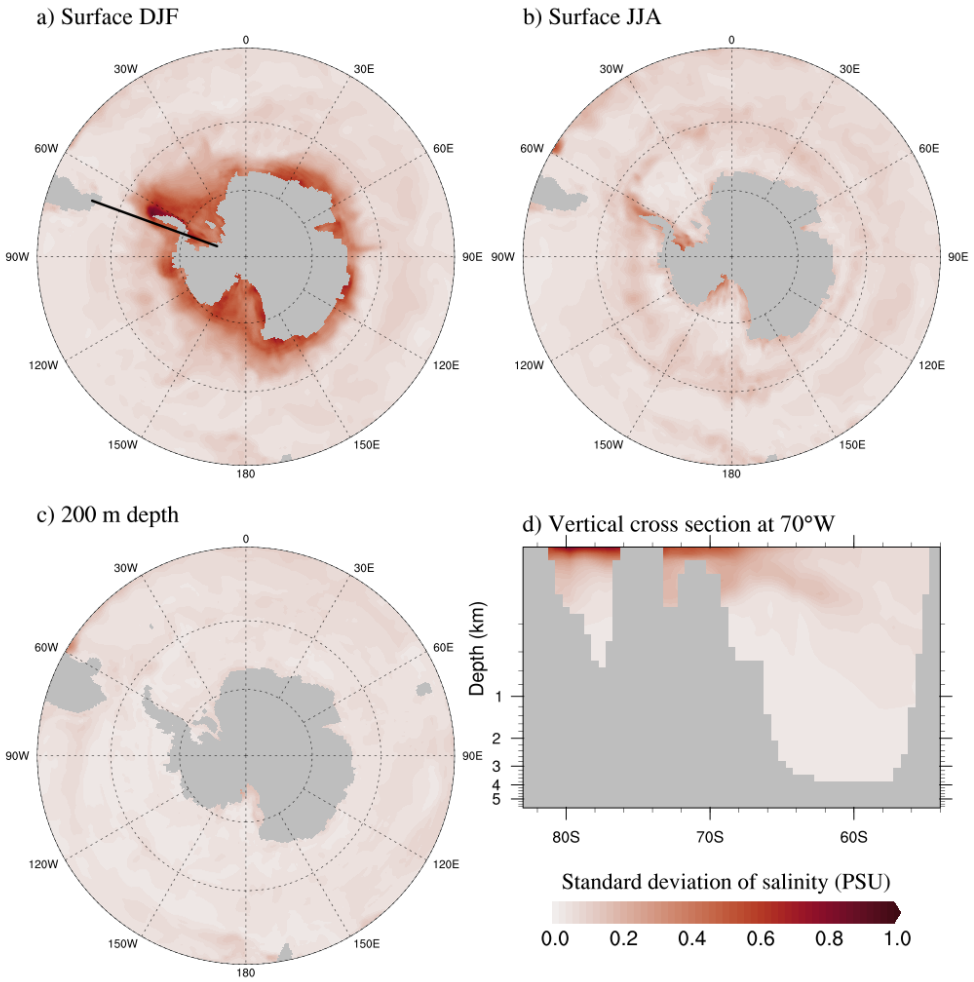

Figure 4.4: Standard deviation of salinity of the austral summer (a), and winter (b) at the surface; of the entire year at 200 m depth (c), and at a vertical cross section between Antarctica and South America at 70°W (d) simulated by the MPIOM T20B1F0 experiment. The black line in (a) marks the location of the vertical cross section.

salinity of the AABW is much lower (*Orsi et al.*, 1999), especially in the Weddell Sea, where *Gordon et al.* (1993) noted the salinity of 34.63 PSU, these results point out the importance of somehow including the fresh water imput from basal melting of the ice shelves.

Sea level variability (Fig. 4.6) only has a small seasonal dependence, but unlike temperature and salinity that vary more strongly during the austral summer, sea level has a higher variability during the winter due to stronger winds affecting it. The regions of highest variability are independent of the season and located on the southern side of the ACC path. They are most likely caused by the meandars and jets formed in the ACC due to the obstacles at the ocean floor. The region in which the slope of the

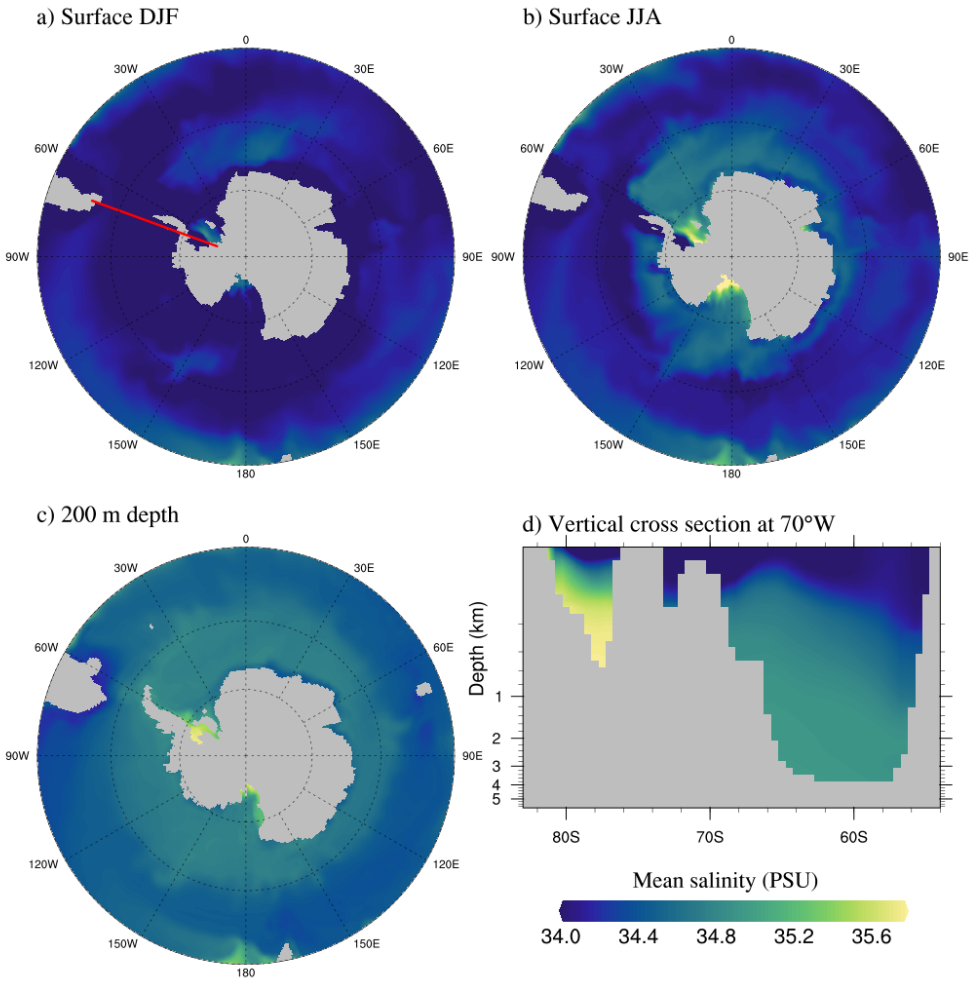

Figure 4.5: Mean salinity of the austral summer (a), and winter (b) at the surface; of the entire year at 200 m depth (c), and at a vertical cross section between Antarctica and South America at 70°W (d) simulated by the MPIOM T20B1F0 experiment. The red line in (a) marks the location of the vertical cross section.

mean sea surface elevation (Fig. 4.7) is the steepest coincides with the outer edge of the Antarctic Circumpolar Current. Because the ACC is to a large extent geostrophic, it usually flows parallel to the contours in the clockwise direction around the sea surface height minimum.

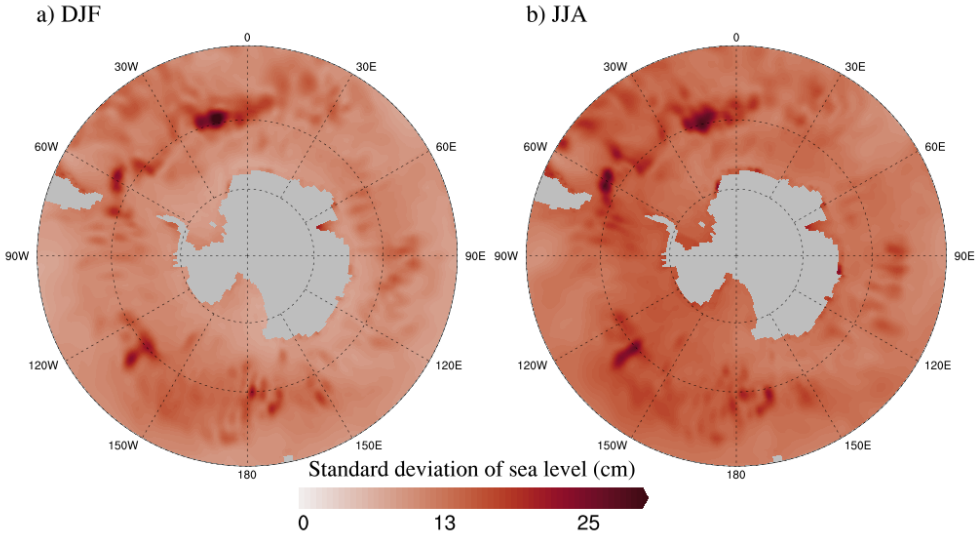

Figure 4.6: Standard deviation of sea surface elevation in the Southern Ocean simulated by the MPIOM T20B1F0 experiment for the austral summer (a) and winter (b).

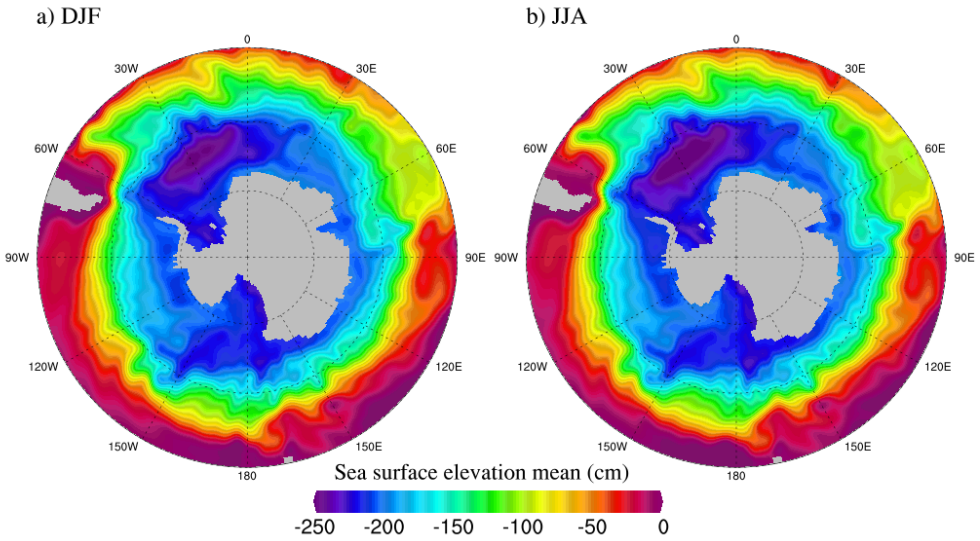

Figure 4.7: Mean sea surface elevation in the Southern Ocean simulated by the MPIOM T20B1F0 experiment for the austral summer (a) and winter (b).

4.3 Changes in the Southern Ocean caused by bathymetry modifications

Differences in mean sea ice thickness, potential temperature, salinity, and sea surface elevation between T20B1F0 and T20B0F0 model experiment are calculated to study the influence of the bathymetry changes in the ocean model on ocean dynamics in the Southern Ocean. Only the grid cells that are wet in both model experiments are used for this comparison. To evaluate whether those changes are significant compared to the typical variability in the respective region, they are compared with the standard deviations of the T20B0F0 experiment.

The ice cover (Fig. 4.8) can highly influence the distribution of other water properties by insulating it from the atmosphere and modifying salinity through freezing and melting of seawater. Extending the ocean domain further south into regions that maintain very cold water temperatures throughout the year results in an increased sea ice thickness. The largest changes in ice thickness are located in the areas with largest bathymetry modifications, i.e. Weddell and Ross Sea. The ice thickness increase is somewhat larger during the summer months, but it persists throughout the year. The average sea ice extent is mostly not affected by changes of the model bathymetry, with the exception of a region near the Antarctic Peninsula, where the average summer ice extent simulated by the T20B0F0 experiment leaves the tip of the peninsula ice-free,

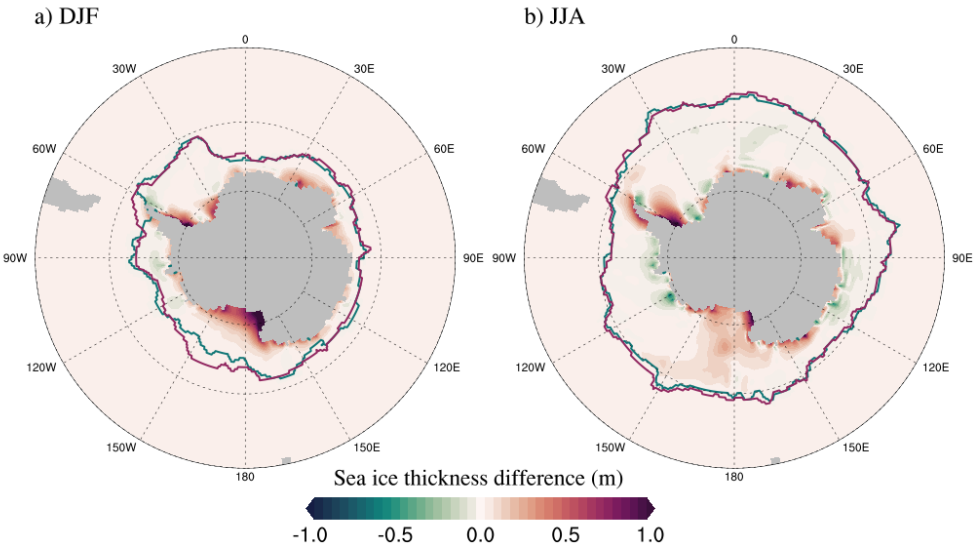

Figure 4.8: Difference in mean sea ice thickness of the austral summer (a), and winter (b) between model experiments T20B1F0 and T20B0F0. The green lines mark the sea ice extent in the T20B0F0 experiment, and purple in the T20B1F0 experiment.

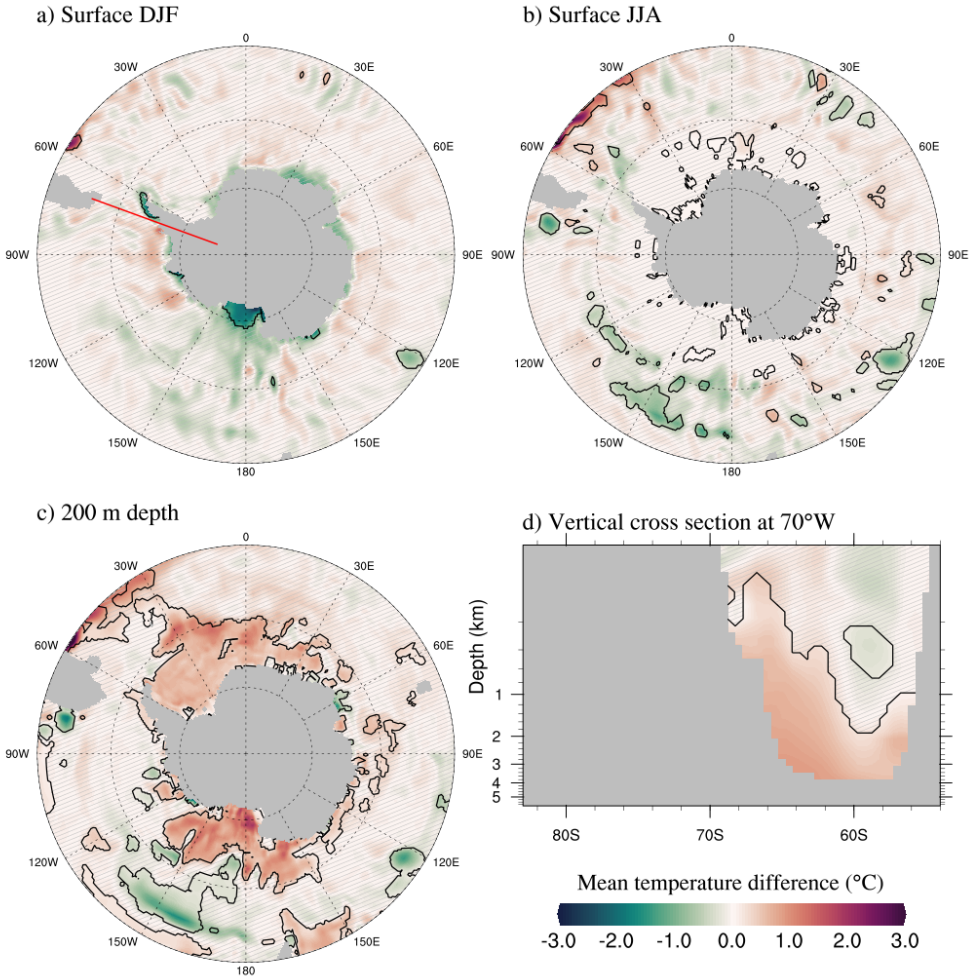

Figure 4.9: Difference in mean temperature of the austral summer (a), and winter (b) at the surface of the Southern Ocean; of the entire year at 200 m depth (c), and at a vertical cross section between Antarctica and South America at 70°W (d) between model experiments T20B1F0 and T20B0F0. Areas where the difference between model experiments does not exceed the standard deviation of the T20B0F0 experiment are striped and their boundary is marked with black lines. The red line in (a) marks the location of the vertical cross section.

while in the T20B1F0 experiment the ice just north of the peninsula melts later in the summer and forms earlier, resulting in a somewhat larger ice extent.

Changes in mean sea surface potential temperature are rather small, especially in comparison with its usual day-to-day variability. The increase of water depth generally causes a decrease in temperature in those and nearby regions and the mean difference can reach 2 °C. During the austral summer (Fig. 4.9 a), changes are larger and mainly focused in the vicinity of the coast, but only exceed the usual temperature variability in

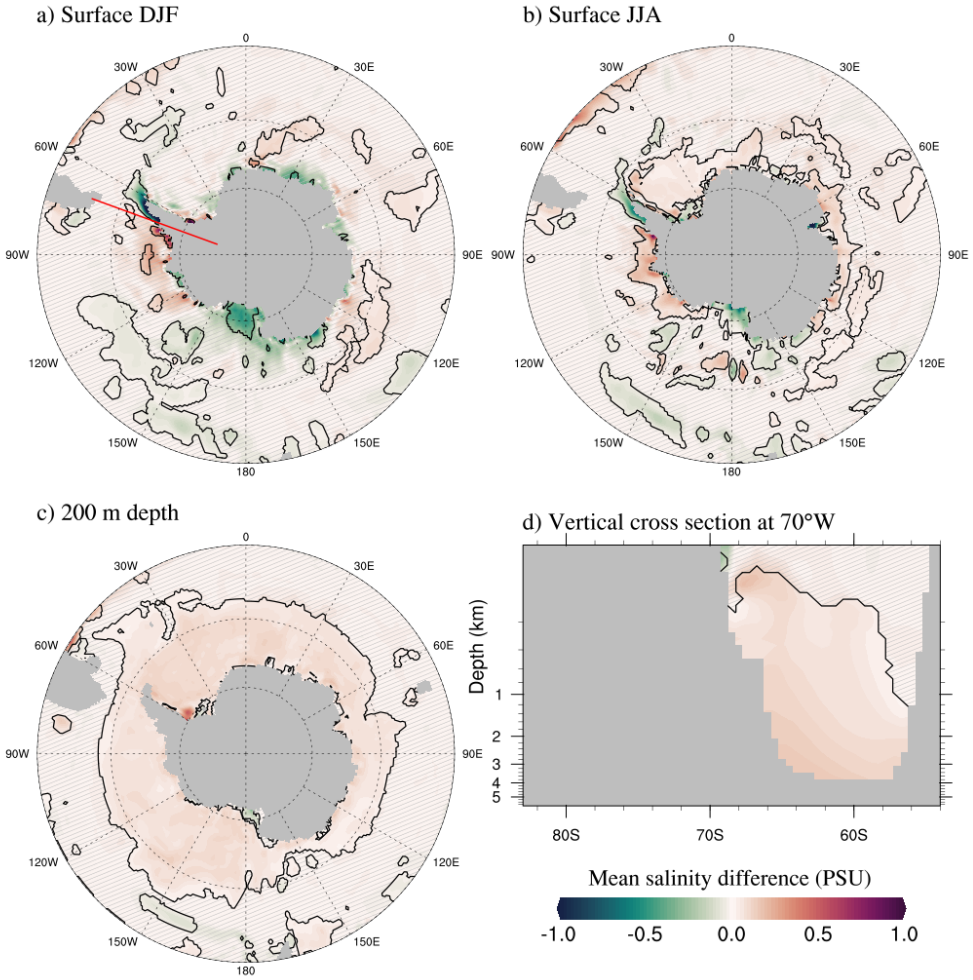

Figure 4.10: Difference in mean salinity of the austral summer (a), and winter (b) at the surface of the Southern Ocean; of the entire year at 200 m depth (c), and at a vertical cross section between Antarctica and South America at 70°W (d) between model experiments T20B1F0 and T20B0F0. Areas where the difference between model experiments does not exceed the standard deviation of the T20B0F0 experiment are striped and their boundary is marked with black lines. The red line in (a) marks the location of the vertical cross section.

the Ross Sea and at the tip of Antarctic Peninsula. There are almost no differences near the coast during the winter (Fig. 4.9 b), but small changes further in the open ocean, especially Southern Pacific, are still present. Since water cooled at the surface is denser, and therefore heavier, it sinks to the bottom, resulting in temperature modifications extending through the whole water column. At 200 m depth (Fig. 4.9 c) changes caused by bathymetry modifications are much larger than at the surface. While the surface cooled at and near the newly introduced shallow basins, the temperature at 200 m depth increased in most of the Southern Ocean, probably due to the increased ice

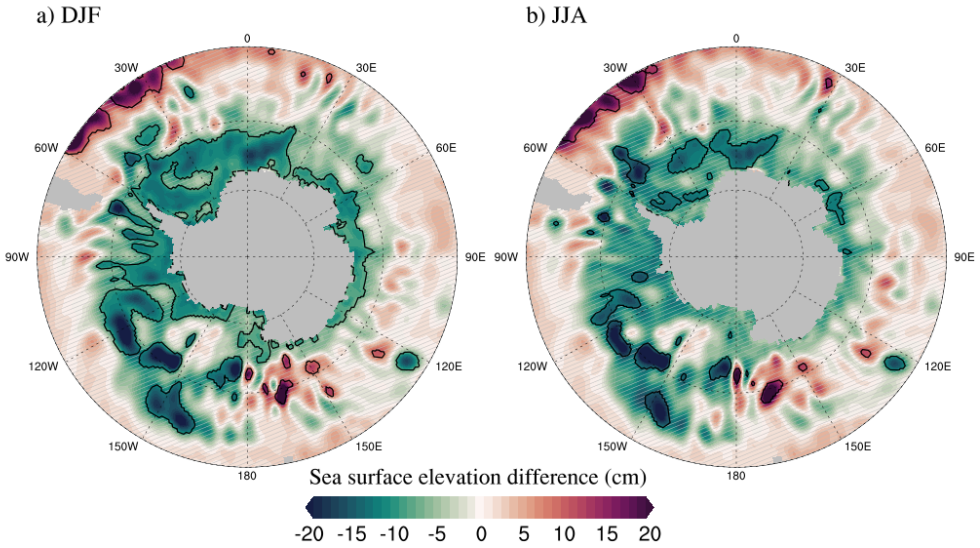

Figure 4.11: Difference in mean sea surface elevation of the austral summer (a), and winter (b) in the Southern Ocean between model experiments T20B1F0 and T20B0F0. Areas where the difference between model experiments does not exceed the standard deviation of the T20B0F0 experiment are striped and their boundary is marked with black lines.

cover that provides better insulation. The temperature of the AABW flowing from the Antarctic continental slope to the ocean basin floor (Fig. 4.9 d) is also increased.

Changes in surface salinity are mostly limited to areas near the Antarctic coast. During the summer (Fig. 4.10 a), they are somewhat larger, but less significant compared to the typical inter-seasonal variability. During the winter (Fig. 4.10 b) however, the difference between the two model experiments exceeds the inter-seasonal variability in most areas along the coast. In both seasons, there is a decrease in salinity around the Antarctic Peninsula and in the Ross Sea and an increase near the coast of West Antarctica. The increase in surface salinity arises from the increased ice formation in the T20B1F0 experiment, while relatively fresh water is produced through melting of the sea ice along the Antarctic coast. It is advected and mixed by the eastward currents. The bathymetry modifications of the Antarctic Peninsula reduce the smoothness of the coastline, diverting the currents around the tip of the peninsula, which influences the distribution of salinity. At 200 m depth (Fig. 4.10 c), there is a small and rather uniform increase in salinity due to intensified sea ice formation in the whole Southern Ocean. From the vertical cross section (Fig. 4.10 d), it can be seen that this increase extends through the whole water column, increasing the water density and counteracting the density decrease from raised temperature.

The difference in sea surface elevation between the model experiments with different bathymetries (Fig. 4.11) shows patterns that reflect those modifications. Since the largest increase in depth is in the Ross and Weddell Sea, the decrease in sea level is also largest in and near those areas, often reaching 10 cm or more. As expected, there is almost no seasonal change in the sea level differences caused by the changes in the bathymetry. The low sea surface on the southern side of the ACC is further decreased by including the full extent of the Weddell and the Ross Sea, while the elevation in the rest of the ocean is increased. When the new oceanic areas are added, the depth is increased in areas that were previously forming a coast, and the water level adjusts to the bathymetry change by sinking in that region. The sea surface elevation in the remaining ocean then rises to compensate for this change. The changes in the steepness of the sea surface elevation slope in the ACC region could cause some changes in the speed of the current, but regions with the largest gradient remain unchanged.

4.4 Changes in the Southern Ocean caused by ice shelf forcing

Extending the model domain to include the areas beneath the Antarctic ice shelves proved to highly influence ocean properties below the surface. Some of these changes might even be excessive due to the increased sea ice formation in the newly introduced shallow basins, which are treated as open ocean in the T20B1F0 model experiment, without taking into account the insulating influence and the additional fresh water input that the ice shelves provide. The T20B1F1 model experiment partially corrects that by including some of the factors relevant for the ice shelf – ocean interaction into the atmospheric forcing. The influence of ice shelf forcing on ocean water properties is analysed by comparing the T20B1F0 and T20B1F1 experiment.

The differences in mean sea surface temperature due to modification of atmospheric forcing (Fig. 4.12 a, b) show a strong seasonal dependence. They are far more prominent during the austral summer, when thermal forcing from the ice shelf decreases the temperature in the Bellingshausen Sea by more than 2 °C. That is because even when the ice shelves are not simulated, during the winter the ocean is covered with sea ice, which has a similar effect on temperature as the ice shelves, insulating the seawater from the harsh winter atmosphere. The temperature difference between the atmospheric forcing and the simulated ice shelf forcing is much smaller in the Ross and Weddell Sea, where summer air temperature is usually well below 0 °C, than near the Antarctic Peninsula, where it sometimes exceeds 5 °C. Therefore, the changes caused by the small ice shelves on the western side of Antarctic Peninsula are much larger than those

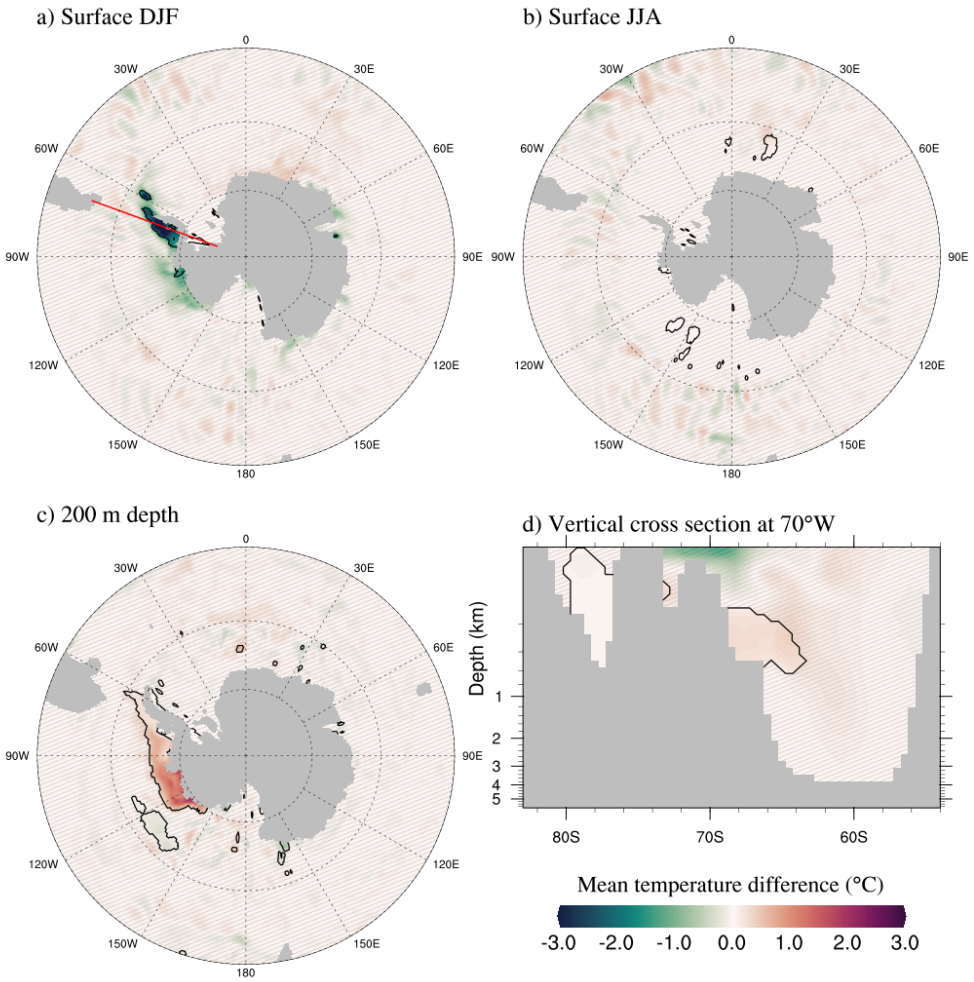

Figure 4.12: Difference in mean temperature of the austral summer (a), and winter (b) at the surface of the Southern Ocean; of the entire year at 200 m depth (c), and at a vertical cross section between Antarctica and South America at 70°W (d) between model experiments T20B1F1 and T20B1F0. Areas where the difference between model experiments does not exceed the standard deviation of the T20B1F0 experiment are striped and their boundary is marked with black lines. The red line in (a) marks the location of the vertical cross section.

caused by the three major ice shelves. At a depth of 200 m (Fig. 4.12 c), the changes are much smaller and simulating the ice shelves causes a temperature increase in the same region. Below 200 m (Fig. 4.12 d) the changes are mostly negligible.

Applying ice shelf forcing only affects the sea ice thickness (Fig. 4.13) along the coast of the Antarctic Peninsula, but the magnitude of the increase is much larger than that induced by bathymetry modifications. While extending the bathymetry beneath the Ross and Filcher-Ronne ice shelves already resulted in permanent sea ice formation

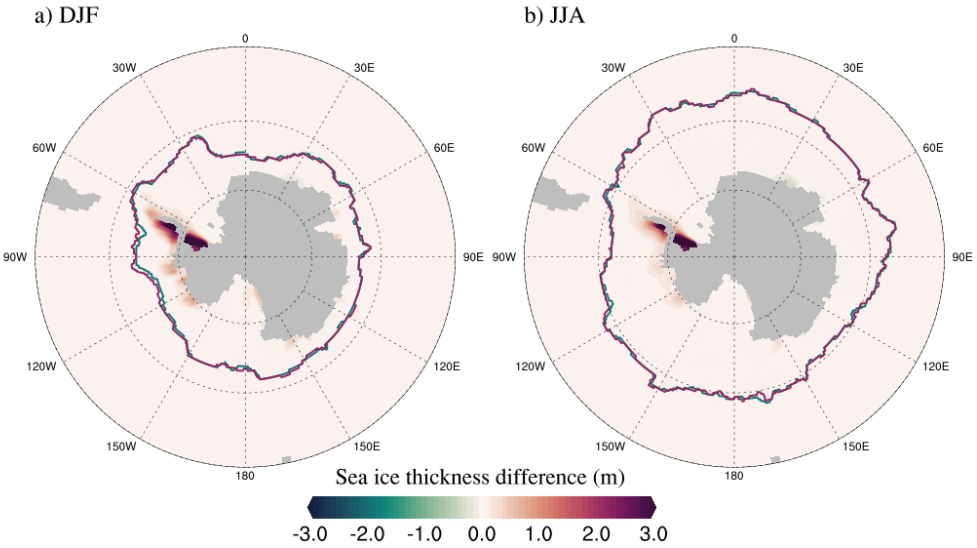

Figure 4.13: Difference in mean sea ice thickness of the austral summer (a), and winter (b) between model experiments T20B1F1 and T20B1F0. The green lines mark the sea ice extent in the T20B1F0 experiment, and purple in the T20B1F1 experiment.

due to their shallow water and below freezing temperature throughout the year, the peninsula remained partially ice-free during the summer in the T20B1F0 experiment. Including constant below freezing temperature forcing from the ice shelves changes that, resulting in permanent sea ice formation around the Antarctic Peninsula.

As expected, introducing ice shelf basal melting into the forcing of the ocean model has the largest influence on salinity in areas near the Antarctic Peninsula and West Antarctica (Fig. 4.14), which have the highest melt rates. Melting of the ice shelves causes a decrease in salinity, especially directly beneath the ice shelves, due to the input of fresh water. During the winter and summer months, salinity is affected very similarly by forcing from the ice shelves because seasonal variations of ice shelf melting rates are not taken into account in this model experiment. The changes are limited to the upper 200 m of the ocean.

The sea surface elevation changes caused by simulating the existence of ice shelves with modifications of the atmospheric forcing (Fig. 4.15) are much smaller compared to those caused by changes in the bathymetry, rarely exceeding 5 cm, and insignificant compared to the usual intra-seasonal variability described by the standard deviation of the T20B1F0 experiment. Most of the changes appear to be rather randomly distributed stripes. The only exception is a small but rather uniform sea level rise along the coast of Western Antarctica that can be explained by input of freshwater from ice shelf melting, but that also does not exceed the usual variability.

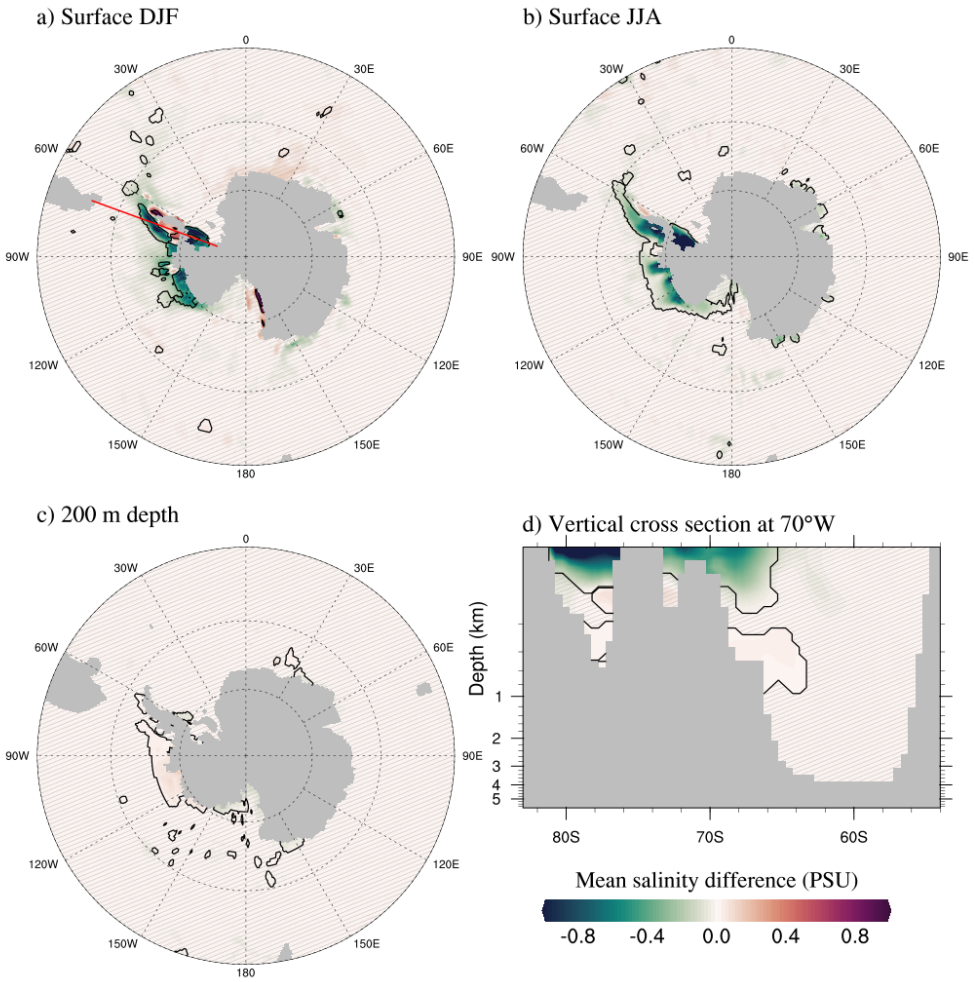

Figure 4.14: Difference in mean salinity of the austral summer (a), and winter (b) at the surface of the Southern Ocean; of the entire year at 200 m depth (c), and at a vertical cross section between Antarctica and South America at 70°W (d) between model experiments T20B1F1 and T20B1F0. Areas where the difference between model experiments does not exceed the standard deviation of the T20B1F0 experiment are striped and their boundary is marked with black lines. The red line in (a) marks the location of the vertical cross section.

4.5 Influence on global ocean circulation

As seen in the previous two sections, including the Antarctic ice shelves by modifying the bathymetry around Antarctica and masking the atmospheric forcing has a large influence in the regions where the modifications were made and their immediate vicinity. However, the changes in the model experiment results are not limited to the Southern Ocean, they influence the global ocean circulation and cause changes in ocean water properties in areas far away from Antarctica. In this section, the consequences for

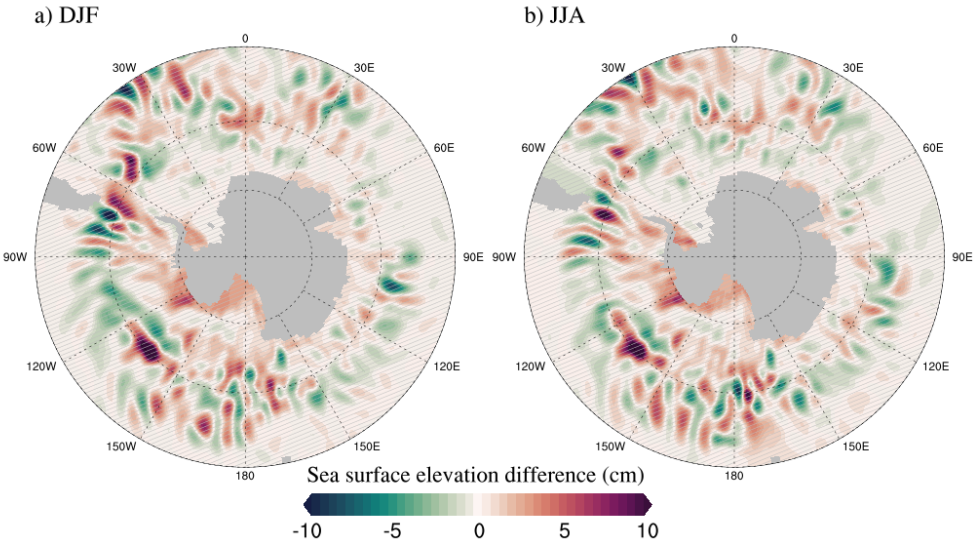

Figure 4.15: Difference in mean sea surface elevation of the austral summer (a), and winter (b) in the Southern Ocean between model experiments T20B1F1 and T20B1F0. Areas where the difference between model experiments does not exceed the standard deviation of the T20B1F0 experiment are striped and their boundary is marked with black lines.

the global temperature and salinity distribution are analysed, with a special consideration of the Atlantic Meridional Overturning Circulation (AMOC), which is one of the mechanisms responsible for the propagation of changes across the ocean. The AMOC extends from the Southern Ocean to the Nordic Seas, transporting heat northwards through the South and North Atlantic, and sinking carbon and nutrients into the deep ocean (*Frajka-Williams et al.*, 2019). Since the changes caused by bathymetry modifications and those caused by ice shelf forcing have a similar spatial distribution further away from the Antarctic coast, they are not considered independently in this section. Instead, the differences between T20B0F0 and T20B1F1 model experiment are analysed. In order to study the changes at depth, the 500 m (averaged 485-560 m) layer is considered to make sure that the seasonal surface changes are excluded. Finally, to study the effect the changes implemented into the model have on the AMOC, a vertical cross section along the 32°W meridian is analysed, and the meridional heat and volume transport are calculated for 26.5°N and compared with observations.

The induced changes in global sea surface temperature (Fig. 4.16 a) are very small compared to the typical seasonal and interseasonal variability. It is nevertheless obvious that the North Atlantic, in particular the downwelling region near the southern coast of Greenland, is affected by the inclusion of Antarctic ice shelves to the same extent as the Southern Ocean, indicating possible changes to the AMOC. At 500 m depth

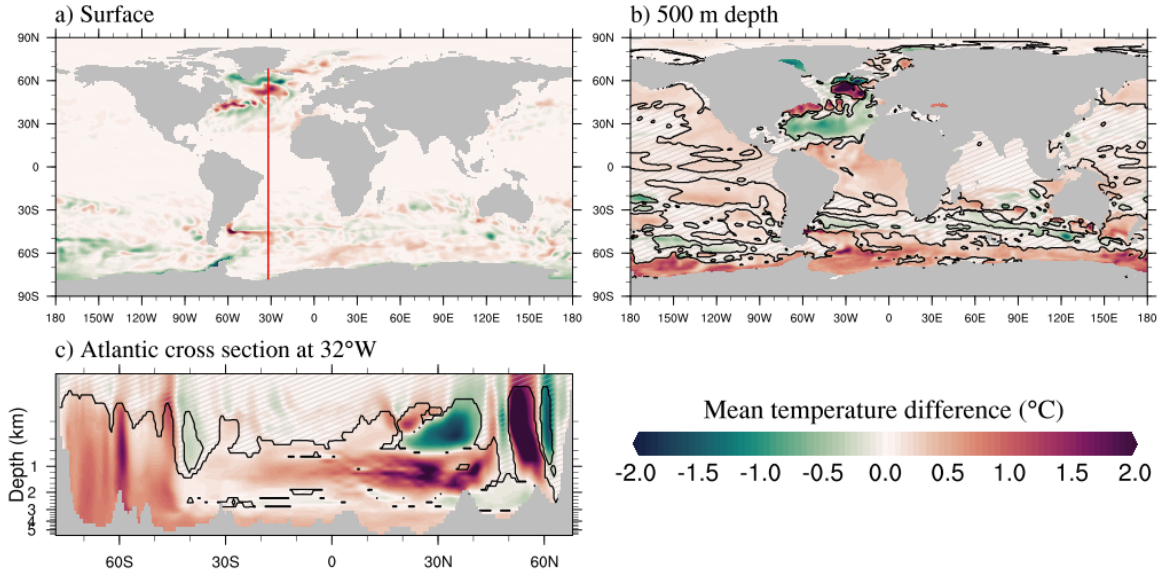

Figure 4.16: Difference in mean temperature between model experiments T20B1F1 and T20B0F0 in the surface layer (a), at 500 m depth (b), and in a vertical cross section through the Atlantic Ocean at 32°W (c). Areas where the difference between model experiments does not exceed the standard deviation of the T20B0F0 experiment are striped and their boundary is marked with black lines. The red line in (a) marks the location of the vertical cross section.

(Fig. 4.16 b), where atmospheric influence and seasonal variability can be neglected, including the ice shelves substantially affects global temperature, especially in the Atlantic Ocean. The changes are considerable at all latitudes in the Atlantic and often much larger in the abyssal and deep ocean (Fig. 4.16 c) than at the surface. The warmer bottom water formed in the enlarged Weddell Sea flows down the continental slope and all the way into the North Atlantic, increasing the temperature of the deep Atlantic compared to the T20B0F0 experiment by approximately 1 °C. That further causes a strong increase in temperature in some parts of the North Atlantic and a decrease in other regions.

Since some of the changes manifest as a series of stripes of alternating temperature increases and decreases, it is likely that they are a result of insufficient integration time, that did not allow the model simulation to reach a steady state under the new conditions. The time necessary for the model to settle after such large changes in bathymetry near Antarctica is determined by the longest processes that are affected by those changes. Since production of AABW is one of the drivers of global thermohaline circulation (*Foldvik et al.*, 2004), and more than half of the total AABW flux is believed to have its origin in the Weddell Sea (*Orsi et al.*, 1999), changing the bathymetry in the

Weddell Sea can have a severe influence on the global conveyor belt. However, it can take thousands of years to completely exchange water through thermohaline circulation, indicating that the 500 years of spin-up might not be long enough. However, high computational costs are associated with an extension of the spin-up time, which was hence kept at 500 years while evaluating the impact of changes to the ocean simulation. After the advantages of the new model experiments are confirmed, the simulation will be continued until the steady state is reached and the artefacts are removed. The ice shelf forcing also causes some stripes, which can probably be fixed by running the model experiment for 30 instead of only 10 years, or by switching on the ice shelf forcing for the last 20–30 years of the spin-up.

Changes in mean surface salinity (Fig. 4.17 a) are largest in both polar regions and in the North Atlantic. In some parts of the North Atlantic they even exceed the standard deviation of the T20B0F0 experiment. At 500 m depth (Fig. 4.17 b) the changes are again more prominent than at the surface and affect the Atlantic Ocean most, while the changes in the Pacific are much smaller and the Indian Ocean is barely affected despite being closer to the origin of the changes. The vertical cross section in the Atlantic Ocean (Fig. 4.17 c) shows that the difference in salinity caused by bathymetry

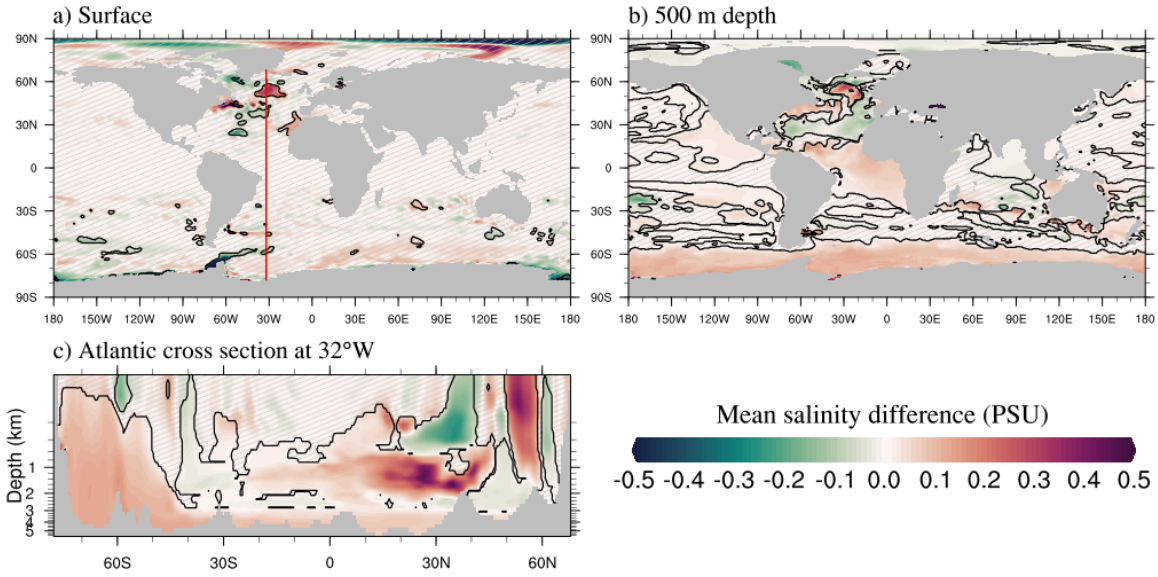

Figure 4.17: Difference in mean salinity between model experiments T20B1F1 and T20B0F0 in the surface layer (a), at 500 m depth (b), and in a vertical cross section through the Atlantic Ocean at 32°W (c). Areas where the difference between model experiments does not exceed the standard deviation of the T20B0F0 experiment are striped and their boundary is marked with black lines. The red line in (a) marks the location of the vertical cross section.

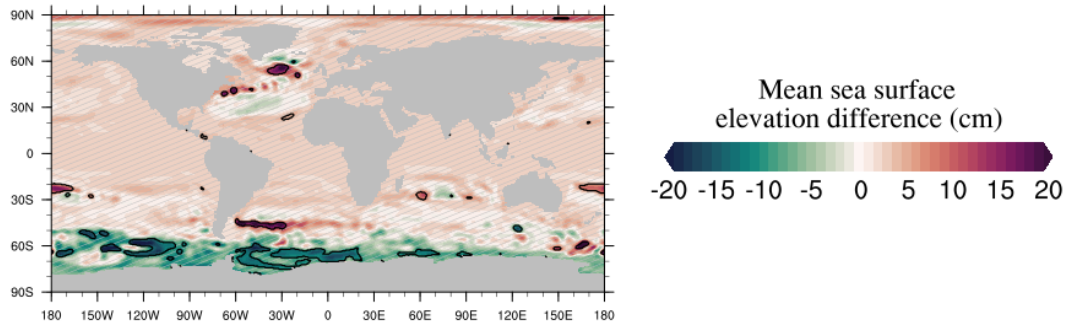

Figure 4.18: Difference in mean sea surface elevation between model experiments T20B1F1 and T20B0F0. Areas where the difference between model experiments does not exceed the standard deviation of the T20B0F0 experiment are striped and their boundary is marked with black lines.

modifications has a distribution very similar to the temperature difference. Regions of increased (decreased) temperature coincide with regions of increased (decreased) salinity because they are both advected by the same currents and their distribution is affected by the bathymetry of the Atlantic. An increase in both temperature and salinity at approximately 2 km depth in front of the Mid-Atlantic Ridge, for example, is caused by the accumulation of water in front of the obstacle, while the decrease in temperature and salinity behind it exists because the water in the Newfoundland Basin is not directly connected with the AABW. Since an increase in temperature reduces the water density, while an increase in salinity results in a density increase, these two changes between the T20B0F0 and T20B1F1 experiment partially cancel each other, thus affecting the formation of the AABW less than either temperature or salinity individually.

The changes in mean sea surface elevation (Fig. 4.18) are much larger in the Southern Ocean than in the rest of the world oceans. Apart from a very small region in the North Atlantic, they are insignificant compared to the standard deviation of sea surface elevation. There is also no seasonal dependence of sea level changes.

AMOC volume transport is defined as the maximum of the stream function, which can be calculated by integrating meridional velocity at a particular latitude:

$$\psi(z) = \int_{x_w}^{x_e} \int_{-H}^{z} v(x,z) dz dx \,, \tag{4.3}$$

where x_w and x_e are western and eastern boundaries, H is ocean depth, z is the vertical coordinate, and $v(x,z)$ is the simulated meridional velocity (*Stepanov et al.*, 2006). In most cases the transport is obtained by integrating the whole water column from ocean

bottom to the surface, but when the surface currents are predominantly southward the maximum of the stream function is located a few levels below the surface. The meridional heat transport across a trans-basin section is similarly calculated as:

$$Q = \int_{x_w}^{x_e} \int_{-H}^{0} \rho_0 c_p v(x,z)\theta(x,z) dx dz \,, \tag{4.4}$$

where ρ_0 is the average density of seawater, c_p is the specific heat capacity of seawater, and $\theta(x,z)$ is the simulated potential temperature. For both heat and volume positive values indicate a northward transport, while negative values represent predominantly southward transport. The transports are calculated for the 26.5°N latitude, to allow the comparison with in situ observations from the Rapid Climate Change Programme (RAPID) (*McCarthy et al.*, 2015). Since both volume and heat transport vary greatly from day to day, the time series are smoothed with a Gaussian-weighted moving average 60 days window, and the averages and standard deviations are calculated from the smoothed time series. Because average RAPID transports from *McCarthy et al.* (2015) and *Stepanov et al.* (2006) are calculated from the period between April 2004 and October 2007, simulated mean meridional transports are calculated from the same time span.

Despite the good quality of the simulated AMOC, most numerical models underestimate the meridional heat transport values compared to RAPID (e.g. *Mo and Yu*, 2012; *Haines et al.*, 2013; *Stepanov et al.*, 2006). The average meridional volume and heat transports calculated from the model output are given in Table 4.3, with the RAPID transports from *Stepanov et al.* (2006) for reference. The average volume transport from the RAPID array is 19±3 Sv (1 Sv = 10^6 m^3/s). As expected, all MPIOM

Table 4.3: Average meridional volume and heat transport through the Atlantic Ocean at 26.5°N calculated from the three MPIOM experiments, for the April 2004 – October 2007 time span, compared with the RAPID array observations (*Stepanov et al.*, 2006). Mean and standard deviation of the model experiments are calculated from the time series smoothed with a Gaussian-weighted moving average filter, while the RAPID array values are calculated from the monthly means.

	Volume (Sv)		Heat (PW)	
	Mean	SD	Mean	SD
T20B0F0	11.6	3.5	1.78	0.23
T20B1F0	6.6	6.3	1.26	0.15
T20B1F1	6.5	6.2	1.23	0.15
RAPID	18.8	3.4	1.33	0.40

experiments underestimate the AMOC transport, with 12±4 Sv obtained from the T20B0F0 experiment, and even lower value of 7±6 Sv from both experiments with modified model bathymetry. Nevertheless, all three values are within the usual range of simulated AMOC transports. It is unfortunate that the bathymetry modifications near Antarctica result in an even larger underestimation of the AMOC, but as previously mentioned, the system did not reach steady state, so it is possible that after a longer spin-up simulation with the new bathymetry, the simulated transport will be larger. Furthermore, MPIOM with its coarse 1° spatial resolution necessitates the use of many subgridscale parametrizations, such as horizontal and vertical viscosity or eddy-induced mixing. These parameters are a combination of those available from the literature, those gained via past experience with the HOPE or OMCT models, and those that were calibrated to give improved results as part of the model development process. The calibrated parameters, such as friction, diffusion, convection, and wind mixing are obtained with the T90B0F0 model experiment. Therefore, their values are most likely not the best options for the new model experiments, thus affecting the ocean circulation in a negative way. Tuning of the model is not a part of this study because its focus is the impact of bathymetry changes, which could be clouded by the new parameter choices. Before the model is used for any further study or as a part of AOD1B, however, the parameters need to be recalibrated with the new bathymetry and a shorter time step.

The heat transport, however, is overestimated in the T20B0F0 experiment, with its value of 1.8±0.2 PW, compared to 1.3±0.4 PW from the RAPID array. The values from both the T20B1F0 and the T20B1F1 experiment, 1.3±0.2 PW and 1.2±0.2 PW respectively, are much closer to the observed heat transport. Even though the new experiments increase the temperature of the Antarctic Bottom Water, the simulated decrease in meridional speed on average results in a decreased meridional heat transport.

The temporal variability of the meridional volume and heat transport (Fig. 4.19) shows that differences between the model experiments are not uniform. While the T20B1F1 volume transport is lower than that calculated from the T20B0F0 experiment during most of the simulated time span, there are periods with barely any difference, such as in late 2004 and early 2005, and during year 2009, as well as periods when the T20B1F0 and T20B1F1 experiments simulate larger transport, such as during year 2010. The heat transport simulated by the experiments with the new bathymetry is significantly lower throughout the whole simulated time span, with the exception of a short time during year 2010. This heat transport decrease is caused by a layer of decreased temperature at around 500 – 1,000 m depth, as well as by small decreases in meridional velocity. While the difference between the T20B0F0 and T20B1F0 model

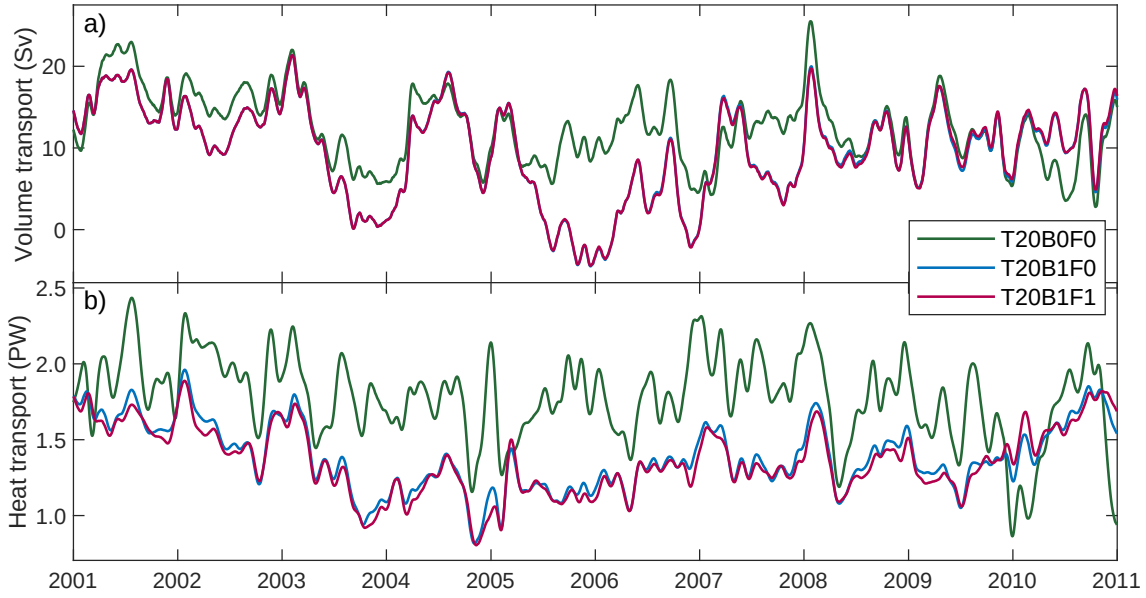

Figure 4.19: Meridional volume (a), and heat (b) transport through the Atlantic Ocean at 26.5°N calculated from three MPIOM model experiments, smoothed with a Gaussian-weighted moving average filter with 60 days window length.

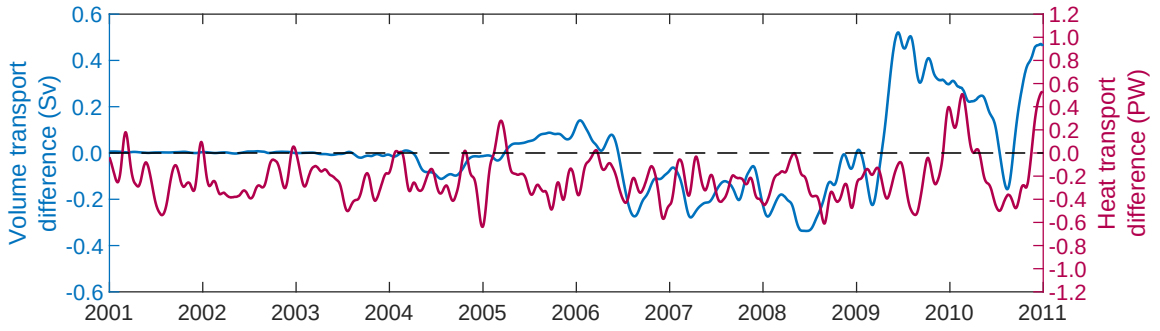

Figure 4.20: Difference in meridional volume and heat transport through the Atlantic Ocean at 26.5°N between T20B1F1 and T20B1F0 model experiments, smoothed with a Gaussian-weighted moving average filter with 60 days window length.

experiment in both volume and heat transport is pretty obvious, the impact of ice shelf forcing is much smaller. Since it is not possible to distinguish between the two volume transports from Fig. 4.19, the difference between T20B1F1 and T20B1F0 model experiment is shown in Fig. 4.20. No difference in volume transport between the two experiments is noticeable for the first 4 years after including the ice shelf forcing into the simulation. The difference becomes larger only towards the end of the simulation, indicating that if the simulation is continued for several decades, the ice shelf melting

rates and temperature forcing might have an impact on the AMOC transport at 26.5°N. At a first glance, the impact of ice shelf forcing on heat transport seems pretty large compared to the impact of bathymetry changes. However, time is necessary for any change originating near Antarctica to propagate to the northern hemisphere, so the fact that the magnitude of the difference does not change from the beginning until the end of the simulation is an indicator that those differences are random fluctuations, not a result of physical processes related to ocean – ice shelves interactions near Antarctica.

4.6 Comparison against global ocean reanalysis data

It was demonstrated that modifying the bathymetry around Antarctica and simulating the influence of Antarctic ice shelves changes the ocean model results not just in the vicinity of modified regions, but also in the whole ocean, especially the Northern Atlantic. To investigate whether those changes bring the model output closer to the observed state of the ocean, the results are compared with an independent dataset, the GLORYS2v4 ocean reanalysis (*Garric and Parent*, 2018), in which the outputs from a numerical ocean general circulation model are combined with observations to generate a synthesized estimate of the state of the global ocean.

The ocean model used for the GLORYS2v4 dataset is Nucleus for European Models of the Ocean (NEMO) version 3.1, with a tripolar ORCA grid type (*Madec and Imbard*, 1996) at 1/4° horizontal resolution, which corresponds to 27 km at the equator and 12 km at high latitudes. The vertical grid has 75 z-levels and the bathymetry used in the system is a combination of the interpolated ETOPO1 database (*Amante and Eakins*, 2009) in regions deeper than 300 m and GEBCO8 (*Becker et al.*, 2009) in regions shallower than 200 m, with linear interpolation in the 200 – 300 m layer. At the surface the reanalysis system is driven by the ERA-Interim reanalysis products (*Dee et al.*, 2011), with corrections applied to the precipitation and radiative fluxes due to their known biases. The assimilated data consist of satellite measured sea surface temperature (SST) and sea level anomaly (SLA) data, in situ temperature and salinity profiles, and sea ice concentration. SLA is provided by CMEMS SLA TAC from the SEALEVEL-GLO-SLA-L3-REP-OBSERVATIONS-008-001-b product, which includes data from all altimeter missions: Sentinel-3A/B, Jason-3, HY-2A, Saral[-DP]/AltiKa, Cryosat-2, OSTM/Jason-2, Jason-1, Topex/Poseidon, Envisat, GFO, and ERS-1/2 (*Pujol and Mertz*, 2019). The SST is assimilated from the daily Reynolds 1/4° AVHRR-only SST version 2 product (*Reynolds et al.*, 2007). In situ temperature and salinity profiles are assimilated from the CORA 4.1 database provided by CMEMS IS TAC (*Szekely*, 2019), and the sea ice concentration is taken from the IFREMER/CERSAT

products (*Ezraty et al.*, 2007).

Temperature and salinity from the three MPIOM experiments are compared to the temperature and salinity from GLORYS2v4. GLORYS2v4 also provides sea surface height fields, but since those fields are given as the sea surface height above the geoid, while the sea level calculated by the MPIOM experiments is the surface elevation above the highest vertical level, those two values are not comparable without including a third dataset that provides the geoid information. Comparison with sea level from altimetry would be affected by the same issue. Because GLORYS2v4 has a higher spatial resolution, both in the horizontal and in the vertical, it has been interpolated to the same 1° grid as the MPIOM experiments and the values from the top 6 vertical layers, covering the water layer from the surface to 6.54 m depth, are averaged to compare them with the MPIOM surface layer. Only surface temperature and salinity are used for validation of the new MPIOM experiments even though the GLORYS2v4 dataset provides information for the whole water column, because most of the assimilated observations in GLORYS2v4 are satellite based, so their impact is the largest at the surface, while the information at the depths is mostly model based.

For validation standard deviation reductions are calculated, i.e. the reduction in standard deviation of the GLORYS2v4 reanalysis, when an MPIOM experiment has been subtracted from it (Eq. 2.1). It is calculated for each grid point separately, which allows us to distinguish the areas where the model performs well and to pinpoint the regions where the model might have issues in simulating the processes contained in the reanalysis. A positive standard deviation reduction indicates that a substantial amount of variability contained in the reanalysis dataset is also predicted by the MPIOM model experiment, and zero or negative values suggest that the model simulates virtually no variability contained in the reanalysis. Seeing that the standard deviation reductions are fairly similar for different MPIOM experiments, thus hindering their visual comparison, only the standard deviation reductions for the T20B0F0 model experiment are shown. For the other experiments, the differences between two experiments are calculated, clearly showing the regions with improvements (positive values) and degradations (negative values) between the two MPIOM model experiments.

The reduction of standard deviation of surface temperature (Fig. 4.21 a) calculated for the MPIOM T20B0F0 experiment shows that temperature is very well simulated by MPIOM. It is positive everywhere in the mid-latitudinal ocean, with values usually exceeding 80 %. The correspondence is not that good in the equatorial area, even though the values of standard deviation reduction are usually positive, with an area in the Western Pacific having small negative values as an exception. The largest issue exists in the polar regions, especially near the Antarctic coast, where there is no

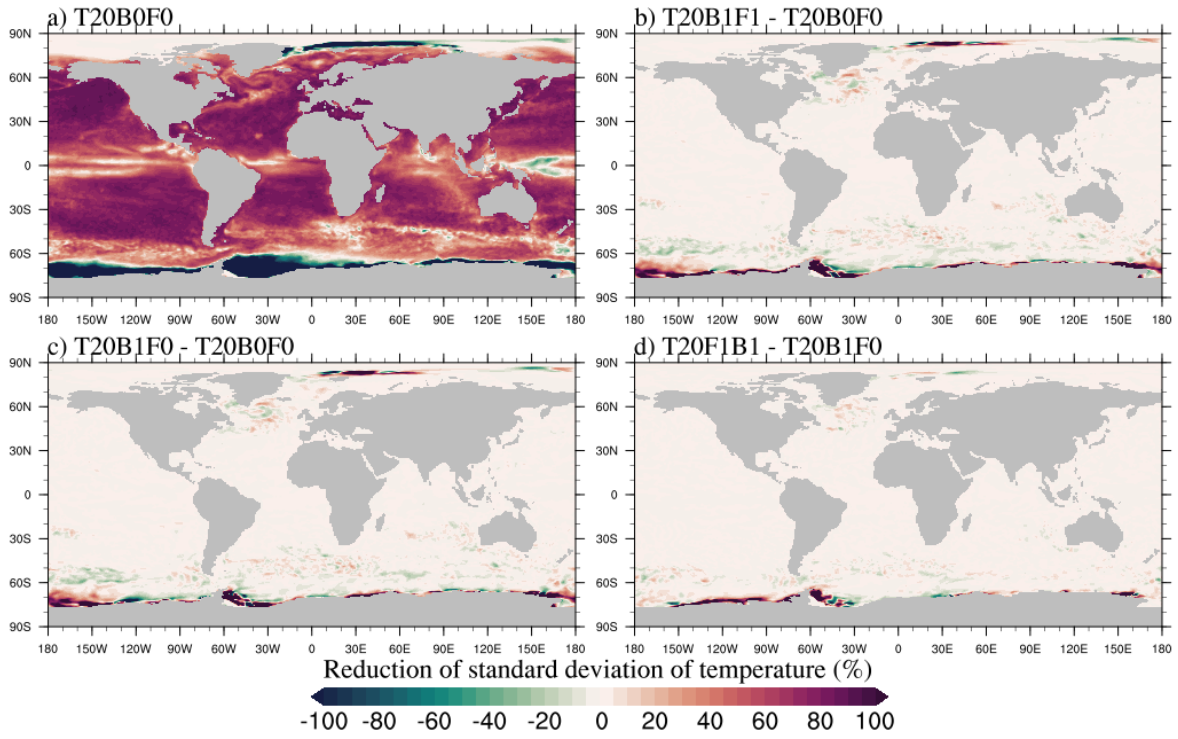

Figure 4.21: Reduction of standard deviation of temperature when MPIOM T20B0F0 has been subtracted from GLORYS2v4 (a). Improvement in standard deviation reduction when the bathymetry has been modified and ice shelf forcing taken into account (b), when considering only the bathymetry modifications (c), and when considering only ice shelf forcing (d).

correspondence at all between MPIOM and the reanalysis. The improvement in the simulation of temperature when the ice shelf influence is included into MPIOM is considerable (Fig. 4.21 b). It is mostly limited to the coast of Antarctica and the Arctic, which are the regions in which MPIOM T20B0F0 has the poorest results, with some minor changes in the North Atlantic. The impact of bathymetry changes (Fig. 4.21 c) and the inclusion of ice shelf forcing (Fig. 4.21 d) have a similar magnitude, but are most prominent in slightly different regions. While the bathymetry changes have the largest influence in the Ross and the Weddell Sea, where the bathymetry modifications are the largest, the ice shelf forcing affects most the areas off the coast of West Antarctica, where the ice shelf melting is the fastest and the difference between ice shelf and atmospheric temperature is the largest.

Standard deviation reduction of surface salinity (Fig. 4.22 a) of the MPIOM T20B0F0 model experiment is overall much lower than for temperature. It rarely exceeds 60 % anywhere and there are several areas where it is negative. Salinity has worst correspondence in the ACC region and in the North Atlantic, which are the regions most

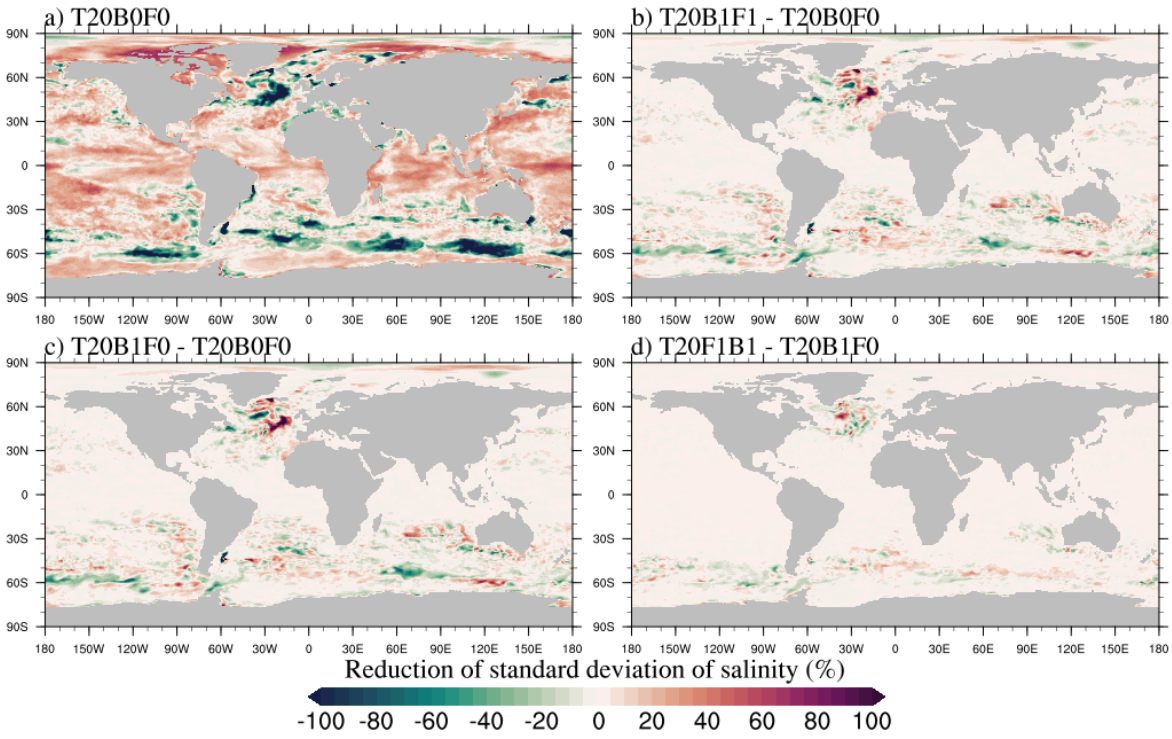

Figure 4.22: Reduction of standard deviation of salinity when MPIOM T20B0F0 has been subtracted from GLORYS2v4 (a). Improvement in standard deviation reduction when the bathymetry has been modified and ice shelf forcing taken into account (b), when considering only the bathymetry modifications (c), and when considering only ice shelf forcing (d).

affected by the Antarctic bathymetry and the thermohaline circulation. The total improvements (Fig. 4.22 b) are indeed mainly visible in those regions, increasing the very low standard deviation reductions and somewhat reducing the area with negative reductions. Surprisingly, the impact is stronger in the North Atlantic than in the vicinity of the changes implemented into the model. The improvements caused by the bathymetry modifications (Fig. 4.22 c) are larger and cover larger areas than those purely due to the ice shelf forcing (Fig. 4.22 d).

There are some areas where the changes made to the model cause a decrease in standard deviation reductions, deteriorating the model results compared to the reanalysis. The degradations related to bathymetry modifications might be prevented by using a longer spin-up and by recalibrating the subgridscale parameters for the new model domain. The recalibration was not performed in this case because changing other parameters would cloud the influence of bathymetry and forcing changes. The degradations caused by ice shelf forcing suggest that the temperature and ice shelf melting rates used in the T20B1F1 simulation are not accurate enough, which could be fixed by using more

realistic values, for instance by taking into account different temperatures and melting rates for each ice shelf, or by considering their temporal variability. Another possible cause for some of the degradations can be found in the reanalysis. To allow the validation of new MPIOM experiments, the GLORYS2v4 reanalysis dataset is considered as a perfect representation of the true state of the ocean, which is not entirely correct. By assimilating observations, it is much closer to reality than the unconstrained MPIOM, but it is still largely based on a model experiment that does not simulate the dynamics under the ice shelves. Therefore, it can be expected that a model simulation that uses a comparable bathymetry (T20B0F0) will in some aspects resemble the reanalysis better than one that uses a significantly different bathymetry. Nevertheless, there are improvements visible in both sea surface temperature and salinity fields after the areas beneath the ice shelves are included and the ice shelf forcing is simulated, indicating that the new model experiments with MPIOM are promising and can help to improve the model.

5

Development of AOD1B

GRACE and GRACE-FO satellites measure the variations in the Earth's gravity field due to the redistribution of mass in the Earth's hydrosphere, cryosphere, atmosphere, oceans, and solid Earth. Typically, data from 30 days are accumulated to calculate one global gravity field model (*Dobslaw et al.*, 2013). Even though GRACE can capture the low frequency variations and long-term trends caused by processes in the solid Earth, ice, and terrestrial water pretty well, ocean and atmosphere are dominated by submonthly processes. When data from 30 days of observations are combined into one gravity field, submonthly atmospheric and oceanic variability can alias into the gravity solution. Therefore, such processes are usually simulated with an a priori background model and removed from GRACE data. Using background models also allows the vertical separation of the signal, because satellite gravimetry is inherently insensitive to discriminate between signals above, on, and below the surface.

Atmosphere and Ocean Dealiasing Level 1B (AOD1B) product, currently at release 06, is used for estimating and removing non-tidal atmospheric and oceanic variability from GRACE. It is based on ocean bottom pressure simulated by an ocean general circulation model, forced by temperature, moisture and pressure fields from the European Centre for Medium Range Weather Forecasts (ECMWF) reanalysis and weather prediction model. It is important to continuously work on improving the AOD1B product because any improvements in the background models reduce the GRACE error budget.

5.1 Validation of AOD1B RL06

This section is based on the publication C1:
H. Dobslaw, I. Bergmann-Wolf, R. Dill, **L. Poropat**, M. Thomas, C. Dahle, S. Esselborn, R. König, and F. Flechtner (2017): **A new high-resolution model of non-tidal atmosphere and ocean mass variability for de-aliasing of satellite gravity observations: AOD1B RL06**, Geophysical Journal International, 211, 263-269, doi: 10.1093/gji/ggx302.

Validation against in situ ocean bottom pressure (OBP) time series was a very valuable tool during the development of AOD1B RL06. There are several differences between AOD1B RL05 and RL06, the largest of them being the change in the ocean model. The decision to switch from the Ocean Model for Circulation and Tides (OMCT; *Thomas*, 2002), which is used in AOD1B RL05, to the Max Planck Institute Ocean Model (MPIOM; *Jungclaus et al.*, 2013), is mainly based on the validation against in situ OBP. While the performance of the two models is very similar in most regions of the world ocean, MPIOM has a clear advantage in the Arctic Ocean, due to its curvilinear grid that allows better positioning of the model poles. MPIOM is modified for usage in AOD1B based on the experience with OMCT. After each modification, OBP from the new model experiment is validated against in situ observations by calculating the relative explained variances (Eq. 2.1).

In the end, when the suitable modifications are implemented, the difference in relative explained variance between RL05 and RL06 is calculated (Fig. 5.1). Since the model is used for dealiasing GRACE monthly solutions, the focus of the validation is on submonthly frequencies. Therefore, both in situ and simulated time series are separated into three distinct submonthly frequency bands. The lower frequencies are not considered here because uninterrupted in situ records are typically shorter than 2 years, the contribution of barystatic sea level changes not modelled by AOD1B increases at seasonal to interannual time-scales, and reliability of in situ observations decreases at longer periods due to sensor aging and resulting non-linear drifts in the time series. The validation concentrates only on years 2004 – 2008 because the global coverage with in situ OBP observations is best during that timespan.

In the 1 – 3 days period band, the improvements are largest in the Arctic Ocean, where the ocean dynamics benefit most from the curvilinear grid used in MPIOM. There are also significant improvements throughout the Pacific, but the RL06 performs worse in the Gulf of Alaska. Both versions of AOD1B perform best in the 3 – 10 days period band, but there are significant improvements in the ACC region, as well as again in the Arctic. For the longest analysed periods, 10 – 30 days, relative explained variances

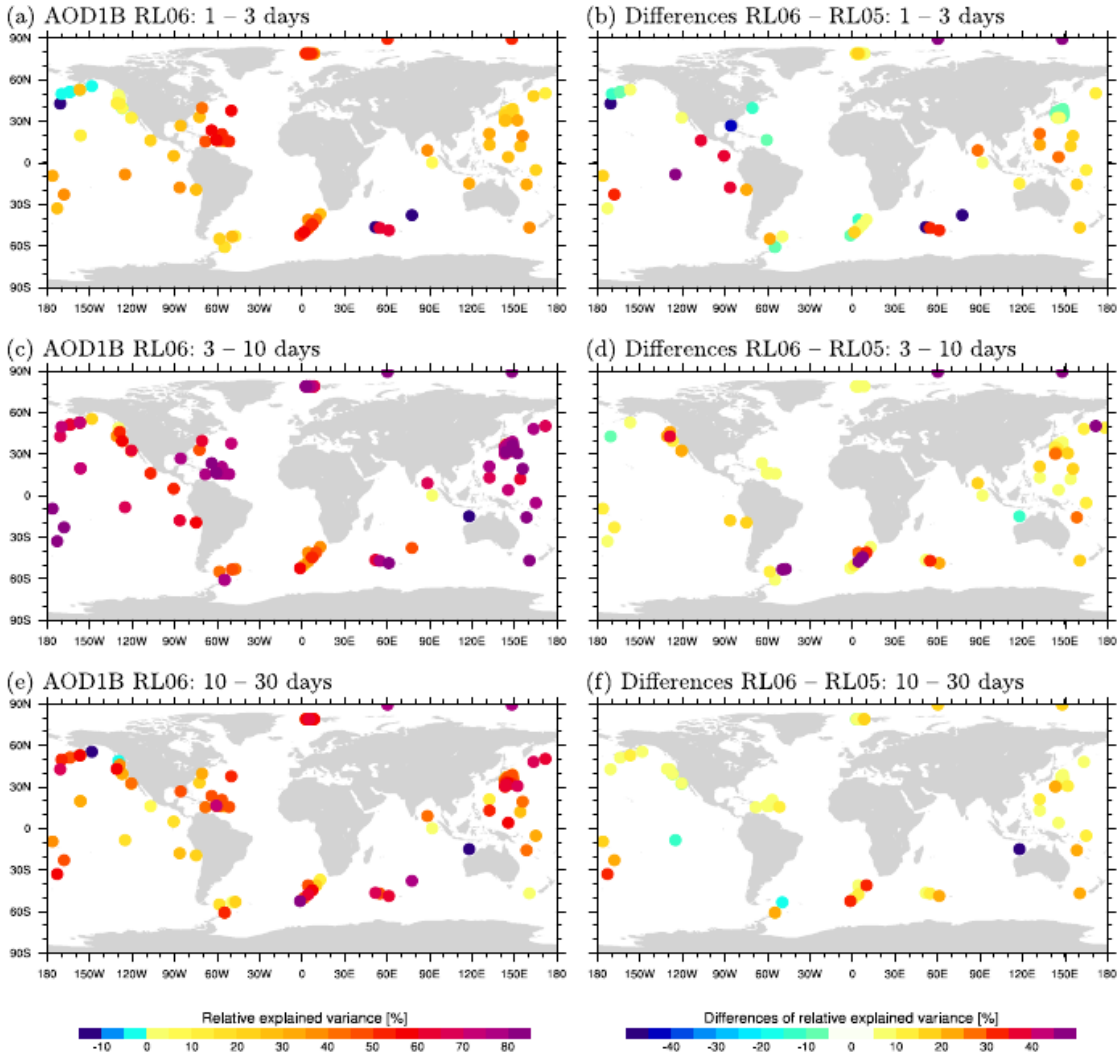

Figure 5.1: Relative variances (percent) of in situ ocean bottom pressure observations explained by AOD1B RL06 (left), and the differences between relative variances explained by RL06 and RL05 (right) that have been bandpass filtered for periods of 1 – 3 days (top), 3 – 10 days (middle) and 10 – 30 days (bottom).

are generally lower and both releases show an approximately similar fit to the in situ observations.

5.2 Towards AOD1B RL07

Already during the development of AOD1B RL06, it was known that among many improvements achieved by replacing OMCT with MPIOM, there was one thing that OMCT did better: unlike MPIOM, it did simulate the dynamics beneath the Antarctic ice shelves. While the advantages overpowered the downside, allowing AOD1B RL06 to be published without the inclusion of the full area of the Southern Ocean, those areas need to be included eventually to improve the dealiasing model for GRACE even more. After performing new MPIOM experiments with modified bathymetry, they are tested in the same way as AOD1B RL06 was, by comparing them with in situ ocean bottom pressure time series. Ocean bottom pressure is used because, in order to use it as a dealiasing background model, it is important to know how the model predicts variations of mass due to the ocean dynamics.

Ocean bottom pressure from T20B0F0, T20B1F0, and T20B1F1 model experiments is separated into three bands: periods smaller than 3 days, 3 – 10 days periods, and 10 – 30 days periods. Only the submonthly variability is analysed because it is most relevant for the dealiasing model. The standard deviation of differences between the three model experiment and for the three frequency bands is calculated (Fig. 5.2),

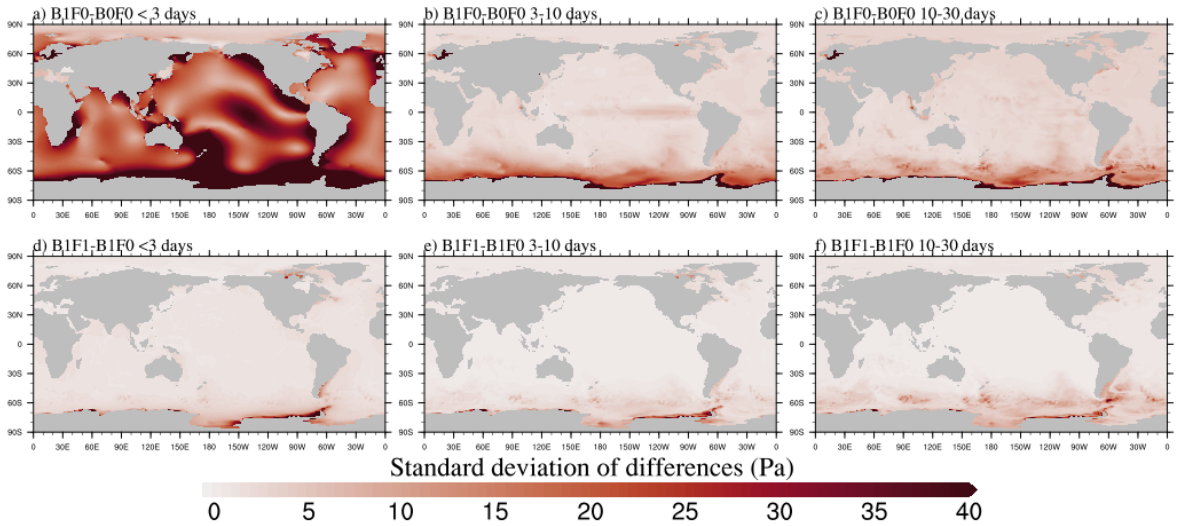

Figure 5.2: Standard deviation of differences in ocean bottom pressure between the T20B1F0 and T20B0F0 model experiment (top), and between the T20B1F1 and T20B1F0 model experiment (bottom) calculated separately for the < 3 days (left), 3 – 10 days (middle), and 10 – 30 days (right) period band. The color scale does not display the full variability in (a), which exceeds 150 Pa near Antarctica, to make it comparable with the other figures.

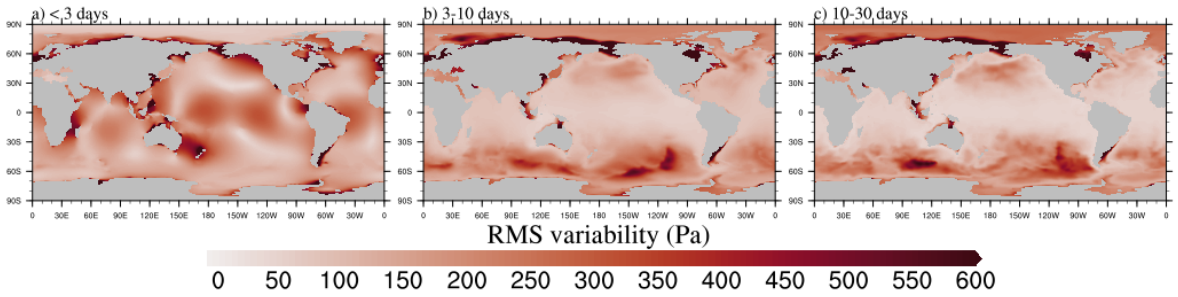

Figure 5.3: Standard deviation of ocean bottom pressure in < 3 days (a), $3 - 10$ days (b), and $10 - 30$ days (c) period band calculated from the T20B1F1 model experiment.

and can be compared with the standard deviation computed from the T20B1F1 model experiment (Fig. 5.3), which displays the typical geographical distribution of variability in each frequency band.

Periods shorter than 3 days are clearly dominated by the ocean response to the atmospheric tides, specifically the S2 constituent with a period of 12 h. When the bathymetry is modified, the amplitude maxima and phase lags of the tides are shifted to adjust to the new bathymetry, resulting in an increased variability band from the Ross Sea, over New Zealand, to the east coast of Australia. Changes in variability due to bathymetry modifications are much smaller and mostly limited to the Southern Ocean on other frequency bands. The largest changes in areas further away from the Antarctic coast are related to the maxima in the ACC variability. There is also a noticeable change at the equator in the $3 - 10$ days band, which might be a result of model characteristics instead of realistic physical processes. MPIOM is known to overestimate the quantities in that region and it can be sensitive to small changes. A very large change in the Baltic Sea is caused by the local bathymetry modifications, but it does not extend further away from the Baltic.

Simulating the ice shelf forcing has a much smaller influence. For the shortest periods, it is almost completely limited to the coast of Antarctica, but it surprisingly also causes some changes on the other side of the world, in Baffin Bay. These changes are not reflected in the mean changes of temperature, salinity or sea surface elevation. Since there are no known processes on such a short temporal scale that could originate on the southern hemisphere and affect the northern polar region, it is most likely a numerical artefact that needs to be taken care of before the model experiment can be used in an official dealiasing product. For longer periods, changes in the Arctic decrease, while changes in the Southern Ocean spread further away from the continent, extending to 40°S. As expected, the largest changes in variability are found in the vicinity and east of the areas with strongest ice shelf forcing, West Antarctica, and Antarctic Peninsula.

Finally, OBP simulated by the new MPIOM experiments is validated against in situ OBP. Although for most of the analysis, only the second half of the simulation results was utilized to allow the model enough time to adjust to the new forcing data, using the same timespan for validation against in situ OBP results in only approximately 50 time series comparisons. To be able to fully utilize the in situ OBP database, the whole simulated timespan (2001 – 2010) is used, resulting in relative explained variances at 154 locations across the world ocean. Since the differences between the model simulations are very small, only the explained variances for T20B1F1 experiment are shown (Fig. 5.4). The results of OBP validation of the T90B0F0 model experiment, which is the starting point for this study, are shown in Fig. 2.5. Apart from a longer time step, it is equivalent to the T20B0F0 experiment used for comparison throughout this work.

In terms of OBP variability, MPIOM performs best for periods between 3 and 10 days. In this band relative explained variances are positive for every single in situ time series, most of them are above 60 % and more than half of them exceed 80 %. Variability in OBP at these periods is largely dominated by the wind-driven ocean circulation, suggesting that the physics behind that process is already well implemented into MPIOM. For periods between 10 and 30 days, when density effects have an increasingly growing influence on the in situ measurements, most stations have relative explained variances in the 50 – 60 % range, with only a few negative stations. The worst results are obtained for the shortest periods. Even though the tidal signals are removed from the in situ time series by means of classical harmonic analysis, for many stations some tidal residuals are left in the series. Furthermore, while the ocean tides are not simulated by MPIOM, the atmospheric tides are are included in the atmospheric forcing from ERA-Interim, resulting in quite prominent response of the ocean on approximately diurnal and semidiurnal periods (as seen in Fig. 5.3 a). To avoid those signals affecting the validation, a low pass filter has been applied to both in situ and simulated time series, in order to filter out most of the residual tidal signals from the highest analysed frequency band. Consequently, the results for the periods below 3 days are worse than for the longer periods, but still positive for most of the in situ stations. There is also a clear geographical dependency of the explained variances, with results in the Atlantic, Southern, and Arctic Ocean being much better than in the Pacific.

Finally, the differences in relative explained variances between the T20B1F1 and the T20B0F0 model experiment are calculated (Fig. 5.5). For the longer periods there is virtually no difference between the model experiments. All differences in explained variances are negligible (<2 %), and are more or less equally divided between improvements and deteriorations. Considering the excellent results already for the MPIOM T90B0F0 model experiment (Fig. 2.5), with relative explained variances often exceed-

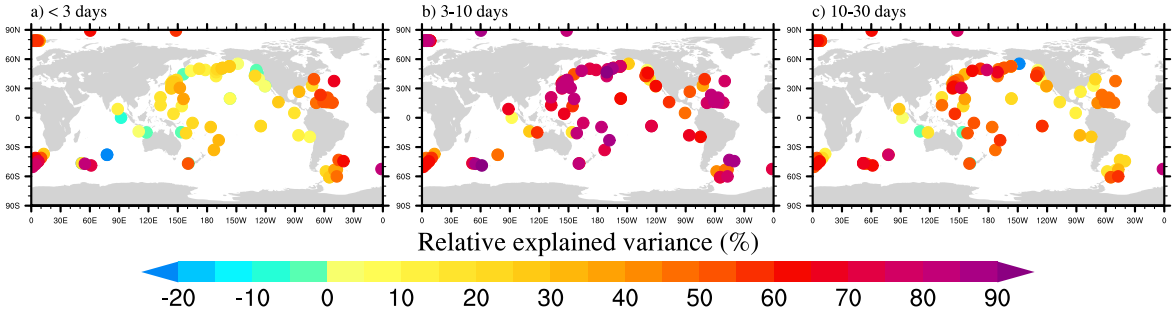

Figure 5.4: Relative explained variance of the in situ OBP data when the MPIOM T20B1F1 model experiment has been subtracted for the < 3 days (a), 3 – 10 days (b), and 10 – 30 days (c) period band.

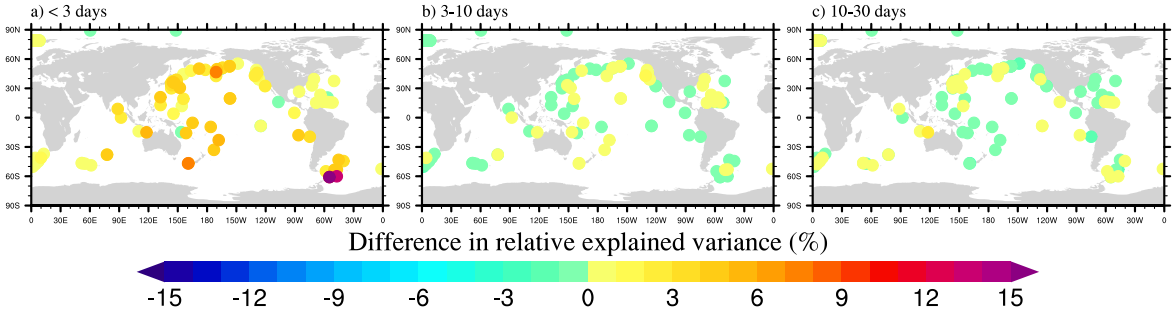

Figure 5.5: The difference in relative explained variances between the T20B1F1 and T20B0F0 model experiment for the $<$ 3 days (a), 3 – 10 days (b), and 10 – 30 days (c) period band.

ing 90 % for the 3 – 10 days periods, it is unlikely that a global ocean model can surpass that. Even with the difficulties of perfect general ocean circulation simulation set aside, there are always measuring and data processing errors that make the possibility of a 100 % correspondence between any two independent datasets highly unlikely. Therefore, improvements on that frequency band are not expected. For the shortest periods, however, a significant improvement is caused by the changes in the model experiments. The geographical distribution of the improvements corresponds almost perfectly with the areas of lowest relative explained variances in the older model experiment (Fig. 2.5 b), increasing the relative explained variances in the Pacific Ocean by on average 5 %. Somewhat unexpectedly, the improvements in the simulation of ocean bottom pressure are larger in the Pacific than in the Atlantic, as could be anticipated from the global mean temperature, salinity, and sea level changes from Section 4.5. However, that can easily be explained by the geographical distribution of in situ stations in the Atlantic, namely there are no stations in the area of the North Atlantic, which is most affected by the bathymetry changes in the model. The largest improvements can be found in the few southernmost stations that directly measure the

variability in the ACC, where the improvements in OBP relative explained variance exceed 10 %.

The analysis of the high frequency OBP variability obtained with the T20B1F0 and T20B1F1 MPIOM experiments demonstrates the impact of changes on high frequency ocean mass redistribution relevant for the GRACE dealiasing model AOD1B. Apart from showing the extent of the influence of the dynamics beneath Antarctic ice shelves, it also points out some suspicious signals that need to be studied further and possibly fixed before this model experiment is ready to be included into the next release of AOD1B. However, the validation against in situ OBP confirms that the changes done to the MPIOM bathymetry and the subsequent attempt to include the influence ice shelf melting and temperature might have on ocean circulation, are undeniably in the right direction. After including some further changes into the model, recalibration, and a longer spin-up simulation, the MPIOM T20B1F1 experiment will be the basis for the new AOD1B RL07.

6

Conclusions and outlook

In this dissertation, ocean signals observed by in situ OBP recorders and GRACE satellites, as well as simulated by an ocean general circulation model, are analysed and intercompared. The combined results of all the incorporated studies demonstrate that to get a clear picture of the ocean mass variability, all three sources of data are necessary. The in situ OBP data have the highest accuracy and temporal resolution for the locations in which the pressure recorders are deployed, but those are very sparse and irregularly distributed, covering the northern hemisphere relatively well, but with barely any coverage in the southern hemisphere. GRACE satellites provide a global coverage for measurements of oceanic (and other) mass variations, but the provided GRACE gravity fields typically have only monthly temporal resolution. To study the high frequency mass variability throughout the ocean, not just at a few selected location, we usually still need to use global ocean models, although GRACE is also showing an ability to capture at least some submonthly signals. To properly separate the signals from GRACE and prevent aliasing an ocean model is also needed.

Ocean bottom pressure signals: The analysis of OBP time series observed by satellites and in situ and simulated by an ocean model is the topic of the first study, which confirms that those three data sources are indeed comparable. A procedure to use in situ measured OBP time series for validation of models and GRACE gravity fields is explained. Comparing the model output from an MPIOM experiment with highly accurate in situ measurements from the few locations with available in situ data shows

that the model performs well at those locations, which increases the confidence into the model and its performance in the locations for which we do not have observations. The same principle can be applied to GRACE gravity fields, although it is shown that the validation against in situ OBP works better for high frequency signals than for monthly means, which is the typical sampling of GRACE fields. One difference between GRACE and in situ OBP that needs to be kept in mind when performing such comparisons is that in situ measurements are pointwise, while GRACE only detects averages over large areas. That can impact the validation results in regions with high spatial variability, where the in situ time series might not be representative for the larger area captured by GRACE. For that reason, using a pattern filter to detect regions of coherent variability around each in situ station improves the results when validating GRACE data. If an attempt to compare different GRACE solutions by means of validation against in situ OBP data is made, all GRACE solutions need to be post-processed in the same way, because it is shown that post-processing choices can severely impact the results.

GRACE: In the second part of the dissertation, which is focused on GRACE observations, a comparsion is done between five monthly GRACE gravity field solutions from different institutions, as well as with a combined solution created within the EGSIEM project. The validation against in situ OBP shows that the CSR RL05, ITSG-Grace2016, and EGSIEM solutions outperform the JPL RL05.1, GFZ RL05a, and AIUB RL02 solutions, which is confirmed by the validation against GNSS data. A detailed analysis of the ITSG-Grace2016 daily Kalman solutions and their comparison against in situ OBP demonstrates that there are significant submonthly signals captured by GRACE, that are not simulated by the dealiasing background model applied to the GRACE data.

MPIOM experiments: Initially instigated by the need to improve the dealiasing background model for GRACE, but also motivated by the importance of polar regions for the world's climate, new model experiments with MPIOM are performed, to demonstrate the influence of Antarctic ice shelves on the simulated ocean circulation. Modifying the bathymetry to include the full extent of the Weddell and the Ross Sea, as well as the areas beneath most of the smaller ice shelves at the coast of Antarctica has a large influence on sea ice thickness, temperature, salinity, and sea surface elevation, not just in the vicinity of Antarctica, but also in the North Atlantic, confirming the assumption that the processess near Antarctica affect the meridional overturning circulation to a high degree. The changes in the mean temperature exceed 1 °C in some areas, while those in salinity are of the 0.5 PSU order of magnitude. The changes are much larger and more significant at and below 200 m depth than they are at the surface. The mean sea level is affected in the whole ocean, with a large decrease of more than 10 cm near Antarctica and a much smaller increase of approximately 3 cm

everywhere else, but those changes are not significant compared to the usual day-to-day sea level variability. The influence of the ice shelves on ocean dynamics is included into the model by a simple modification of atmospheric forcing. Since the ice shelves are blocking the interaction between the ocean and the atmosphere, the wind stress is masked in areas covered by ice shelves, and the atmospheric temperature and precipitation are replaced by simple estimates of ice shelf base temperatures and melting rates. The resulting changes are mostly limited to the areas in the immediate vicinity of the ice shelves and to the upper 200 m water layer. During the austral summer there is a temperature decrease along the West Antarctic coast, and during the whole year there is a decrease in salinity beneath and near the ice shelves with largest melting rates. Some of the patterns in the mean differences, especially those in the vertical cross-section through the Atlantic, indicate that the spin-up time of only 500 years is not long enough for the model to adapt to the changes because the meridional overturning circulation is much slower. The ice shelf forcing should also be applied for a longer period to fully influence the global circulation. The AMOC volume and heat transports are lowered in the new experiments, which underestimates the volume transport, but brings the heat transport closer to the values from the RAPID array observations. The MPIOM model experiments are compared with the GLORYS2v4 ocean reanalysis, demonstrating that the changes caused by the model modifications are bringing the MPIOM output closer to the state of the ocean contained in the reanalysis, especially in the regions where the difference between MPIOM and the reanalysis dataset is the largest.

AOD1B development: In the last part, in situ OBP time series are used to compare different releases of AOD1B. It is shown that RL06 is an improvement compared to RL05 in almost all locations and all frequency bands. The largest improvement is seen in the Arctic Ocean, where the difference in relative explained variance is 50 %, indicating that it was a good decision to switch from a model with equiangular grid with poles located at geographical poles, to a model that uses a curvilinear grid that allows positioning of the poles over the continents, thus avoiding a singularity at the north pole. The analysis of ocean bottom pressure simulated by the new MPIOM model experiments shows the extent of changes in high frequency oceanic variability caused by the bathymetry changes near Antarctica, and by the implementation of simple ice shelf forcing. It also exposes some issues with the results that need to be checked and fixed before the implementation of the new model experiment into AOD1B RL07. Nevertheless, the validation of the new experiment against in situ OBP demonstrates that simulating the dynamics under the Antarctic ice shelves improves the MPIOM OBP simulation for the highest frequencies, making it a first step towards the next AOD1B release.

The findings of this thesis highlight that the changes in ocean circulation caused by bathymetry modifications around Antarctica are significant enough that they should be included in the global ocean model. With those improvements, the new release of the AOD1B product will further improve the quality of the GRACE gravity field solutions, which in turn will allow us to monitor the mass induced component of the sea level with GRACE even better. In the future, the new experiments with MPIOM need to be continued with a much longer spin-up time, before including them into the new AOD1B release. Additional experiments with varying ice shelf melting rates or even ice shelf areas can be performed, to test how the melting of the ice shelves due to the ongoing climate changes can affect the ocean circulation. Ideally, a coupled ocean – ice sheet model could be used to fully capture the influence of Antarctic ice shelves on global circulation, as well as to simulate the effect changes in seawater temperature and ocean circulation have on ice shelf basal melting rates and thus on the mass loss of the Antarctic ice sheet.

Nomenclature

List of Symbols

C	Courant number	
c	wave speed	[m s^{-1}]
c_p	specific heat capacity of seawater	[J kg^{-1} K^{-1}]
Δt	time step	[s]
Δx	distance between two grid points in the zonal direction	[m]
G	GRACE observations	
g	acceleration of gravity	[m s^{-2}]
H	water depth	[m]
m	model	
o	in situ observations	
ψ	stream function	[Sv]
Q	merdional heat transport	[PW]
ρ_0	mean density of seawater	[kg m^{-3}]
S	standard deviation	
SR	standard deviation reduction	[%]
t	time	[s]
θ	seawater potential temperature	[°C]
v	meridional ocean speed	[m s^{-1}]
VE	relative explained variance	[%]
x	spatial coordinate in the zonal direction	[m]
z	vertical coordinate	[m]

Abbreviations

ACC	Antarctic Circumpolar Current
AIUB	Astronomical Institute of the University of Bern
AABW	Antarctic Bottom Water
AMOC	Atlantic Meridional Overturning Circulation
AOD1B	Atmosphere and Ocean Dealiasing Level 1B
ASOF–N	Arctic–Subarctic Ocean Fluxes North
AWI	Alfred Wegener Institute
BPR	Bottom Pressure Recorder
CFL	Courant-Friedrichs-Lewy
CSR	Center for Space Research
DART	Deep-ocean Assessment and Reporting of Tsunamis
DJF	December, January, and February (northern winter and austral summer)
ECMWF	European Centre for Medium-Range Weather Forecasts
EGSIEM	European Gravity Service for Improved Emergency Management
GFZ	*GeoForschungsZentrum* (German Research Centre for Geosciences)
GNSS	Global Navigational Satellite System
GPS	Global Positioning System
GRACE	Gravity Recovery and Climate Experiment
GRACE–FO	GRACE Follow-On
JJA	June, July, and August (northern summer and austral winter)
JPL	Jet Propulsion Laboratory
KESS	Kuroshio Extension System Study
LSDM	Land Surface Discharge Model
LEGOS	*Laboratoire d'Etudes en Géophysique et Océanographie Spatiales*
MOVE	Meridional Overturning Variability Experiment
MPIOM	Max Planck Institute Ocean Model
OBP	Ocean Bottom Pressure
OMCT	Ocean Model for Circulation and Tides
PIES	Pressure Inverted Echo Sounder
RL	Release
SLA	Sea Level Anomaly
SST	Sea Surface Temperature

List of Figures

List of Tables

Bibliography

Amante, C., and B. Eakins (2009), ETOPO1 Global Relief Model converted to PanMap layer format, doi:10.1594/PANGAEA.769615.

Becker, J., D. Sandwell, W. Smith, J. Braud, B. Binder, J. Depner, D. Fabre, J. Factor, S. Ingalls, S.-H. Kim, R. Ladner, K. Marks, S. Nelson, A. Pharaoh, R. Trimmer, J. Von Rosenberg, G. Wallace, and P. Weatherall (2009), Global Bathymetry and Elevation Data at 30 Arc Seconds Resolution: SRTM30_PLUS, *Mar. Geod.*, *32*(4), 355–371, doi:10.1080/01490410903297766.

Bergmann, I., and H. Dobslaw (2012), Short-term transport variability of the Antarctic Circumpolar Current from satellite gravity observations, *J. Geophys. Res.*, *117*, C05044, doi:10.1029/2012JC007872.

Bernales, J., I. Rogozhina, and M. Thomas (2017), Melting and freezing under Antarctic ice shelves from a combination of ice-sheet modelling and observations, *J. Glaciol.*, *63*(240), 731–744, doi:10.1017/jog.2017.42.

Beszczynska-Möller, A., E. Fahrbach, U. Schauer, and E. Hansen (2012), Variability in Atlantic water temperature and transport at the entrance to the Arctic Ocean, 1997–2010, *ICES J. Mar. Sci.*, *69*(5), 852–863, doi:10.1093/icesjms/fss056.

Bettadpur, S. (2012), UTCSR Level-2 Processing Standards Document, *Tech. rep.*, Center for Space Research, University of Texas, Austin, TX, USA.

Bishop, S. P., and D. R. Watts (2014), Rapid Eddy-Induced Modification of Subtropical Mode Water during the Kuroshio Extension System Study, *J. Phys. Oceanogr.*, *44*(7), 1941–1953, doi:10.1175/JPO-D-13-0191.1.

Böning, C., R. Timmermann, A. Macrander, and J. Schröter (2008), A pattern-filtering method for the determination of ocean bottom pressure anomalies from GRACE solutions, *Geophys. Res. Lett.*, *35*, L18611, doi:10.1029/2008GL034974.

British Oceanographic Data Centre (BODC) (2014), The GEBCO_2014 Grid, version 20150318, available from www.gebco.net.

Bryan, K. (1969), A numerical method for the study of the circulation of the world ocean, *J. Comput. Phys.*, *4*(3), 347–376, doi:10.1016/0021-9991(69)90004-7.

Cazenave, A., K. Dominh, S. Guinehut, E. Berthier, W. Llovel, G. Ramillien, M. Ablain, and G. Larnicol (2009), Sea level budget over 2003–2008: A reevaluation from GRACE space gravimetry, satellite altimetry and Argo, *Global Planet Change*, *65*(1–2), 83–88, doi:10.1016/j.gloplacha.2008.10.004.

Chambers, D. (2006), Observing seasonal steric sea level variations with GRACE and satellite altimetry, *J. Geophys. Res. Oceans*, *111*(C3), C03010, doi:10.1029/2005JC002914.

Chen, Q., L. Poropat, L. Zhang, and H. Dobslaw (2018), Validation of the EGSIEM GRACE gravity fields using GNSS coordinate time series and in situ ocean bottom pressure records, *Remote Sensing*, *10*(12), 1976, doi:10.3390/rs10121976.

Dahle, C., F. Flechtner, C. Gruber, D. König, R. König, G. Michalak, and K. Neumayer (2012), GFZ GRACE Level-2 processing standards document for Level-2 product release 005, *Tech. Rep. STR 12/02*, GeoForschungsZentrum Potsdam, Potsdam, Germany, doi:10.2312/GFZ.b103-12020.

Dahle, C., C. Gruber, E. Fagiolini, and F. Flechtner (2016), Gravity Field Mapping from GRACE: Different Approaches – Same Results?, in *VIII HOTINE-MARUSSI SYMPOSIUM ON MATHEMATICAL GEODESY*, *International Association of Geodesy Symposia*, vol. 142, edited by N. Sneeuw, P. Novak, M. Crespi, and F. Sanso, pp. 165–175, Springer, Cham, doi:10.1007/1345_2015_8.

Davis, J., P. Elósegui, J. Mitrovica, and M. Tamisiea (2004), Climate-driven deformation of the solid Earth from GRACE and GPS, *Geophys. Res. Lett.*, *31*(24), L24605, doi:10.1029/2004GL021435.

Dee, D., S. Uppala, A. Simmons, P. Berrisford, P. Poli, S. Kobayashi, U. Andrae, M. Balmaseda, G. Balsamo, P. Bauer, P. Bechtold, A. Beljaars, L. van de Berg, J. Bidlot, N. Bormann, C. Delsol, R. Dragani, M. Fuentes, A. Geer, L. Haimberger, S. Healy, H. Hersbach, E. Holm, L. Isaksen, P. Kallberg, M. Kohler, M. Matricardi, A. McNally, B. Monge-Sanz, J.-J. Morcrette, B.-K. Park, C. Peubey, P. de Rosnay, C. Tavolato, J.-N. Thepaut, and F. Vitart (2011), The ERA-Interim reanalysis: configuration and performance of the data assimilation system, *Q. J. Royal Meteorol. Soc.*, *137*, 553–597, doi:10.1002/qj.828.

Dijkstra, H. (2008), *Dynamical Oceanography*, 407 pp., Springer, Berlin, Germany.

Dill, R. (2008), Hydrological model LSDM for operational Earth rotation and gravity field variations, *Tech. rep.*, Deutsches GeoForschungsZentrum GFZ, Potsdam, doi:10.2312/GFZ.b103-08095.

Dill, R., H. Dobslaw, and M. Thomas (2018), Improved 90-day Earth orientation predictions from angular momentum forecasts of atmosphere, ocean, and terrestrial hydrosphere, *Journal of Geodesy*, *92*, doi:10.1007/s00190-018-1158-7.

Dobslaw, H., F. Flechtner, I. Bergmann-Wolf, C. Dahle, R. Dill, S. Esselborn, I. Sasgen, and M. Thomas (2013), Simulating high-frequency atmosphere-ocean mass variability for dealiasing of satellite gravity observations: AOD1B RL05, *J. Geophys. Res. Oceans*, *118*, 3704–3711, doi:10.1002/jgrc.20271.

Dobslaw, H., I. Bergmann-Wolf, E. Forootan, C. Dahle, T. Mayer-Gürr, J. Kusche, and F. Flechtner (2016), Modeling of present-day atmosphere and ocean non-tidal de-aliasing errors for future gravity mission simulations, *J. Geodesy*, *90*(5), 1–14, doi:10.1007/s00190-015-0884-3.

Dobslaw, H., I. Bergmann-Wolf, R. Dill., L. Poropat, and M. Thomas (2017), A new high-resolution model of non-tidal atmosphere and ocean mass variability for de-aliasing of satellite gravity observations: AOD1B RL06, *Geophys. J. Int.*, *211*, 263–269, doi:10.1093/gji/ggx302.

Eble, M., and F. Gonzales (1990), Deep-ocean pressure measurements in the Northeast Pacific, *JTECH*, *8*, 221–233, doi:10.1175/1520-0426(1991)008<0221:DOBPMI>2.0.CO;2.

Ezraty, R., F. Girard-Ardhuin, J. Piolle, L. Kaleschke, , and G. Heygster (2007), *Arctic and Antarctic sea ice concentration and Arctic sea ice drift estimated from Special Sensor Microwave data*, user's Manuel Version 2.1.

Foldvik, A., T. Gammelsrød, S. Østerhus, E. Fahrbach, E. Rohardt, M. Schröder, K. Nicholls, L. Padman, and R. Woodgate (2004), Ice shelf water overflow and bottom water formation in the southern Weddell Sea, *J. Geophys. Res.*, *109*, C02015, doi:10.1029/2003JC002008.

Frajka-Williams, E., I. Ansorge, J. Baehr, H. Bryden, M. Chidichimo, S. Cunningham, G. Danabasoglu, S. Dong, K. Donohue, P. Elipot, S.and Heimbach, N. Holliday, R. Hummels, L. Jackson, J. Karstensen, M. Lankhorst, I. Le Bras, M. S. Lozier, E. McDonagh, C. Meinen, H. Mercier, B. Moat, R. Perez, C. Piecuch, M. Rhein, M. Srokosz, K. Trenberth, S. Bacon, G. Forget, G. Goni, D. Kieke,

J. Koelling, T. Lamont, G. McCarthy, C. Mertens, U. Send, D. Smeed, S. Speich, M. van den Berg, D. Volkov, and C. Wilson (2019), Atlantic Meridional Overturning Circulation: Observed Transport and Variability, *Front. Mar. Sci.*, *6*, 260, doi:10.3389/fmars.2019.00260.

Garric, G., and L. Parent (2018), *Product user manual For Global Ocean Reanalysis Products GLOBAL-REANALYSIS-PHY-001-025*, 4.1 ed., available from http://resources.marine.copernicus.eu/documents/PUM/CMEMS-GLO-PUM-001-025.pdf.

Gordon, A., B. Huber, H. Hellmer, and A. Efield (1993), Deep and Bottom Water of the Weddell Sea's western rim, *Science*, *262*(5130), 95–97, doi:10.1126/science.262.5130.95.

Haines, K., V. Stepanov, M. Valdivieso, and H. Zuo (2013), Atlantic meridional heat transports in two ocean reanalyses evaluated against the RAPID array, *Geophys. Res. Lett.*, *40*(2), 343–348, doi:10.1029/2012GL054581.

Hellmer, H. (2004), Impact of Antarctic ice shelf basal melting on sea ice and deep ocean properties, *Geophys. Res. Lett.*, *31*, L10307, doi:10.1029/2004GL019506.

Hellmer, H., and D. Olbers (1989), A two-dimensional model for the thermohaline circulation under an ice shelf, *Antarct. Sci.*, *1*(4), 325–336, doi:10.1017/S0954102089000490.

Hellmer, H., M. Rhein, G. Heinemann, J. Abalichin, W. Abouchami, O. Baars, U. Cubasch, K. Dethloff, L. Ebner, E. Fahrbach, M. Frank, G. Gollan, R. Greatbatch, J. Grieger, V. Gryanik, M. Gryschka, J. Hauck, M. Hoppema, O. Huhn, T. Kanzow, B. Koch, G. König-Langlo, U. Langematz, G. Leckebusch, C. Lüpkes, S. Paul, A. Rinke, B. Rost, M. Rutgers van der Loeff, M. Schröder, G. Seckmeyer, T. Stichel, V. Strass, R. Timmermann, S. Trimborn, U. Ulbrich, C. Venchiarutti, U. Wacker, S. Willmes, and D. Wolf-Gladrow (2016), Meteorology and oceanography of the Atlantic sector of the Southern Ocean – a review of German achievements from the last decade, *Ocean Dynam.*, *66*, 1379–1413, doi:10.1007/s10236-016-0988-1.

Jaggi, A., M. Weigelt, F. Flechtner, A. Güntner, T. Mayer-Gürr, S. Martinis, S. Bruinsma, J. Flury, S. Bourgogne, H. Steffen, U. Meyer, Y. Jean, A. Sušnik, A. Grahsl, D. Arnold, K. Cann-Guthauser, R. Dach, Z. Li, Q. Chen, T. van Dam, C. Gruber, L. Poropat, B. Gouweleeuw, A. Kvas, B. Klinger, J.-M. Lemoine, R. Biancale, H. Zwenzner, T. Bandikova, and A. Shabanloui (2019), European Gravity Service for Improved Emergency Management (EGSIEM) – from concept to implementation, *Geophys. J. Int.*, *218*(3), 1572–1590, doi:10.1093/gji/ggz238.

Jean, Y., U. Meyer, and A. Jäggi (2018), Combination of GRACE monthly gravity field solutions from different processing strategies, *J. Geod.*, *92*(11), 1313–1328, doi:10.1007/s00190-018-1123-5.

Jones, P. (1998), First- and Second-Order Conservative Remapping Schemes for Grids in Spherical Coordinates, *Mon. Weather Rev.*, *127*, 2204–2210, doi:10.1175/1520-0493(1999)127<2204:FASOCR>2.0.CO;2.

Jungclaus, J. H., N. Fischer, H. Haak, K. Lohmann, J. Marotzke, D. Matei, U. Mikolajewicz, D. Notz, and J. S. von Storch (2013), Characteristics of the ocean simulations in the Max Planck Institute Ocean Model (MPIOM) the ocean component of the MPI-Earth system model, *JAMES*, *5*(2), 422–446, doi:10.1002/jame.20023.

Kantha, L., and C. Clayson (2000), *Numerical Models of Oceans and Oceanic Processes*, *International Geophysics Series*, vol. 66, 949 pp., Academic Press, San Diego, USA.

Kanzow, T., F. Flechtner, A. Chave, R. Schmidt, P. Schwintzer, and U. Send (2005), Seasonal variation of ocean bottom pressure derived from Gravity Recovery and Climate Experiment (GRACE): Local validation and global patterns, *J. Geophys. Res. Oceans*, *110*, C09001, doi:10.1029/2004JC002772.

Kanzow, T., U. Send, W. Zenk, A. Chave, and M. Rhein (2006), Monitoring the integrated deep meridional flow in the tropical North Atlantic: Long-term performance of a geostrophic array, *Deep-Sea Res. I*, *53*, 528–546, doi:10.1016/j.dsr.2005.12.007.

Köhler, J., C. Mertens, M. Walter, U. Stöber, M. Rhein, and T. Kanzow (2014), Variability in the Internal Wave Field Induced by the Atlantic Deep Western Boundary Current at 16°N, *J. Phys. Oceanogr.*, *44*, 492–516, doi:10.1175/JPO-D-13-010.1.

Kurtenbach, E., A. Eicker, T. Mayer-Gürr, M. Holschneider, M. Hayn, M. Fuhrmann, and J. Kusche (2012), Improved daily GRACE gravity field solutions using a Kalman smoother, *J. Geodyn.*, *59-60*, 39–48, doi:10.1016/j.jog.2012.02.006.

Leuliette, E., and L. Miller (2009), Closing the sea level rise budget with altimetry, Argo, and GRACE, *Geophys. Res. Lett.*, *36*, L04608, doi:10.1029/2008GL036010.

Llovel, W., S. Guinehut, and A. Cazenave (2010), Regional and interannual variability in sea level over 2002–2009 based on satellite altimetry, Argo float data and GRACE ocean mass, *Ocean Dynamics*, *60*, 1193–1204, doi:10.1007/s10236-010-0324-0.

Luthcke, S., T. Sabaka, B. Loomis, A. Arendt, J. McCarthy, and J. Camp (2013), Antarctica, Greenland and Gulf of Alaska land-ice evolution from an iterated GRACE global mascon solution, *J. Glaciol.*, *59*(216), 613–631, doi:10.3189/2013JoG12J147.

Macrander, A., C. Böning, O. Boebel, and J. Schröter (2010), Validation of GRACE gravity fields by in-situ data of ocean bottom pressure, in *System Earth via Geodetic-Geophysical Space Techniques*, Springer, Berlin.

Madec, G., and M. Imbard (1996), A global ocean mesh to overcome the North Pole singularity, *Climate Dynamics*, *12*(6), 381–388, doi:10.1007/BF00211684.

Mayer-Gürr, T., S. Behzadpour, M. Ellmer, A. Kvas, B. Klinger, and N. Zehentner (2016), ITSG-Grace2016 - Monthly and Daily Gravity Field Solutions from GRACE, GFZ Data Services, doi:10.5880/icgem.2016.007.

McCarthy, G. D., D. A. Smeed, W. E. Johns, E. Frajka-Williams, B. I. Moat, D. Rayner, M. O. Baringer, C. S. Meinen, J. Collins, and H. L. Bryden (2015), Measuring the Atlantic Meridional Overturning Circulation at 26°N, *Prog. Oceanogr.*, *130*, 91–111, doi:10.1016/j.pocean.2014.10.006.

Meinen, C., and D. Watts (1998), Calibrating Inverted Echo Sounders Equipped with Pressure Sensors, *JTECH*, *15*, 1339–1345, doi:10.1175/1520-0426(1998)015<1339:CIESEW>2.0.CO;2.

Meinig, C., S. Stalin, A. Nakamura, and H. Milburn (2005), Real-Time Deep-Ocean Tsunami Measuring, Monitoring, and Reporting System: The NOAA DART II Description and Disclosure.

Meyer, U., A. Jggi, Y. Jean, and G. Beutler (2016), AIUB-RL02: An improved time series of monthly gravity fields from GRACE data, *Geophys. J. Int.*, *205*(2), 1196–1207, doi:10.1093/gji/ggw081.

Mo, H.-E., and Y.-Q. Yu (2012), Simulation of Volume and Heat Transport along 26.5°N in the Atlantic, *Atmos. Oceanic Sci. Lett.*, *5*(5), 373–378, doi:10.1080/16742834.2012.11447019.

Moore, S., and J. Fisher (2012), Challenges and Opportunities in GRACE-Based Groundwater Storage Assessment and Management: An Example from Yemen, *Water Resour. Manag.*, *26*(6), 1425–1453, doi:10.1007/s11269-011-9966-z.

Morison, J., J. Wahr, and C. Peralta-Ferriz (2007), Recent trends in Arctic Ocean mass distribution revealed by GRACE, *Geophys. Res. Lett.*, *34*(7), L07602, doi:10.1029/2006GL029016.

National Oceanic and Atmospheric Administration (NOAA) (1998), ETOPO5 bathymetry/topography data. Digital relief of the surface of the Earth, data Announcement: 88-MGG-02.

Orsi, A., G. Johnson, and J. Bullister (1999), Circulation, mixing, and production of Antarctic Bottom Water, *Prog. Oceanogr.*, *43*, 55–109, doi:10.1016/S0079-6611(99)00004-X.

Padman, L., H. A. Fricker, R. Coleman, S. Howard, and L. Erofeeva (2002), A new tide model for the Antarctic ice shelves and seas, *Annals of Glaciology*, *34*, 247–254, doi:10.3189/172756402781817752.

Park, J.-H., D. Watts, K. Donohue, and S. Jayne (2008), A comparison of in situ bottom pressure array measurements with GRACE estimates in the Kuroshio Extension, *Geophys. Res. Lett.*, *35*(17), L17601, doi:10.1029/2008GL034778.

Park, J.-H., D. Watts, K. Donohue, and K. Tracey (2012), Comparisons of sea surface height variability observed by pressure-recording inverted echo sounders and satellite altimetry in the Kuroshio Extension, *J. Oceanogr.*, *68*(3), 401–416, doi:10.1007/s10872-012-0108-x.

Pawlowicz, R., B. Beardsley, and S. Lentz (2002), Classical tidal harmonic analysis including error estimates in MATLAB using T_TIDE, *Comput. Geosci.*, *28*, 929–937, doi:10.1016/S0098-3004(02)00013-4.

Peralta-Ferriz, C., J. Morison, S. Stalin, and C. Meinig (2014), Measuring Ocean Bottom Pressure at the North Pole, *Mar. Technol. Soc. J.*, *48*(5), 52–68, doi:10.4031/MTSJ.48.5.11.

Piecuch, C., K. Quinn, and R. Ponte (2013), Satellite-derived interannual ocean bottom pressure variability and its relation to sea level, *Geophys. Res. Lett.*, *40*(12), 3106–3110, doi:10.1002/grl.50549.

Poropat, L., H. Dobslaw, L. Zhang, A. Macrander, O. Boebel, and M. Thomas (2018), Time variations in ocean bottom pressure from a few hours to many years: in situ data, numerical models, and GRACE satellite gravimetry, *J. Geophys. Res. Oceans*, *123*, 5612–5623, doi:10.1029/2018JC014108.

Pujol, M.-I., and F. Mertz (2019), *Product User Manual for Sea Level SLA products.*

Reynolds, R., T. Smith, C. Liu, D. Chelton, K. Casey, and M. Schlax (2007), Daily High-Resolution-Blended Analyses for Sea Surface Temperature, *J. Climate*, *20*, 5473–5496, doi:10.1175/2007JCLI1824.1.

Rignot, E., S. Jacobs, J. Mouginot, and B. Scheuchl (2013), Ice-Shelf Melting Around Antarctica, *Science*, *341*, 266–270, doi:10.1126/science.1235798.

Rintoul, S., C. Hughes, and D. Olbers (2001), Chapter 4.6 The antarctic circumpolar current system, in *Ocean Circulation and Climate: Observing and Modelling the Global Ocean*, *International Geophysics*, vol. 77, edited by G. Siedler, J. Church, and J. Gould, pp. 271–302, Academic Press, doi:10.1016/S0074-6142(01)80124-8.

Rodell, M., I. Velicogna, and J. Famiglietti (2009), Satellite-based estimates of groundwater depletion in India, *Nature*, *460*(7258), 999–1002, doi:10.1038/nature08238.

Send, U., M. Lankhorst, and T. Kanzow (2011), Observation of decadal change in the Atlantic meridional overturning circulation using 10 years of continuous transport data, *Geophys. Res. Lett.*, *38*, L24606, doi:10.1029/2011GL049801.

Stepanov, V., D. Iovino, S. Masina, A. Storto, and A. Cipollone (2006), Methods of calculation of the Atlantic meridional heat and volume transports from ocean models at 26.5°N, *J. Geophys. Res. Oceans*, *121*, 1459–1475, doi:10.1002/2015JC011007.

Szekely, T. (2019), *Product User Manual For Global Delayed Mode Insitu Dataset INSITU_GLO_TS_REP_OBSERVATIONS_013_001_b called CORA*.

Tapley, B. D., S. Bettadpur, M. Watkins, and C. Reigber (2004), The gravity recovery and climate experiment: Mission overview and early results, *Geophys. Res. Lett.*, *31*, L09607, doi:10.1029/2004GL019920.

Thomas, M. (2002), Ocean induced variations of Earth's rotation – Results from a simultaneous model of global circulation and tides, Ph.D. thesis, University of Hamburg, Hamburg, Germany.

Velicogna, I. (2009), Increasing rates of ice mass loss from the Greenland and Antarctic ice sheets revealed by GRACE, *Geophys. Res. Lett.*, *36*(19), L19503, doi:10.1029/2009GL040222.

Wahr, J., and I. Velicogna (2003), What might GRACE contribute to studies of post glacial rebound?, *Space Sci. Rev.*, *108*(1–2), 319–330, doi:10.1023/A:1026183526762.

Watkins, M., and T. Yuan (2012), JPL Level-2 Processing Standards Document for Level-2 Product Release 05, *Tech. rep.*, NASA JPL, Pasadena, CA, USA.

Watts, D., and H. Kontoyiannis (1990), Deep-Ocean Bottom Pressure Measurement - Drift Removal and Performance, *J. Atmos. Oceanic Tech.*, *7*(2), 296–306, doi:10.1175/1520-0426(1990)007<0296:DOBPMD>2.0.CO;2.

Willis, J., D. Chambers, and R. Nerem (2008), Assessing the globally averaged sea level budget on seasonal to interannual timescales, *J. Geophys. Res. Oceans*, *113*(C6), C06015, doi:10.1029/2007JC004517.

Acknowledgements

Throughout my entire PhD time, I received a great deal of support and assistance from my colleagues, family, and friends. I would like to take this opportunity to express my gratitude to all of them.

First of all, I would like to thank my advisor Prof. Dr. Maik Thomas. He was always supportive and ready to help whenever I had a question about research, publishing or administrative side of GFZ.

I would also like to thank my supervisor Dr. Henryk Dobslaw for giving me the opportunity to do this work and for his guidance and support every step of the way.

I thank Prof. Dr. Frank Flechtner for reviewing my thesis and for traveling to Berlin so that I could defend it.

I thank Dr. Qiang Chen for inviting me to write a paper with him that later became a part of this dissertation.

I also thank Prof. Dr.-Ing. Torsten Mayer-Gürr and Dr. Andreas Kvas for their contribution to the paper that I published as a part of my PhD studies.

A special thanks to Dr. Jorge Bernales for his explanations about ice shelves, which were crucial for my work.

I also thank Dr. Carina Haeger for proofreading my thesis. Without her my dissertation, and especially the German abstract, would have many more mistakes.

I am grateful to the entire Section 1.3. for providing a great work environment, always answering any questions I had and helping me every time I needed something translated to or from German. I never believed I could find so many good friends at work.

I thank my friends, both newly made in Germany and old friends from Croatia, for all the interesting conversations, fun board game sessions, and other breaks from work, as well as for their moral support. You made my life much nicer.

Finally, I would like to thank my family for their encouragement and help. I thank my parents, Vesna and Davor Poropat, for always being proud of me. I thank my sister Marta for always listening to me when I needed to vent about the difficulties of doing a PhD. I thank Zara for her calming influence, which helped me immensely when things were going wrong and writing was difficult.

Appendix

Publications

The appendix contains the abstracts and author contributions of all papers incorporated into this dissertation. An overview of contributions of Lea Poropat to each of the publications is given in Table 1. The contributions are separated into idea, computation, analysis, figure preparation, and writing. All papers have been published in peer reviewed journals.

Table 1: Contributions of Lea Poropat to papers included in this dissertation. Papers for which Lea Poropat is the main author are labeled with F, while co-authored publications are labeled with C.

	F1	F2	C1	C2
Idea	50 %	30 %	0 %	20 %
Computation	90 %	50 %	20 %	50 %
Analysis	80 %	50 %	20 %	50 %
Figures	100 %	70 %	66 %	44 %
Writing	90 %	65 %	0 %	40 %

F1 Time variations in ocean bottom pressure from a few hours to many years: in situ data, numerical models, and GRACE satellite gravimetry

L. Poropat, H. Dobslaw, L. Zhang, A. Macrander, O. Boebel, and M. Thomas (2018): **Time variations in ocean bottom pressure from a few hours to many years: in situ data, numerical models, and GRACE satellite gravimetry**, Journal of Geophysical Research: Oceans, 123, 5612–5623, doi: 10.1029/2018JC014108.

Abstract

In situ ocean bottom pressure (OBP) obtained from 154 different locations irregularly scattered over the globe is carefully processed to isolate signals related to the ocean general circulation and large-scale sea-level changes. Comparison against a global numerical ocean model experiment indicates poor correspondence for periods below 24 hours, possibly related to residual tidal signals and small timing errors in the atmospheric forcing applied to the ocean model. Correspondence increases rapidly for periods between 3 and 10 days, where wind-driven dynamics are already well understood and consequently well implemented into numerical models. Coherence decreases again for periods around 30 days and longer, where processes not implemented into ocean general circulation models as barystatic sea-level changes become more important. Correspondence between in situ data and satellite-based OBP as obtained from the GRACE GFZ RL05a gravity fields critically depends on the post-processing of Level-2 Stokes coefficients that also includes the selection of appropriate averaging regions for the GRACE-based mass anomalies. The assessment of other available GRACE Level-2 products indicate even better fit of more recent solutions as ITSG-Grace2016 and the CSR and JPL RL05 mascons. In view of the strong high-frequency component of OBP, however, a higher temporal resolution of the oceanic GRACE products would be rather advantageous.

Declaration of contribution

The idea to write this paper was developed by H. Dobslaw and L. Poropat. A. Macrander and O. Boebel provided the in situ ocean bottom pressure data, H. Dobslaw provided the model experiment output, and L. Zhang processed GRACE data to make them comparable with other utilized datasets. L. Poropat processed the in situ data, and performed the comparison with ocean model output and GRACE gravity fields, including the production of all images. L. Poropat wrote the bulk of the manuscript, with the help of H. Dobslaw. M. Thomas reviewed the manuscript and provided useful feedback.

F2 Mitigating temporal aliasing effects of high-frequency geophysical fluid dynamics in satellite gravimetry

L. Poropat, A. Kvas, T. Mayer-Gürr, and H. Dobslaw (2020): **Mitigating temporal aliasing effects of high-frequency geophysical fluid dynamics in satellite gravimetry**, Geophysical Journal International, 220(1), 257–266, doi: 10.1093/gji/ggz439.

Abstract

Temporal aliasing errors induced by high-frequency tidal and non-tidal mass variability in the Earth system are among the three most important error sources that limit the accuracy of present-day surface mass estimates from satellite gravimetry. By means of end-to-end simulations, we demonstrate that the Kalman Smoother approach developed by *Kurtenbach et al.* (2012) effectively captures non-tidal submonthly variability, and thereby reduces temporal aliasing errors way beyond the level of simply subtracting the standard dealiasing model AOD1B. Validation against in situ ocean bottom pressure observations confirms that the Kalman Smoother solutions published together with the ITSG-Grace2016 monthly gravity fields contain high-frequency signal over the oceans not predicted by AOD1B. The daily gravity fields therefore reduce aliasing artefacts in the monthly gravity fields, and at the same time provide observational evidence on submonthly bottom pressure variability presently not reflected in state-of-the-art numerical ocean circulation models. It is thus recommended to include a Kalman Smoother approach into any standard GRACE processing scheme. For a hypothetical double-pair configuration currently under consideration as a future mass change mission, we find that the benefit of the Kalman Smoother is much smaller thanks to the increased number of observations taken at different inclinations, which lead to generally reduced aliasing errors and much more isotropic spatial error correlations. We also reassess the idea of pre-eliminating low-resolution daily gravity fields and find large distortions in the monthly-mean gravity solution at spatial wavelengths around the cutoff-degree of the daily fields. We thus recommend further study for any satellite gravity mission concept that critically relies on such pre-elimination schemes for reaching its science objectives.

Declaration of contribution

For this paper L. Poropat analysed the geophysical signals in the daily gravity fields, performed the in situ validation, and wrote the manuscript together with H. Dobslaw. A. Kvas performed the satellite mission simulation experiments. T. Mayer-Gürr and H. Dobslaw designed the study and contributed to the interpretation of results.

C1 A new high-resolution model of non-tidal atmosphere and ocean mass variability for de-aliasing of satellite gravity observations: AOD1B RL06

H. Dobslaw, I. Bergmann-Wolf, R. Dill, **L. Poropat**, M. Thomas, C. Dahle, S. Esselborn, R. König, and F. Flechtner (2017): **A new high-resolution model of non-tidal atmosphere and ocean mass variability for de-aliasing of satellite gravity observations: AOD1B RL06**, Geophysical Journal International, 211, 263–269, doi: 10.1093/gji/ggx302.

Abstract

The release 06 (RL06) of the Gravity Recovery and Climate Experiment (GRACE) Atmosphere and Ocean De-Aliasing Level-1B (AOD1B) product has been prepared for use as a time-variable background model in global gravity research. Available since the year 1976 with temporal resolution of 3 hr, the product is provided in Stokes coefficients up to degree and order 180. RL06 separates tidal and non-tidal signals, and has an improved long-term consistency due to the introduction of a time-invariant reference orography in continental regions. Variance reduction tests performed with globally distributed in situ ocean bottom pressure recordings and sea-surface height anomalies from Jason-2 over a range of different frequency bands indicate a generally improved performance of RL06 compared to its predecessor. Orbit tests for two altimetry satellites remain inconclusive, but GRACE K-band residuals are reduced by 0.031 $\mathrm{nm\,s^{-2}}$ in a global average, and by more than 0.5 $\mathrm{nm\,s^{-2}}$ at numerous places along the Siberian shelf when applying the latest AOD1B release. We therefore recommend AOD1B RL06 for any upcoming satellite gravimetry reprocessing effort.

Declaration of contribution

For this paper L. Poropat performed the validation of AOD1B releases against in situ ocean bottom pressure and generated the affiliated figures.

C2 Validation of the EGSIEM GRACE gravity fields using GNSS coordinate time series and in situ ocean bottom pressure records

Q. Chen, **L. Poropat**, L. Zhang, H. Dobslaw, M. Weigelt, and T. van Dam (2018): **Validation of the EGSIEM GRACE gravity fields using GNSS coordinate time series and in situ ocean bottom pressure records**, Remote Sensing, 10(12), 1976, doi: 10.3390/rs10121976.

Abstract

Over the 15 years of the Gravity Recovery and Climate Experiment (GRACE) mission, various data processing approaches were developed to derive time-series of global gravity fields based on sensor observations acquired from the two spacecrafts. In this paper, we compare GRACE-based mass anomalies provided by various processing groups against Global Navigation Satellite System (GNSS) station coordinate time-series and in-situ observations of ocean bottom pressure. In addition to the conventional GRACE-based global geopotential models from the main processing centers, we focus particularly on combined gravity field solutions generated within the Horizon2020 project European Gravity Service for Improved Emergency Management (EGSIEM). Although two validation techniques are fully independent from each other, it is demonstrated that they confirm each other to a large extent. Through the validation, we show that the EGSIEM combined long-term monthly solutions are comparable to CSR RL05 and ITSG2016, and better than the other three considered GRACE monthly solutions AIUB RL02, GFZ RL05a, and JPL RL05.1. Depending on the GNSS products, up to 25.6 % mean Weighted Root-Mean-Square (WRMS) reduction is obtained when comparing GRACE to the ITRF2014 residuals over 236 GNSS stations. In addition, we also observe remarkable agreement at the annual period between GNSS and GRACE with up to 73 % median WRMS reduction when comparing GRACE to the 312 EGSIEM-reprocessed GNSS time series. While the correspondence between GRACE and ocean bottom pressure data is overall much smaller due to lower signal to noise ratio over the oceans than over the continents, up to 50 % agreement is found between them in some regions. The results fully confirm the conclusions found using GNSS.

Declaration of constribution

L. Poropat did the work pertaining to the validation of GRACE gravity fields against in situ OBP in this paper: from performing the experiments, through results analysis, to writing parts of the manuscript that describe it.